Pain-relevant behavior associated with VGF expression in primary afferent neurons

A THESIS
SUBMITTED TO THE FACULTY OF THE
UNIVERSITY OF MINNESOTA
BY

Jaclyn A. Dykstra

IN PARTIAL FULFILLMENT OF THE REQUIREMENTS
FOR THE DEGREE OF
DOCTOR OF PHILOSOPHY

Advisors: Lucy Vulchanova, Ph.D., Alvin Beitz, Ph.D.

July 2015

Acknowledgements

A very special thank you to all the people that helped me through this process:

To my advisor, Lucy Vulchanova, for her consistent guidance, scientific support, discerning critique, enthusiasm, tenacity, and patience. You kept your focus even when I lost mine, and without you, this thesis would not have been possible.

To my co-advisor, Alvin Beitz, and to my committee members, Cathy Carlson, Alessandro Bartolomucci, and Chris Honda, for their valuable insight and unwavering encouragement.

To Maureen Riedl and Galina Kalyuzhnaya, for thoughtful discussions and extensive technical support.

To past and present collaborators, especially Dan Schuster, Kelley Kitto, Rebecca Speltz, Cristina Peterson, Steve Schnell, Martin Wessendorf, David Brown, Jennifer Marlo-Triemstra, Colin Reich, Hannah Springer, and Breanna Pearson, for your assistance, expertise, interest, and sympathy.

To my funding sources, including the Comparative Medicine and Pathology Training Fellowship supported by the National Institutes of Health, the Dr. Bee Hanlon and Dr. JoAnne Schmidt-O'Brien Research Fellowship, and the University of Minnesota Graduate School Doctoral Dissertation Fellowship, for your investment and helping me achieve my career goals.

To my husband, Josh, for constructing behavioral testing equipment, enduring countless weekend weanings, programming eccentricities in Excel, procuring a wrist brace after I circled too many neurons, proofreading pathobiological mumbo jumbo, and all the little things in-between.

To my family, particularly my parents, Thomas and JoAnn Harry, and my sister, Tina Harry, for your love, understanding, support, and relentless belief in me.

To Lorene Dykstra, for proofreading through all the sciencey stuff.

To Wicket and Garrus, for being steadfast companions on this adventure.

To Aperture Science, for reminding me that science is not about asking why, it is about asking why not.

Now these points of data make a beautiful line. And we're out of beta, we're releasing on time. So I'm glad I got burned. Think of all the things we learned for the people who are still alive.

– Jonathan Coulton, *Still Alive,* 2007

Abstract

Previously published work by our lab evaluating injury-induced changes in sensory neuron protein expression identified substantially increased levels of the neurosecretory protein VGF (non-acronymic), a neuropeptide precursor. To further characterize the functional role of VGF-derived peptides in sensory neuron signaling and in the development of pain-relevant behavior, we utilized animal models, behavior analyses, and complementary morphologic and molecular techniques to pursue two approaches: using adeno-associated virus (AAV) vectors to modulate VGF expression in primary afferent neurons, and exploring whether VGF up-regulation is limited to somatic pain. From this work, we learned intrasciatic administration of AAV5 vectors yields inefficient and variable transduction of sensory and motor neurons, reminiscent of the AAV8 serotype. Intrathecal administration of AAV5-VGF resulted in successful transduction of the choroid plexus but poor expression in dorsal root ganglion (DRG) sensory neurons. Unexpected DRG sensory neuron degeneration was observed following highly-efficient transduction of AAV9, warranting caution in future experiments utilizing this vector serotype. Antibiotic-induced visceral hypersensitivity was associated with up-regulation of VGF and other nociceptive neuropeptides in sensory neurons of the sixth lumbar DRG. However, contrary to expectations, referred cutaneous allodynia associated with antibiotic-induced visceral hypersensitivity was not readily detected using a non-invasive mechanical stimulation assay. Collectively, these findings encourage a re-evaluation of the tools employed to modulate VGF expression in primary afferent neurons *in vivo*, support the investigation of this novel signaling system beyond models of nerve injury, and are presented such that they can be used as an aid in the design of future work.

Table of Contents

List of Tables

List of Figures

List of Abbreviations

AAV	Recombinant adeno-associated virus
AEB	Acetone-evoked behavior
ANOVA	Analysis of variance
AQEE-30	VGF-derived bioactive peptide, designated by the four N-terminal amino acids and total length
AUC	Area under the paw withdrawal threshold curve
BL	Baseline
CBA	Chicken β-actin promoter
CGRP	Calcitonin gene-related peptide
CMV	Cytomegalovirus
Cre	Cre-recombinase
Cy2	Cyanine 2 fluorescent dye
Cy3	Cyanine 3 fluorescent dye
Cy5	Cyanine 5 fluorescent dye
DRG	Dorsal root ganglion
GFP	Green fluorescent protein
hADC	Human arginine decarboxylase
hVGF	Mouse line in which the coding sequence of mouse VGF_{1-617} is replaced by human VGF_{1-615} (B6;129Sv-*Vgf* $^{tm(VGF)}$/J)
IB_4	Isolectin B_4
IBS	Irritable bowel syndrome
IC	Intracolonic
IHC	Immunohistochemistry

-IR	Immunoreactivity
L4	Fourth lumbar (in reference to vertebral segment)
L5	Fifth lumbar (in reference to vertebral segment)
L6	Sixth lumbar (in reference to vertebral segment)
MBP	Myelin basic protein
MGV	Mean grey value
MHC	Major histocompatibility complex
mVGF	Mouse line with the same genetic background as hVGF but lacking the targeted mutation (B6;129Sv/J)
PBS	Phosphate buffered saline
PCR	Polymerase chain reaction
PDGF	Platelet-derived growth factor
PWT	Paw withdrawal threshold
SEM	Standard error of the mean
SGC	Satellite glial cell
SNI	Spared nerve injury
SP	Substance P
SUDO	Simplified up-down (method of mechanosensitivity assessment)
TLQP-21	VGF-derived bioactive peptide, designated by the four N-terminal amino acids and total length
TLQP-62	VGF-derived bioactive peptide, designated by the four N-terminal amino acids and total length; parent peptide of TLQP-21 and AQEE-30
TRPV1	Transient receptor potential vanilloid 1
VGF	Not an abbreviation, protein name is non-acronymic

Chapter 1

Introduction

The purpose of this research was to investigate the functional role of VGF-derived peptides in sensory neuron signaling and in the development of pain-relevant behavior. These hypothesis-driven projects utilized genetic models, behavior analyses, and complementary morphologic and molecular techniques to further characterize this novel signaling system.

Neuropathic pain. Pain is an unpleasant sensory and emotional experience associated with actual or potential tissue damage (Loeser and Treede, 2008). Neuropathic pain is a distinct, complex, and chronic pain state initiated by a primary lesion or disease affecting the somatosensory nervous system (Grubb, 2010). This condition is estimated to affect 2-3% of the population, with an estimated prevalence of 4 million adults, and accounts for 25-50% of all visits to pain clinics (Wallace, 2005; Gilron et al., 2006). Etiologies of nervous system pathology are varied and include direct nerve and spinal cord trauma, viral infections including *Herpes zoster*, and metabolic derangements including diabetes mellitus. While neuropathic pain may result from lesions to the peripheral nervous system, central nervous system, or both, peripheral somatic nerves are most commonly involved (Hayes et al., 2002; Irving, 2005). Key symptoms are spontaneous burning or piercing pain, paradoxical sensory loss, and hypersensitivity, which may manifest as *allodynia* – pain evoked by innocuous stimuli such as light touch, *hyperalgesia* – exaggerated pain in response to noxious stimuli, and *hyperpathia* – explosive abnormal pain that persists beyond a stimulus (Kehlet et al., 2006).

Despite being a common and severe condition, therapy is often unsatisfactory. Neuropathic pain is frequently resistant to available pharmacologic options, including over-the-counter analgesics and opioids. The impact of this disabling condition on

patients can be devastating, with an increased prevalence of depression, anxiety, and sleep disorders; decreased quality of life; and impairment of daily living activities and work performance (Gilron et al., 2006; Haanpää and Treede, 2010). The underlying pathophysiology of neuropathic pain is heterogeneous, complex, and incompletely understood. A better mechanistic understanding of the development and maintenance of neuropathic pain will likely identify new therapeutic targets as well as potential biomarker candidates for improved diagnosis.

Neurosecretory protein VGF. Dorsal root ganglion (DRG) sensory neurons are the first relay for the transmission of pain signals from the periphery to the central nervous system. Peripheral nerve injury induces changes in sensory neuron gene expression, resulting in alterations of neuron function. These modifications may impact the excitability, responsiveness, transmission, or survival of sensory neurons, and may or may not be reversible (Kehlet et al., 2006). Previously published work by our lab evaluating injury-induced changes in sensory neuron protein expression identified substantially increased levels of the neurosecretory protein VGF (non-acronymic), a neuropeptide precursor (Riedl et al., 2009). The nerve growth factor responsive *Vgf* gene is expressed in neurons within the central and peripheral nervous system and in various endocrine cells. The encoded 617 amino acid protein is cleaved into a number of peptides, including several bioactive peptides from the highly conserved C-terminal region (Figure 1-1; Bartolomucci et al., 2011).

In addition to rapid, robust, and persistent expression of VGF in injured sensory neurons, acute intrathecal administration of bioactive peptides derived from the C-terminal region of VGF to naïve animals resulted in thermal hyperalgesia and microglial p38 activation.

These and the findings of others have suggested that the VGF C-terminal peptides likely play an important functional role in neuronal signaling at the onset of nerve injury, mediating interactions between sensory neurons and spinal neurons or microglia (Moss et al., 2008; Riedl et al., 2009).

To further characterize this novel signaling system, we questioned whether VGF overexpression in somatic sensory neurons would be sufficient to induce pain-related behavior (Chapter 2). Conjointly, we investigated whether VGF upregulation was evident in sensory neurons in a model of visceral hypersensitivity, which also served to complement and inform other ongoing research (Chapter 3). Additionally, in the course of this work we identified and analyzed potential methodology process improvements (Chapter 4).

Genetic manipulation of VGF. A powerful tool for studying gene function in an intact animal is the use of targeted mutations to regulate expression levels of the gene product. However, genetic manipulation of VGF in primary sensory neurons has faced certain challenges. Although well-characterized, constitutive VGF knockout mice exhibit a wide range of abnormalities – such as reduced postnatal survival – that preclude their use in the study of neuropathic pain (Hahm et al, 1999). The development of sensory neuron-specific knock-out or knock-in mouse lines has been hampered by the lack of a tissue-specific promoter. The most promising candidate is the *Advillin* gene, which is expressed almost exclusively in peripheral sensory neurons (Hasegawa et al., 2007). Unfortunately, the particular sequence of the *Advillin* promoter has not yet been determined, and sensory neuron-specific transgenic mouse lines are not commercially available.

A more tenable technique to manipulate gene expression in primary afferent neurons is to utilize viral-mediated gene transfer. Recombinant adeno-associated virus (AAV) vectors have emerged as powerful vehicles for genetic manipulation of primary sensory neurons, mediating efficient, stable, and nontoxic transduction (Daya and Berns, 2008; Schultz and Chamberlain, 2008). AAV are non-pathogenic, single-stranded DNA viruses in the *Dependovirus* genus of the *Parvoviridae* family. The "gutless" recombinant vectors are devoid of viral genes (retaining only the inverted terminal repeats), can target non-dividing cells *in vivo*, and drive long-term expression of the transgene (Beutler and Reinhardt, 2009). While the small packaging capacity of around 4400 bp for regulatory elements and the transgene can be a detriment, the capacity is sufficient to accommodate the encoding sequence for VGF (~ 1850 bp) and a standard ubiquitous promoter. Sensory neuronal tropism has been demonstrated for multiple capsid serotypes of AAV, including AAV1 (Hollis et al., 2008; Homs et al., 2011); AAV2 (Boulis et al., 2003; Xu et al., 2003; Gu et al., 2005; Homs et al., 2011); AAV5 (Mason et al., 2010; Vulchanova et al., 2010; Xu et al., 2012); AAV6 (Towne et al., 2009); AAV8 (Vulchanova et al., 2010); and AAVrh20 (Pleticha et al., 2014b). Not all sensory neuron subpopulations were equally targeted by each serotype, suggesting differential tropism based on the protein structure of the capsid.

Viral access to primary afferent neurons is typically achieved through intrathecal, intraneural, or direct ganglionic injection. Intrathecal administration by acute lumbar puncture presents less risk of direct traumatic damage to nervous tissue, but provides the vector access to spinal and supraspinal structures via the cerebrospinal fluid (Hylden and Wilcox, 1980). Unintentional contamination of the cerebrospinal fluid has also been

observed following intraganglionic injection (Mason et al., 2010). The neurotropism of AAV vectors is not limited to sensory neurons, and genetic manipulation of VGF in these off-target sites could complicate and confound the interpretation of behavioral analysis, particularly as VGF within the central nervous system has been implicated in mood and antidepressant responses (Hunsberger et al., 2007). Identifying a route of administration that would sequester the vector to the region of interest is an important step in investigating the utility of viral-mediated gene transfer to further characterize the VGF signaling system in sensory neurons.

Visceral pain. Visceral pain, pain sensed as arising from the internal organs of the body, affects up to 25% of the population at any one time and is a prominent symptom of many clinical conditions (Moloney et al., 2015). The neurobiological mechanisms of visceral pain differ from those involved in somatic pain, and clinically, visceral pain is characterized by diffuse and poorly localized pain that may be associated with referred pain to a somatic structure (Cervero and Laird, 1999). Treatment is often insufficient and unsatisfactory. Much like neuropathic pain, enhanced understanding of the underlying mechanisms of visceral pain is needed to aid in the development of novel therapeutics.

Irritable bowel syndrome (IBS) is the most common functional gastrointestinal disorder, with key symptoms including abdominal pain or discomfort and altered lower bowel function (Sayuk and Gyawali, 2015). The prevalence is estimated to be 10-15% in Western countries, although as few as 25% of IBS sufferers actually seek professional care (Hungin et al., 2005). The multifactorial pathogenesis of IBS is incompletely understood, but involves psychosocial factors, altered signaling between the gut and

brain, alterations in the normal composition of the gut commensal microbiota, and low-grade intestinal immune activation (Aguilera et al., 2015). Inspired by the work of Verdú and colleagues (2006) describing the development of a murine visceral (colonic) hypersensitivity model by deliberate antibiotic-induced perturbation of the gut microflora, our laboratory sought to replicate this model principally to investigate mucosal neuroimmune interactions in the face of intestinal dysbiosis. While the scope of this companion project goes beyond the work reported here, access to these mice provided a unique opportunity to examine sensory neurons innervating the gut for potential changes in VGF expression.

OBJECTIVES

The first series of experiments presented in Chapter 2 investigated the transduction efficiency of an AAV serotype 5 (AAV5) vector driving overexpression of VGF in lumbar DRG sensory neurons. Through our collaborators, we received an AAV5 vector containing the rodent VGF sequence. We expected that viral-mediated overexpression of VGF in primary afferent neurons would induce behavioral hypersensitivity. Previous work in our lab had demonstrated sensory neuron tropism of AAV5 following intrathecal injection (Vulchanova et al., 2010). However, we sought to avoid promiscuous transduction of distant, off-target sites following biodistribution by the cerebrospinal fluid. We questioned whether direct injection of AAV5 into the peripheral nerve would mediate efficient retrograde gene transfer limited to sensory neurons of the lumbar DRG. Following the initial experimental work in rats, we performed a pilot study using transgenic mice to better visualize the vector distribution and viral-mediated overexpression of rodent VGF following intrathecal administration.

In the latter section of Chapter 2, we report an unexpected sensory neuronopathy associated with AAV serotype 9 (AAV9)-mediated expression of green fluorescent protein. These findings raised some concerns regarding the use of this AAV serotype in the DRG, particularly as random sensory neuron loss may complicate data interpretation in studies investigating sensory neuron signaling.

The series of experiments presented in Chapter 3 investigated the behavioral phenotype and changes in sensory neuron protein expression associated with a murine model of antibiotic-induced dysbiosis. We questioned whether intestinal dysbiosis and subsequent visceral hypersensitivity could be monitored non-invasively through evaluation of referred cutaneous allodynia. In addition, we expected visceral hypersensitivity to be associated with upregulation of nociceptive neuropeptides including VGF.

In Chapter 4, the method developed during the course of this work to clarify the positive cutoff values for immunofluorescence images of sensory neurons is discussed in detail. Finally, a time-saving modification to the common up-down method for assessing mechanosensitivity in rodents was recently published. The original up-down method was utilized extensively in the experiments in Chapter 2. We questioned the reliability of the recently proposed method for mechanosensitivity measurements in rodents and provide critical analysis of the limitations of this proposed testing method.

FIGURES

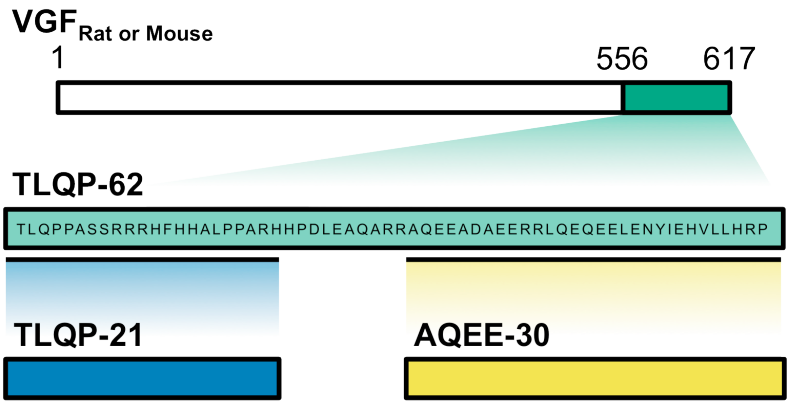

Figure 1-1, Schematic representation of the VGF C-terminal peptides. By convention, VGF-derived peptides are designated by their four N-terminal amino acids and total length. Bioactive peptides include TLQP-62, which contains TLQP-21 and AQEE-30.

Chapter 2

Viral-mediated gene transfer to sensory neurons

2.1 AAV5-mediated protein overexpression in sensory neurons following intrasciatic delivery in rats

2.2 AAV5-mediated protein overexpression in sensory neurons following intrathecal delivery in transgenic mice

2.3 Unexpected sensory neuronopathy following AAV9-mediated gene transfer

Portions of the work described in this chapter were included in the following:

Dykstra JA, Schuster DJ, Riedl MS, Kitto KF, Fairbanks CA, Vulchanova L. Unexpected sensory neuronopathy following adeno-associated virus mediated gene transfer. Poster session presented at: University of Minnesota College of Veterinary Medicine Points of Pride Research Day; Oct 2, 2013; Saint Paul, MN.

Schuster DJ, Dykstra JA, Riedl MS, Kitto KF, Belur LR, McIvor RS, Elde R, Fairbanks CA, Vulchanova L. Biodistribution of adeno-associated virus serotype 9 after intrathecal and intravenous delivery in the mouse. *Front Neurosci.* Special research topic on neuroanatomy, invited peer-reviewed contribution. 2014 Jun; 8:42.

Dykstra JA, Riedl MS, Kitto KF, Lin W, Salton S, Fairbanks CA, Vulchanova L. Gene transfer mediated by sciatic nerve delivery of AAV5-GFP and AAV5-VGF vectors. Poster session presented at: Neuroscience 2014. 44th Annual Meeting of the Society for Neuroscience; Nov 15-19, 2014; Washington, DC.

SUMMARY

Adeno-associated virus (AAV) vectors have emerged as powerful vehicles for genetic manipulation of primary sensory neurons, mediating efficient, stable, and nontoxic transduction. Differential targeting of subtypes of dorsal root ganglia neurons by AAV5 and AAV8 following intrathecal delivery by direct lumbar puncture has been demonstrated. To determine whether increased expression of VGF in dorsal root ganglion (DRG) neurons is sufficient for induction of hypersensitivity, we sought to overexpress VGF using an AAV-mediated approach. From this work, we learned intrasciatic administration of AAV5 vectors yields inefficient and variable transduction of sensory and motor neurons, reminiscent of the AAV8 serotype. Intrathecal administration of AAV5-VGF resulted in successful transduction of the choroid plexus but poor expression in DRG sensory neurons. A distinct behavioral phenotype was not evident in vector-treated rats or mice; however, this lack of desired biological effect is consistent with the absence of detectable transgene overexpression within neurons. It is not clear whether the apparent paucity of neurotropism by AAV5-VGF is a consequence of poor transduction, low transgene expression, or failure of the transgene to yield bioactive peptides. Finally, unexpected DRG sensory neuron degeneration was observed following highly efficient transduction of AAV9, warranting caution in future experiments utilizing this vector serotype.

INTRODUCTION

VGF is endogenously expressed in sensory neurons, and is rapidly and robustly upregulated following peripheral inflammation and nerve injury (Moss et al., 2008; Riedl et al., 2009). Several bioactive VGF-derived peptides from the C-terminus and adjacent region have acute pronociceptive effects when administered intrathecally, including TLQP-62 (Moss et al., 2008), AQEE-30 (Riedl et al., 2009), and TLQP-21 (Fairbanks et al., 2014). However, the precise role played by VGF-derived peptides in the peripheral nervous system remains unclear.

We hypothesized that VGF activity in sensory neurons modulates nociception and hypersensitivity in rodents, as measured by assays of pain-relevant behavior. Studying the response of sensory neurons in the absence of VGF function has been hampered by the unavailability of a serviceable constitutive or conditional knock-out model. Pharmacologic blockade has also been hindered by the lack of a known endogenous protein receptor, with a receptor for just one of the peptides (TLQP-21) described only recently (Hannedouche et al., 2013). To further understand the role played by VGF in nociception, rather than ablate VGF, we opted to overexpress VGF in primary afferent DRG neurons using viral-mediated gene transfer. We expected prolonged endogenous expression of VGF would manifest as pain-related behavior, with a similar facilitatory role as exogenous peptide administered intrathecally.

2.1.1 AAV5-MEDIATED PROTEIN OVEREXPRESSION IN SENSORY NEURONS FOLLOWING INTRASCIATIC DELIVERY IN RATS

Viral access to primary afferent neurons is typically achieved through injection into the cerebrospinal fluid or directly into the peripheral nervous tissue. However, access of the vector to the cerebrospinal fluid allows potential transduction and viral-mediated gene transfer to supraspinal structures. VGF is also endogenously expressed by neurons within the central nervous system, and overexpression in these off-target sites could complicate and confound the interpretation of behavioral analysis. We questioned whether neuronal transduction by AAV5 could be confined to our region of interest by injecting the vector into the peripheral nerve. Several AAV serotypes have been demonstrated as capable of transducing sensory or motor neurons following intrasciatic administration in rodent models, including AAV6 (Towne et al., 2009); AAV2 (Boulis et al., 2003; Xu et al., 2003; Gu et al., 2005; Homs et al., 2011); AAV1 (Hollis et al., 2008; Homs et al., 2011); and AAVrh20 (Pleticha et al., 2014b). To our knowledge, there are no reports on the tropism and efficacy of AAV5 administered intraneurally.

We investigated if direct injection of AAV5 into the sciatic nerve would mediate efficient retrograde gene transfer to sensory neurons of the lumbar DRG while reducing the likelihood of promiscuous transduction of distant, off-target sites. Simultaneously, we tested whether viral-mediated overexpression of VGF in sensory neurons would induce behavioral hypersensitivity.

2.1.2 METHODS

***Animals*.** The experimental procedures were reviewed and approved by the Institutional Animal Care and Use Committee of the University of Minnesota. Male Sprague-Dawley rats (200–250g; Harlan Labs, Madison, Wisconsin USA) were maintained in a specific

pathogen free vivarium with a 12:12 light/dark cycle (lights on at 07:00 h) and ambient temperature of 21±2°C. The animals were housed in groups of 2–3 in transparent plastic cages with corncob bedding, paper nesting material, and *ad libitum* access to water and standard rodent chow. The rats were allowed to habituate for at least 4 days under these conditions before intraneural injection. Two separate experiments with groups of 4–10 rats were performed.

AAV vector. AAV5 containing a chicken β-actin promoter (CBA)-regulated rodent VGF sequence was produced by the University of North Carolina Vector Core (Chapel Hill, North Carolina USA) and was kindly provided by Dr. Stephen Salton (Icahn School of Medicine at Mount Sinai, New York, New York USA). AAV5-CBA-GFP was purchased from the University of North Carolina Vector Core (AAV5.ss.PEM.BOL.CBA.GFP).

Vector administration. Animals were randomly divided into control and experimental groups. Under isoflurane anesthesia, the left sciatic nerve was aseptically exposed at the mid-thigh level. The nerve was elevated slightly to allow a thin strip of parafilm (~10 mm wide) to be gently threaded underneath to provide support. Five microliters of vehicle (sterile saline) or suspended viral vector were injected slowly into the left sciatic nerve using a 26G needle and a Hamilton syringe. For both AAV5-GFP and AAV5-VGF, the construct solution contained 8×10^{12} viral vector genomes per milliliter. The injection site was estimated to be proximal to the branching of the sural, peroneal, and tibial nerves; however, there is anatomical variability in the specific location of this branching, and the possibility of inadvertent injection into one of the branches could not be excluded. Following intraneural injection, the overlying muscles were apposed and the skin was closed with surgical wound clips.

Behavioral analysis. Rats were serially evaluated for vector-induced changes in mechanical and thermal sensitivity. All rats were allowed to acclimate to the testing room environment in their home cages for at least 60 min prior to testing. Behavior analysis occurred between 09:00 and 17:00 h and was performed by an investigator blinded to treatment groups. Pain-relevant behavior was investigated two times prior to the injections. Values from the second test day were used as the baseline.

Mechanical sensitivity was assessed in rats using calibrated von Frey filaments (Stoelting Co., Wood Dale, Illinois USA) and the up-down method as adapted for rodents (Chaplan et al., 1994). The rats were placed in individual plastic cages on a wire mesh platform and allowed at least 15 minutes to acclimate to the experimental setup. A series of eight von Frey filaments (0.4–15 g, corresponding filament numbers 3.61–5.18) with logarithmically incremental stiffness were utilized, and testing was initiated with the middle filament (2.0 g, filament number 4.31). The filament was applied vertically to the mid-plantar surface of the hind paw, avoiding the footpads, to the point of bending for 4 sec. A positive response was noted with brisk withdrawal or paw flinching. Paw withdrawals due to locomotion or weight shifting were not counted and the trials were repeated. Following a positive response, the next weakest stimulus was applied, and the next strongest stimulus was applied following a negative response. An interval of at least 30 seconds was provided between stimuli. The resulting pattern of positive and negative responses was used to calculate the 50% paw withdrawal threshold (PWT).

Thermal hyperalgesia was investigated by the Hargreaves method (IITC Life Science, Inc., Woodland Hills, California USA). The rats were placed in acrylic enclosures on a heated glass base maintained at 33–34°C and allowed to acclimate for approximately 10

minutes. A focused, radiant light heat source was directed to the plantar surface and the time to paw withdrawal was recorded. As before, paw withdrawals due to locomotion or weight shifting were not counted. A cut-off of 25 sec was applied to avoid tissue damage. An interval of at least 5 minutes was provided between stimuli. The means of three tests were calculated and used as the withdrawal threshold to heat.

The acetone drop test was used to assess cold allodynia. Similar to von Frey testing, the rats were placed in individual cages on a wire mesh floor. Using a syringe with a blunt needle tip, a drop (30 µL) of acetone was carefully applied to the plantar surface of the hind paw, avoiding any tactile contact, and the animal was observed for acetone-evoked behaviors including elevation of the paw, flinching, and licking. The total time spent in these evoked behaviors over a 1-minute observation period was recorded. An interval of at least 5 minutes was provided between stimuli, and the mean of two tests was recorded for each hind paw.

Tissue preparation. Animals were terminally anesthetized (intramuscular injection of 75 mg/kg ketamine, 5 mg/kg xylazine, and 1 mg/kg acepromazine) and sacrificed by transcardial perfusion with a pre-wash of calcium-free Tyrode's (in mM: 116 NaCl, 5.4 KCl, 1.6 $MgCl_2 \cdot 6H_2O$, 0.4 $MgSO_4 \cdot 7H_2O$, 1.4 NaH_2PO_4, 5.6 glucose, and 26 Na_2HCO_3), followed by modified Zamboni's fixative (4% paraformaldehyde and 0.2% picric acid in 0.1 M phosphate buffer, pH 6.9), and finally 10% sucrose in phosphate-buffered saline (PBS). Brain, spinal cord, lumbar dorsal root ganglia (DRG), sciatic nerves, and liver were collected and incubated in 10% sucrose overnight at 4°C. Tissues were cryosectioned (14 µm) and thaw-mounted onto gelatin-coated slides. For fresh tissue collection, animals were anesthetized as above and sacrificed by exsanguination and

thoracotomy. Harvested tissues were snap-frozen in liquid nitrogen and stored at -80°C. Sciatic nerves were immersed in fixative for two hours, then transferred to 10% sucrose overnight at 4°C.

Immunohistochemistry. Tissue sections were incubated in blocking buffer (PBS containing 0.3% Triton X-100, 1% bovine serum albumin, and 1% normal donkey serum) at room temperature for 30 min, then incubated overnight at 4°C in primary antisera prepared using blocking buffer as diluent. Primary antisera used were: chicken anti-GFP, 1:1000 (ab13870; Abcam, Cambridge, Massachusetts USA), protein A-purified guinea pig anti-VGF, 1:1000 (anti-AQEE-30, generated in our laboratory; Riedl et al., 2009), rabbit anti-calcitonin gene related peptide (CGRP), 1:1000 (24112; ImmunoStar, Hudson, Wisconsin USA), and mouse anti-myelin basic protein (MBP), 1:1000 (Chemicon MAB387; EMD Millipore, Darmstadt, Germany). After rinsing with PBS, sections were incubated with appropriate combinations of cyanine-dye conjugated secondary antisera (Jackson ImmunoResearch, West Grove, Pennsylvania USA) for one hour at room temperature. Sections were rinsed again in PBS and coverslipped using glycerol and PBS containing 0.1% p-phenylenediamine (Sigma Chemical Co., St. Louis, Missouri USA). DRG sections were also incubated with NeuroTrace® 435/355 Blue (Molecular Probes, Inc., Eugene, Oregon USA) per manufacturer's instructions. Images were collected using an Olympus FluoView1000 confocal imaging system, analyzed using ImageJ (National Institutes of Health), and processed for publication using Adobe Photoshop.

Cell counting. DRG were mounted and sectioned perpendicular to the nerve root axis. Five equally spaced sections from each DRG separated by a minimum distance of 266

μm were selected for image collection. The region of interest for imaging was visualized on the NeuroTrace channel, and the entire neuron population was imaged as best possible with non-overlapping fields, resulting in a minimum of 7 images per animal. Neuron cell body size and intensity of fluorescence were analyzed in ImageJ, using the Nissl-like NeuroTrace labeling to manually outline cell margins. Only cells with a visible nucleus were counted.

Image analysis. Semi-quantitative image analysis was conducted as described in detail in Chapter 4. Briefly, quadruple-labeled fluorescent tissue sections were imaged to produce a separate 8-bit greyscale image for each color channel. The red (cyanine-3), green (cyanine-2), and far-red (cyanine-5) channels were used for markers of experimental interest, while the blue channel was exclusively used for Nissl-like NeuroTrace labeling. All images from a specific antibody marker and within a particular color channel were compiled into a stack in ImageJ. The image stack was then binarized using the Auto Threshold ImageJ plugin (version 1.15, Landini G, fiji.sc/Auto_Threshold) using the stack histogram, which would include images from control and experimental animals. Splitting the stack back into individual images, each binarized version was saved with the original greyscale images.

For cell counting, images of the identical microscope field were compiled into stacks of seven images: greyscale blue, greyscale red, binarized red, greyscale green, binarized green, greyscale far-red, and binarized far-red. Manual cell outlining was conducted in the blue (NeuroTrace) channel, and the mean grey value (MGV) and cross-sectional area were simultaneously measured for the outlined region of interest for all images in the stack. A cell was considered negative for a particular marker if the mean grey value

of the binarized channel was 0 (all pixels black). To determine which cells had sufficient fluorescent intensity to be considered positive, the average greyscale MGV for the negative population of cells was calculated. The threshold to be considered positive was determined as 3 standard deviations above the average for the negative population.

Statistical analysis. Data were entered into a spreadsheet for analysis. Statistical tests were performed using GraphPad Prism (version 5.0d, GraphPad Software, San Diego, California USA, www.graphpad.com). Groups were compared by Student's t-test, one-way analysis of variance (ANOVA) with post-hoc Bonferroni's multiple comparison test, or two-way repeated measures ANOVA with post-hoc Bonferroni's multiple comparison test, where best applicable. Data are expressed and plotted as mean ± SEM. A p value of < 0.05 was considered significant.

2.1.3 RESULTS

Experiment 1. Naïve rats were randomly divided into three treatment groups: intraneural injection of AAV5-VGF (n = 10), AAV5-GFP (n = 6), or saline (n = 4). Following injection, behavior testing was performed weekly for 6 weeks. Both the ipsilateral (left, affected) and contralateral (right, naïve) hind paws were evaluated. Reliable behavior data could not be obtained on the 35-day post-injection time point due to adverse environmental conditions in the testing room beyond the experimenter's control, for which that time point was omitted from analysis.

Mechanical sensitivity thresholds of the ipsilateral hind paws in both vector-treated groups declined from baseline and trended lower than the saline-treated group by the

final measurement, but were not statistically different at any time point (Figure 2-1 A). A similar non-significant decay in the PWT was observed in the contralateral hind paws of the vector-treated animals. To reduce the repeated measures design into a single, representative value for each individual, the area under the PWT curve was calculated using the minimum possible threshold value for this filament series (3.39) as the floor value. There was no significant difference in the average area under the curve between the saline-treated group and either vector group for each hind paw (Figure 2-1 B).

Thermal sensitivity measurements included serial evaluation for heat hyperalgesia and one-time assessment of cold allodynia in lieu of Hargreaves testing on the final behavior testing time point. No significant changes in paw withdrawal from radiant heat were observed for either vector-treated group (Figure 2-1 C). Acetone-evoked behaviors were limited to flinching or licking immediately after drop application; no prolonged behaviors consistent with cold allodynia were observed (data not shown).

Successful AAV5-mediated transfer of GFP or VGF could not be determined until the tissues were evaluated by immunohistochemistry. An animal was considered to be positive if AAV5-driven immunoreactivity (-ir) was detectable within the sciatic nerve near or proximal to the injection site, within the associated DRG, or within the spinal cord or supraspinal structures. However, vector-mediated expression of VGF could not be discriminated immunohistochemically from endogenous protein in the DRG or spinal cord. Given that GFP labeling in the DRG or spinal cord was only evident in animals that also showed GFP-ir within the sciatic nerve, and that endogenous VGF-ir in the sciatic nerve was negligible, we utilized the presence or absence of VGF-ir within the injected sciatic nerve to determine if successful transfer occurred. Based on

immunohistochemistry of the left sciatic nerve, AAV5-mediated transfer was confirmed in 3 of 6 animals for GFP and in 5 of 10 animals for VGF.

Behavior outcome measures were re-analyzed including only those subjects determined to be positive for vector transduction by immunohistochemistry. In addition, one animal from the saline treatment group developed persistently reduced tactile thresholds in the right hind paw 7 days post-injection due to an unexplained injury, and was also excluded. Intra- and inter-subject variability was more pronounced, owing in part to the smaller group sizes. There was no significant difference in behavior outcomes in the vector-treated animals (Figure 2-2).

Immunohistochemical analysis revealed AAV5-driven GFP-ir or VGF-ir predominantly in the sciatic nerve in the region of the injection site (Figure 2-3). GFP-ir was widespread within non-neuronal elements. Double-labeling with anti-MBP revealed bounding of myelin by GFP-positive cytoplasm, suggesting AAV5-GFP transduction of Schwann cells (Figure 2-3 A-D). The vector-mediated expression of anti-VGF was less intense and multifocal, appearing more limited than in the animals with GFP-ir, but still in cells with MBP immunoreactivity (Figure 2-3 E-H).

Semi-quantitative image analysis was performed on labeled sections from the ipsilateral fifth lumbar (L5) DRG (Figure 2-4). The total number of neurons counted per animal was 448 ± 17.5. GFP-ir in sensory neurons was limited to two of the animals with positive expression in the sciatic nerves, and the transduction rate was low (1.2 and 1.5%). Too few DRG neurons were positive for GFP to assess preferential transduction based on neuron size. No difference was found in the sensory neuron expression of VGF

between treatment groups, and viral-mediated expression could not be distinguished from endogenous protein (Figure 2-4 M). Similarly, no difference was found in the immunoreactivity to the nociceptive signaling neuropeptide CGRP between treatment groups (Figure 2-4 N).

Limited GFP-ir was evident in the dorsal root and superficial laminae of the ipsilateral dorsal horn of the L5 region of the spinal cord (Figure 2-5 A). Ventral horn motor neurons were also occasionally transduced (Figure 2-5 A, inset). As in the DRG, viral-mediated expression of VGF could not be distinguished from endogenous protein (Figure 2-5 C-D). There was no evidence of viral-driven gene expression in the choroid plexus or brain. Absence of GFP-ir or VGF-ir in the liver was consistent with a lack of systemic distribution.

Thus, intraneural administration of AAV5 vectors resulted in poor and variable transduction efficiency of sensory neurons. Viral transduction was confined to the peripheral nerve and its associated DRG and spinal cord segment; supraspinal structures were spared. Vector-associated changes in hypersensitivity or sensory neuron neuropeptide expression were not evident. However, the 50% success rate in viral transfer led to reduced group sizes for analysis.

Experiment 2. Naïve rats were randomly divided into two treatment groups: intraneural injection of AAV5-VGF (n = 12) or saline (n = 4). Following injection, behavior testing was performed at 6-day intervals on both the ipsilateral (left, affected) and contralateral (right, naïve) hind paws. Assays included serial assessment of tactile and cold allodynia. Fresh DRG and spinal cord were collected and frozen for potential analysis.

Left sciatic nerves were immersion-fixed for immunohistochemical confirmation of AAV5-VGF transduction. Vector-mediated transfer to cellular elements in the sciatic nerve was confirmed by immunohistochemistry in 8 of 12 animals. Analysis of the filament-based von Frey and acetone drop tests was performed including all animals (Figure 2-6) and including only individuals with evident transduction versus the saline-injected controls (Figure 2-7). There was no evidence of a change of mechanical hypersensitivity over time in the vector-treated group. Similarly, no further acetone-evoked behaviors were observed.

As in Experiment 1, intraneural administration of AAV5-VGF yielded no discernable changes in paw withdrawal thresholds from mechanical or cold stimuli.

2.1.4 DISCUSSION

To investigate our hypothesis that VGF activity in sensory neurons modulates nociception and hypersensitivity, we investigated the utility of intrasciatic injection to mediate retrograde viral-mediated gene transfer and protein overexpression in lumbar DRG sensory neurons. AAV5-induced gene expression was observed within sensory and motor neurons contributing to the injected sciatic nerve; however, the overall transduction efficiency of nerve fibers was poor and variable. Viral-driven gene expression predominated in putative Schwann cells in the vicinity of the injection site. There was no observed dissemination of the viral vector to contralateral DRG or spinal cord, supraspinal structures, or liver. A change in mechanical sensitivity was inconsistently observed in vector-treated animals.

Differential tropism and cellular expression. Sensory neuronal tropism of AAV5 has been previously described following intrathecal (Vulchanova et al., 2010; Xu et al., 2012) and direct ganglionic injection (Mason et al., 2010). However, access of the vector to the cerebrospinal fluid by either of these methods, whether intentional or not, allows potential transduction and viral-mediated gene transfer to supraspinal structures. Protein overexpression in these off-target sites could complicate and confound the interpretation of behavioral analysis, particularly as VGF within the central nervous system has been implicated in mood and antidepressant responses (Hunsberger et al., 2007). We questioned whether neuronal transduction by AAV5 could be confined to our region of interest by changing the route of administration. Several AAV serotypes have been demonstrated as capable of transducing sensory or motor neurons following intrasciatic administration in rodent models, including AAV6 (Towne et al., 2009); AAV2 (Boulis et al., 2003; Xu et al., 2003; Gu et al., 2005; Homs et al., 2011); AAV1 (Hollis et al., 2008; Homs et al., 2011); and AAVrh20 (Pleticha et al., 2014b). To our knowledge, there are no reports on the tropism and efficacy of AAV5 administered intraneurally. This prompted us to investigate AAV5 in this aspect.

In our hands, intrasciatic administration of AAV5 resulted in preferential transduction of Schwann cells in the vicinity of the injection site. The transduction pattern, including the apparent loss of neuronal tropism, closely resembles reports of the intrasciatic administration of AAV8 (Homs et al., 2011) and adenoviral vectors (Glatzel et al., 2000). While being mindful of interstudy variations in vector dose, viral titers, injection procedures, promoters, and transgenes, the results of these studies suggest the transduction efficacy and cellular tropism of AAV vectors following intraneural

administration are likely serotype-dependent. We considered several potential causes for this change in viral transduction efficacy.

Access to the target cells. A potential hindrance to vector transduction is the connective tissue ensheathment of the peripheral nerve. The perineurium consists of concentric layers of squamous perineurial cells alternating with layers of extracellular matrix, consisting of as many as 15 cellular lamellae in peripheral nerve trunks. The tight junctions joining perineurial cells and the thickness of the basement membranes create a diffusion barrier. Meanwhile, at the subarachnoid angle of the dorsal root where the meningeal coverings of the spinal cord merge with the peripheral nerve connective tissue ensheathments, the perineurial cells lack tight junctions (Mizisin and Weerasuriya, 2011). This discontinuity allows communication between the subarachnoid and intercellular spaces and permits easier penetration of substances within the cerebrospinal fluid to the dorsal root and proximal aspect of the DRG, as evidenced following intrathecal administration of fluorescein by Abram et al. (2006). This anatomic access to axons in the dorsal root and cell bodies in the proximal ganglion likely explains the success of viral transduction of sensory neurons following intrathecal injection. Other serotypes of AAV seem to be more capable of traversing the diffusion barrier of the peripheral nerve trunk than AAV5. However, the transduction of Schwann cells is evidence of at least some AAV5 viral particles successfully breaching the perineurium.

Receptor-mediated endocytosis. Another possible cause for the change in transduction efficacy may be a difference in the distribution of the AAV5 receptor between the cell soma and the peripheral axon. Interestingly, platelet-derived growth factor (PDGF) receptor has been identified as a co-receptor for AAV5 (Di Pasquale et al., 2003).

PDGF receptor expression in the rat sciatic nerve and dorsal root ganglia is down-regulated in maturity, but these receptors continue to be expressed at high levels in Schwann cells in adult animals (Eccleston et al., 1993). Neuronal tropism may not be lost but may be subject to greater competition from other cellular constituents of the nerve. It seems possible that differences in the expression of these or other unidentified receptors at the injection site may be influencing the effective transduction of this AAV serotype.

Access to the nucleus. Following receptor-mediated endocytosis, the viral vector must be transported retrograde from the point of entry at the axon to the nucleus of the neuron before the viral genome can be expressed. The mechanisms involved in intracellular processing of AAV are incompletely understood (Wu et al., 2006), and it is unknown if AAV5 exploits a different pathway than other AAV serotypes. Impaired trafficking of AAV to the nucleus has been documented as an obstacle for AAV2 transduction in certain cell types (Hansen et al., 2000). Inefficient retrograde trafficking of AAV5 to the cell soma would manifest as a failure of viral-mediated gene expression, even if the vector were able to bind and gain entry to the axon successfully. Retrograde transport of AAV5 has been documented in the brain over distances as large as 6 mm, but was selective for certain subpopulations of neurons (Aschauer et al., 2013; Rothermel et al., 2013).

Viral-mediated gene expression. The promoter driving expression of the experimental or reporter gene must be active in the targeted cell, and the cell must have the necessary machinery for post-translational modification of the mature protein. Poor expression may result in underestimating the number of neurons or other cells targeted by AAV5.

The cytomegalovirus (CMV) early enhancer/promoter and the hybrid CMV enhancer/chicken β-actin (CBA) promoter are commonly used in AAV vectors and typically yield high, ubiquitous expression levels in various cell types (Gray et al., 2011a). However, the mechanisms by which VGF is cleaved and the resulting peptides are modified to become biologically active are not understood. If the viral-driven exogenous protein is improperly processed intracellularly, it could result in a failure of immunohistochemical detection.

Vector dosage. Transduction efficacy may be partially compensated by changing the viral dosage. We questioned how the dose used in our study would compare to those reported for the intrasciatic administration of other AAV serotypes. Unfortunately, viral vector dose may be reported in two different ways. The physical titer is strictly a measurement of the amount of virus present (viral particles or genome copies), while the functional titer is the measurement of infectious virus (transducing units). Given the inability to extrapolate physical titers from functional titers and the lack of a functional titer for our vector, only those that reported physical titers were considered. From the reports referenced above, intrasciatic delivery doses in rats ranged from 7.00×10^7 to 1.20×10^{10} viral particles, and in mice was 1.80×10^9 viral particles, all of which were lower or fairly equivalent to our dose of 4.00×10^{10} viral particles. However, this comparison may not be meaningful, as each titer is from a different AAV serotype. The dose in this study may be below the minimum effective dose for neuronal transduction. The practicality of obtaining a functional titer for future work is also debatable, as *in vitro* infectivity assays do not necessarily predict *in vivo* performance.

Behavior assessment. To assess the functional consequences of intrasciatic injection and viral-mediated gene transfer, rats injected with vector or vehicle were serially tested for tactile allodynia, thermal hyperalgesia, and/or cold allodynia in the plantar region of the hind paw. A change in mechanical sensitivity was inconsistently observed in AAV5-treated animals in the first experiment. This finding was not repeated in the second experimental cohort. While the group sizes in each experiment were decremented due to failure of viral-mediated gene transfer or other aberrations, the number of animals with confirmed vector transduction by immunohistochemistry slightly improved in the second experiment (n = 5 in the first, n = 8 in the second) and the number of saline-treated control animals were similar (n = 3 in the first, n = 4 in the second). The cause of the mechanosensitivity threshold shift is not clear.

An attractive explanation for the change in tactile sensitivity is a physiological response to the viral-driven gene product. Intrathecal administration of exogenous VGF-derived peptides has been shown to induce mechanical and cold allodynia (Moss et al., 2008), as well as thermal hyperalgesia as determined by warm water immersion tail-withdrawal testing (Riedl et al., 2009; Fairbanks et al., 2014). Viral-mediated overexpression of VGF within the somatosensory pathway may be sufficient to induce hypersensitivity, with the specific manifestation subject to the random pattern of transduction. However, there are several concerns with this interpretation. Sensory neuronal transduction could not be quantified for AAV5-VGF, but based on the transduction efficiency of GFP, it is likely that viral-mediated expression of VGF in sensory neurons is similarly low. It seems unreasonable to suspect VGF overexpression in such a limited population of sensory neurons would be sufficient to manifest a change in tactile behavior. On the other hand, transduction of Schwann cells in the vicinity of the injection site was evident. Provided

these cells are capable of appropriate VGF processing, local release of VGF-peptides may mediate neuronal communication and signaling.

Yet this putative regional, unilateral signaling process fails to explain the observed contralateral effect. Mechanosensitivity thresholds tended to decrease in the naïve right hind paw in vector-treated animals comparable to the affected left hind paw. No contralateral dissemination of the viral vector was evident by immunohistochemistry of the DRG or spinal cord. To directly achieve this bilateral response, secreted viral-gene encoded product would have to gain access to either the cerebrospinal fluid or systemic circulation. The cell body-rich regions of the DRG have increased vascular permeability (Hirakawa et al., 2004; Abram et al., 2006), so it may be possible for circulating VGF peptides to globally access other DRG. However, to gain access to the bloodstream, viral-driven gene products released into the endoneurial space would still have to overcome the blood-nerve barrier. The relatively impermeable perineurium and endoneurial capillaries tightly regulate entry into and exit from the endoneurial microenvironment (Weerasuriya and Mizisin, 2011). It is not known if transport of VGF-derived peptides across the blood-nerve barrier is a reasonable expectation.

Another possible explanation for the observed variations in mechanosensitivity thresholds is damage to the nerve. Exposure of the sciatic nerve trunk and application of the injection could potentially result in nerve injury-induced hypersensitivity. If iatrogenic trauma was the sole cause of mechanosensitivity deviations, the effect should have been unilateral, equally possible in both vector-treated and vehicle-treated groups, and likely transient as hypersensitivity would resolve as regeneration occurred. To more thoroughly assess the likelihood of nerve damage, semi-thin, transverse sections of the

nerve distal to the injection site could be analyzed for demyelination and Wallerian degeneration. Damage to the neurons could also be caused by toxic effects secondary to the expression of transduced proteins. Viral-mediated gene overexpression may have induced the death of sensory neurons or, as might be more likely in this case, Schwann cells. Immunofluorescence is not ideal for scoring sciatic nerves for the presence of demyelination, digestion chambers, and axonal loss. Semi-thin analysis may be warranted in future work to rule out neurotoxicity. For a more thorough discussion of transduced proteins being associated with toxic effects, please see the section on sensory neuronopathy later in this chapter.

None of these options satisfactorily explain why shifting of the mechanosensitivity thresholds was evident in the first experimental cohort – in vector-treated animals with and without positive immunoreactivity for the viral gene product – and was not evident in the similarly treated second experimental cohort. Aside from randomness associated with viral vector transduction, we questioned if these experimental groups were different in another meaningful way. This led us to recognize the change in behavior measures between cohorts. Rats in the first experimental groups were serially tested for tactile allodynia and thermal hyperalgesia, while in the second cohort the thermal nociception test was replaced with the acetone drop test for cold allodynia. Sensory thresholds were less stable in the rats evaluated for thermal nociception following von Frey testing. None of the animals exhibited any signs of tissue injury or burns in the plantar region of either hind paw to help explain the change in tactile response.

All behavior evaluations were performed in an isolated designated testing room separate from the vivarium. In part due to scheduling limitations for this shared research space,

the two respective tests were performed on the same day. Despite the assays being in the same location and for similar lengths of time, the testing experience was not equal between the cohorts of rats. In the first experiment, animals were transferred from the von Frey testing table directly to the Hargreaves apparatus without being returned temporarily to their respective home cages. In the second experiment, assays were also conducted back-to-back, but both tests were conducted on the von Frey testing table and the stimuli were non-noxious. Learning can be extremely rapid, and it is possible that the consistent sequence of testing or that non-nociceptive cues within the room, such as unfavorable visual, olfactory, or ultrasonic auditory signals between rats, conditioned individual animals into a state of anticipatory hypervigilance (Detloff et al., 2010). Meanwhile, the tests for allodynia in the second cohort did not seem to generate the same level of apprehension.

Given the similar levels of threshold decay between the affected and unaffected limb in individual animals irrespective of treatment group or outcome, it seems likely that this effect is mediated more globally than by viral-induced protein expression in the vicinity of the left sciatic nerve. The possibility exists that the behavior outcome measures are biased by learning and/or the psychological state of the animals. As cautioned by Le Bars and colleagues in their review on animal models of nociception (2001) regarding mechanical sensitivity, “anticipatory or training phenomena are likely to blur the response, which consequently cannot be interpreted other than in terms of pain.” The sensory threshold decay suggests the development of physiologic hypersensitivity, but may be artificially low due to psychological stress.

2.2.1 AAV5-MEDIATED PROTEIN OVEREXPRESSION IN SENSORY NEURONS FOLLOWING INTRATHECAL DELIVERY IN TRANSGENIC MICE

Intrasciatic administration of AAV5 vectors yielded predominately local transduction with inefficient and variable transduction of sensory and motor neurons. We concluded that peripheral nerve injection was not a viable strategy to limit VGF overexpression to lumbar DRG sensory neurons using an AAV5 vector.

To further investigate the role played by VGF in sensory neurons, we performed a pilot study in mice administering the same vectors by direct lumbar puncture. Based on previous work with this vector serotype and delivery method (Vulchanova et al., 2010), we expected viral transduction to be evident in the lumbar dorsal root ganglia and spinal cord as well as in off-target supraspinal regions. As the overexpression of VGF should manifest through behavioral effects dependent on the region affected, we included behavior assessments of pain-related and depressive-like behaviors, given the antidepressant activity of VGF in the central nervous system (Hunsberger et al., 2007).

A setback of the study in rats was the inability to discriminate endogenous and viral-mediated VGF expression. To better visualize the vector distribution and viral-mediated overexpression of rodent VGF, we used a humanized VGF-knock-in mouse line and antisera lacking cross-reactivity between species.

2.2.2 METHODS

***Animals*.** The experimental procedures were reviewed and approved by the Institutional Animal Care and Use Committee of the University of Minnesota. We utilized the B6;129Sv-*Vgf* $^{tm(VGF)}$/J mouse line and B6;129Sv/J mice on the same genetic background lacking the targeted mutation (hereafter referred to as hVGF and mVGF, respectively). In the hVGF mouse line, the coding sequence of mouse VGF_{1-617} is replaced by human VGF_{1-615}, so that the human protein is expressed from this allele and the wild-type mouse protein is undetectable. The mVGF mouse line expresses endogenous mouse VGF. The generation of this humanized VGF-knock-in mouse line was recently described by the lab of origin (Fargali et al., 2014). N2F1 breeders of each line, donated by Dr. Stephen Salton (Icahn School of Medicine at Mount Sinai, New York, New York USA), were intercrossed to yield homozygous N2F2 progeny and experiments were performed on these mixed-background offspring. Experimental mice were maintained in a conventional vivarium with a 12:12 light/dark cycle (lights on at 07:00 h) and ambient temperature of 21±2°C. The animals were socially housed in groups of 4 in transparent plastic cages with corncob bedding, compact cotton nesting material, and *ad libitum* access to water and standard rodent chow.

AAV vector. AAV5 containing a chicken β-actin promoter (CBA)-regulated rodent VGF sequence was produced by the University of North Carolina Vector Core (Chapel Hill, North Carolina USA) and was kindly provided by Dr. Stephen Salton (Icahn School of Medicine at Mount Sinai, New York, New York USA). AAV5-CBA-GFP was purchased from the University of North Carolina Vector Core (AAV5.ss.PEM.BOL.CBA.GFP).

Vector administration. Adult male hVGF mice (20–25g) were randomly divided into control and experimental groups. Twenty minutes prior to vector injection, 200 µL of

25% mannitol solution was delivered via the tail vein to promote enhanced AAV vector transduction of primary sensory neurons (Vulchanova et al., 2010). AAV vector constructs were delivered intrathecally by direct lumbar puncture in unanesthetized mice as described by Hylden and Wilcox (1980) with a minor modification. To conserve viral vector, a length of PE10 tubing was connected between a 50 µL Luer-hub Hamilton syringe and a 30-gauge, 0.5 inch needle. To administer the injection, the animal was gripped gently at the iliac crest and the needle was inserted, bevel side up, at an approximate 45° angle centered between the hipbones. Puncture of the dura was indicated by a reflexive flick of the tail, and an injection volume of 10 µL of saline or vector construct solution was delivered intrathecally. For both AAV5-GFP and AAV5-VGF, the construct solution contained 8×10^{12} viral vector genomes per milliliter. Following the injection, the animals were returned to their home cages.

Behavioral analysis. Mechanical sensitivity and depression-like behavior were evaluated in hVGF mice treated with saline, AAV5-GFP, or AAV5-VGF, and in age-matched male mVGF mice with no experimental manipulations (naïve). Mechanical responses were serially assessed using an electronic von Frey aesthesiometer (IITC Inc. Life Sciences, Woodland Hills, California USA) by an investigator blinded to treatment groups. Mice were placed in individual glass enclosures on a wire mesh platform and allowed to acclimate for 15 to 30 minutes. The probe was applied to the plantar surface of the hind paw until a brisk withdrawal response terminated application of pressure, which was recorded by the instrument. The mean of three tests was calculated for each hind paw.

Tail suspension was used to assess depression-like behavior in response to a short-term, inescapable stress. Mice were allowed to acclimate to the experimental room for at least 40 minutes prior to the assay. Immediately before the test, a short length of white artist tape was applied perpendicular to the tail approximately 1 cm from the tail base. The free ends of the tape were flattened together and a hole was punched through the double-layered tape. The tail suspension apparatus consisted of a plastic box enclosure with a central ceiling suspension hook and three opaque white walls to contrast with the coat color of the mice. Each mouse was suspended on the hook through the hole in the adhesive tape, facing downward and at least 15 cm away from the surface of the walls or floor. Behavior was video-recorded for 180 seconds. Afterwards, the tape securement was carefully removed from the suspension hook, the adhesive tape was gently separated to liberate the tail, and the mouse was returned to the home cage. During the test, experimenters refrained from making noise, movement, or visual contact to minimize any effects of their presence on animal behavior. Subjects were monitored throughout the test via a rotatable recording screen to ensure the suspension was secure. After each testing session, the equipment was cleaned with ethanol solution to eliminate olfactory cues. The video recordings were indexed, edited to remove subject identification cards recorded before each test, and randomized. An investigator blinded to the treatment groups manually recorded the amount of time individual mice spent immobile. Immobility scores were calculated for the entire duration of the test.

Tissue preparation. Animals were terminally anesthetized with isoflurane and sacrificed by transcardial perfusion with a pre-wash of calcium-free Tyrode's (in mM: 116 NaCl, 5.4 KCl, 1.6 $MgCl_2$•$6H_2O$, 0.4 $MgSO_4$•$7H_2O$, 1.4 NaH_2PO_4, 5.6 glucose, and 26

Na_2HCO_3), followed by modified Zamboni's fixative (4% paraformaldehyde and 0.2% picric acid in 0.1 M phosphate buffer, pH 6.9), and finally 10% sucrose in phosphate-buffered saline (PBS). Brain, spinal cord, lumbar dorsal root ganglia (DRG), and liver were collected and incubated in 10% sucrose overnight at 4°C. Tissues were cryosectioned (14 μm) and thaw-mounted onto gelatin-coated slides.

Immunohistochemistry. Tissue sections were incubated in blocking buffer (PBS containing 0.3% Triton X-100, 1% bovine serum albumin, and 1% normal donkey serum) at room temperature for 30 min, then incubated overnight at 4°C in primary antisera prepared using blocking buffer as diluent. Primary antisera used were chicken anti-GFP, 1:1000 (ab13870; Abcam, Cambridge, Massachusetts USA) and rabbit anti-TLQP-21, 1:1000 (generated in our laboratory; Possenti et al., 2012; Fairbanks et al., 2014). After rinsing with PBS, sections were incubated with appropriate combinations of cyanine-dye conjugated secondary antisera (Jackson ImmunoResearch, West Grove, Pennsylvania USA) for one hour at room temperature. Sections were rinsed again in PBS and coverslipped using glycerol and PBS containing 0.1% p-phenylenediamine (Sigma Chemical Co., St. Louis, Missouri USA).

Statistical analysis. Data were entered into a spreadsheet for analysis. Statistical tests were performed using GraphPad Prism (version 5.0d, GraphPad Software, San Diego, California USA, www.graphpad.com). Groups were compared by Student's t-test, one-way analysis of variance (ANOVA) with post-hoc Bonferroni's multiple comparison test, or two-way repeated measures ANOVA with post-hoc Bonferroni's multiple comparison test, where best applicable. Data are expressed and plotted as mean ± SEM. A p value of < 0.05 was considered significant.

2.2.3 RESULTS

Naïve hVGF mice were randomly divided into three treatment groups: intrathecal injection of AAV5-VGF (n = 7), AAV5-GFP (n = 6), or saline (n = 9). An additional group of naïve mVGF mice (n = 8) received no injections. One animal in the AAV5-GFP group was diagnosed with a spontaneous unrelated disease condition (metastatic thymic lymphosarcoma) late in the course of the study. The euthanasia of this animal preceded the remainder of the cohort by less than one week. The tissues were still utilized for immunohistochemical screening. However, due to the unknown influence of the spontaneous disease condition, behavior data from this animal were excluded.

As in the previous section of this chapter, we questioned whether viral-mediated overexpression of VGF in sensory neurons would manifest as behavioral hypersensitivity. Unexpectedly, mechanical sensitivity thresholds in all treatment groups descended sharply from the initial baseline values over the early testing period (Figure 2-8). After three to four weeks, the paw withdrawal threshold values appeared to plateau at approximately 60% of the baseline force. This response pattern was similarly reproduced in both hind paws and across treatment groups, including both the naïve and vehicle-treated controls. Given the instability of the threshold values, p values resulting from statistical analyses were difficult to interpret and considered potentially misleading. For example, post hoc comparisons of two-way repeated measures ANOVA showed a significant difference between mechanical threshold values of the left hind paw in the hVGF AAV5-VGF group at days 28 and 35 relative to saline-treated hVGF animals ($p < 0.05$ and 0.01, respectively). However, no statistically significant difference was

observed when comparing the threshold values of the right hind paw, and hVGF AAV5-VGF did not significantly differ from the hVGF AAV5-GFP or naïve mVGF groups at any time point. It appears the finding of significance relies more on the unexplained rise in the mechanical thresholds of the hVGF saline group during this time frame. Indisputable confirmation of treatment-induced mechanical hypersensitivity could not be meaningfully interpreted.

In the tail suspension test, mice innately engage in vigorous escape behaviors but eventually succumb to immobility, with longer durations of immobility suggesting a heightened degree of behavioral despair. Decreased immobility times in tail suspension and forced swim assays have been induced through intraventricular or hippocampal delivery of VGF-derived peptides (Hunsberger et al., 2007; Thakker-Varia et al., 2007). As viral transduction of neurons in the hippocampal formation has been observed following viral vector delivery through direct lumbar puncture (Schuster et al., 2014a), we reasoned that viral-mediated overexpression of VGF in this off-target region could manifest as antidepressant behavior. A large proportion of the mice demonstrated a propensity to reach for their tails during the testing session irrespective of treatment group (20 of 29 mice, or 69%). Of these, 7 animals (24%) were able to successfully climb onto their tail and grasp the suspension hook for a substantial portion of the testing session (range = 51 to 167 seconds, mean = 113 ± 17 seconds). Given these 7 individuals “escaped” the stressor, their data were not considered valid and were omitted from further analysis. The omitted subjects included naïve mVGF (n = 2), hVGF with AAV5-VGF (n = 2), hVGF with AAV5-GFP (n = 2), and hVGF with saline (n = 1). In the remaining animals, no significant differences in mean immobility times were identified

between any of the treatment groups by one-way ANOVA with post hoc multiple comparisons (Figure 2-9).

Immunohistochemical analysis was performed to detect the presence of viral-mediated gene expression in vector-treated animals. While highly conserved, variations exist between mouse VGF_{1-617} and human VGF_{1-615} sequences. The rabbit anti-TLQP-21 antibody recognizes an epitope of the VGF-derived peptide that is unique to the rodent sequence, while the guinea pig anti-AQEE-30 antibody used in the prior rat experiments recognizes rodent or human peptide. Thus in the humanized VGF-knock-in mice, the expression of endogenous human VGF could be discriminated from the viral-driven rodent VGF by using the anti-TLQP-21 antisera.

The results of immunohistochemistry are summarized in Table 2-1. Expression of viral-mediated GFP was evident in all animals, but anatomic locations were variable. In one subject, GFP-immunoreactivity (-ir) was entirely within somatosensory pathways including L4 DRG sensory neurons, dorsal roots, the dorsal horns and columns of the spinal cord, and dorsal column nuclei in the brainstem, while in another GFP-ir was instead evident in the ventral horns, ventral and lateral columns of the spinal cord, cerebellar peduncles, and cerebellum. Occasional sensory neuron transduction was evident in 3 of the 6 animals. The most reliable tissue for viral transduction was the choroid plexus of the fourth ventricle. Interestingly, the choroid plexus was the only tissue in which viral-mediated expression of VGF was observed.

2.2.4 DISCUSSION

In this pilot study, we investigated the use of a humanized VGF-knock-in mouse line to better visualize the vector distribution and viral-mediated overexpression of rodent VGF following intrathecal administration. Based on previous work with this vector serotype and delivery method, we expected viral transduction to be evident in the lumbar dorsal root ganglia and spinal cord as well as in off-target supraspinal regions, and the overexpression of VGF would manifest through behavioral effects dependent on the region affected. Successful transduction of AAV5-VGF was only evident immunohistochemically in the choroid plexus despite the widely distributed and variable transduction observed with AAV5-GFP. A distinct behavioral phenotype was not evident in vector-treated mice; however, this lack of desired biological effect is consistent with the absence of transgene overexpression within neurons.

It is not clear whether the apparent paucity of neurotropism by AAV5-VGF is a consequence of poor transduction, low transgene expression, or failure of the transgene to yield bioactive peptides. While advantageous for its species-specificity, the anti-TLQP-21 antibody used to immunohistochemically detect viral-mediated gene expression recognizes the cognate VGF-derived peptide TLQP-21, but not the unprocessed parent peptide (Fairbanks et al., 2014). Viral-driven VGF protein production in neurons may be subject to incomplete or incorrect post-translational processing. Interestingly, viral-driven TLQP-21 was observed within the choroid plexus, so appropriate post-translational processing of the VGF transgene product is possible. To elucidate whether transduction failure is the limiting step for neuronal VGF overexpression, future work using the AAV5-VGF vector should incorporate quantitative real-time PCR of DNA extracted from DRG or other relevant tissue to determine the number of vector genomes per cell. Instead of utilizing a primer targeted against the

transgene, which presents technical challenges given the sequence similarities between human and rodent VGF, primers could be targeted against the viral vector promoter or inverted terminal repeat regions. Decreased transduction efficiency may be potentially overcome with a higher vector dose, but aberrant intracellular processing of the transgene product may require redesigning the vector construct.

This study also utilized mouse lines on a mixed genetic background. Congenic mouse strains are produced by repeatedly backcrossing a locus of interest, such as a targeted mutation, onto a parental inbred strain with the goal of creating a uniform genome that is identical to the inbred strain at all loci except that specific genetic region. A strain is considered to be incipient congenic after five generations of backcrossing (with a statistical percentage of background genome of 96.9%) and fully congenic after ten generations of backcrossing (99.91% background genome). The mice utilized in this study were the offspring of N2 breeders, meaning the parents had been backcrossed for two generations. Further backcrossing was not performed, so the mixed genetic background of these mice was statistically 75% recipient strain (C57BL/6) and 25% donor strain (129Sv/J).

An unintended consequence of this hybrid genetic background may be variability in behavioral outcomes. The C57BL/6 and 129 mouse strains display phenotypic differences in several assays of pain-relevant behavior. Notably, the two strains show significant differences in mechanical sensitivity, with the baseline hind paw withdrawal threshold of 129 mice being substantially lower than that of C57BL/6 mice in the von Frey filament test (Mogil et al., 1999; Lariviere et al., 2001). In the tail suspension test, a strong tendency toward tail-climbing behavior has been reported for C57BL/6 mice but

not in similarly tested 129 mice (Mayorga and Lucki, 2001; Bergner et al., 2010). With the undefined genetic background, individual mice may display a propensity towards "129-like" or "C57BL/6-like" behavior independent of the knock-in versus wild-type differences in our gene of interest. It is possible this genetic confound may have resulted in sufficient behavior variability to mask more subtle experimental-induced test outcomes.

The behavior assays also illustrate some of the challenges involved in evaluation of animal behavior and interpretation of the test read-out values. In the assessment of mechanical sensitivity, significant threshold decay from baseline was similarly evident in all treatment groups over the first few weeks of the experiment. Although these values seemed to stabilize over the later weeks, the uncertainty in the cause of this change in tactile sensitivity precluded meaningful interpretation. One possibility to explain the potentially spurious decline in threshold values is an instrument fault. Unlike the work reported earlier in this chapter assessing mechanosensitivity in rats using classical von Frey filaments, these mice were evaluated using an electronic von Frey aesthesiometer. The fluctuations in the read-out values may be due to a loss of calibration of the electronic instrument (Martinov et al., 2013). Another possibility, as discussed in the section regarding the rats, is anticipatory hypervigilance. The mechanical sensitivity testing was performed in a larger testing room with the possibility of other murine experimental work being performed concurrently. Other stressors, such as unfavorable visual, olfactory, or ultrasonic auditory cues, may have adversely conditioned the mice and negatively influenced their testing experience independent of the experimental treatments (Detloff et al., 2010).

Evaluation of the tail suspension assay was complicated by the propensity for tail-climbing behavior, which ultimately invalidated the trial for multiple mice that reached and grasped the suspension hook. The initial attempt to reach for the tail occurred within the first 60 seconds of the trial in 17 of the 20 mice, suggesting the problem would not be avoided by decreasing the length of the trial. To prevent tail-climbing behavior, Can and colleagues (2012) reported the successful use of cylinders of polycarbonate tubing placed as a baffle around the tail prior to suspension. This may represent an easily obtained, practical solution for future testing of C57BL/6 background mice.

Several mice representing various treatment groups also spent very little time immobile (< 10% of the total trial time). Typically, vigorous escape-oriented behaviors are interspersed with periods of immobility that increase in length as the trial progresses. The low immobility times suggest the testing session may have been too short, as not all individuals succumbed to the inescapable stress. In future work, extending the length of the testing session from 3 minutes to 6 minutes may better differentiate mice with and without depression-like behavior.

2.3.1 UNEXPECTED SENSORY NEURONOPATHY FOLLOWING AAV9-MEDIATED GENE TRANSFER

AAV vectors have emerged as powerful vehicles for genetic manipulation of neurons, mediating efficient, stable, and nonpathogenic transduction (Daya and Berns, 2008; Schultz and Chamberlain, 2008). Differential targeting of subtypes of primary sensory neurons by AAV5 and AAV8 following intrathecal delivery by direct lumbar puncture has been demonstrated (Vulchanova et al., 2010; Schuster et al., 2013). However,

transduction of these DRG neurons required pretreatment with intravenous mannitol, a hyper-osmotic blood-brain barrier interruptive reagent that has also been used to enhance AAV distribution in the brain and spinal cord (Kroll and Neuwelt, 1998; Mastakov et al., 2001; Fu et al., 2003).

Interestingly, recent reports have suggested that another serotype, AAV9, is able to cross the blood-brain barrier in neonatal and adult animals without the concurrent use of any permeabilizing reagents (Gray et al., 2011b; Dayton et al., 2012). While successful transduction of primary sensory neurons by AAV9 vectors has been demonstrated in rodent and non-human primate models (Hirai et al., 2012, 2014; Gray et al., 2013), the expression pattern of AAV9-mediated gene transfer to sensory neurons had not been characterized. The goal of the present study was to evaluate the ability of AAV9-GFP to transduce primary sensory neurons and off-target supraspinal regions following intrathecal or intravenous delivery. However, during the course of immunofluorescence image analysis of DRG sections, aberrant labeling of neuronal Nissl substance was identified in several animals (Figure 2-10), prompting further evaluation. The purpose of this report is to describe the unexpected sensory neuronopathy associated with AAV9-mediated expression of GFP.

2.3.2 METHODS

For this retrospective investigation we utilized tissue cryosections remaining from several experiments, summarized in Table 2-2. The experimental procedures within these studies were reviewed and approved by the Institutional Animal Care and Use Committee of the University of Minnesota. All experiments utilized adult male mice (20–

25g; Harlan Labs, Madison, Wisconsin USA). AAV9-GFP was purchased from the University of Pennsylvania Vector Core (AAV9.CB7.CI.eGFP.WPRE.rBG; Philadelphia, Pennsylvania USA). AAV9-human arginine decarboxylase (hADC)-GFP and AAV5-CAG-GFP were acquired from the University of Florida Vector Core Lab of the Gene Therapy Center (Gainesville, Florida USA). Animals were sacrificed by perfusion fixation as described within earlier sections of this chapter. Harvested tissues were cryosectioned (14 μm) and thaw-mounted onto gelatin-coated slides.

In the inciting experiment, C57BL/6 mice received AAV9-GFP through intrathecal (IT) or intravenous (IV) routes of delivery and in the presence or absence of mannitol pretreatment (Schuster et al., 2014b). The viral dose was 3.3×10^{11} vector genomes per injectate. These mice were maintained until a 3-week endpoint. As shown in the fluorescence micrographs in Figure 2-10, DRG immunohistochemistry included chicken anti-GFP primary antisera, 1:1000 (ab13870; Abcam, Cambridge, Massachusetts USA) with Cy2-conjugated secondary antisera, 1:300 (Jackson ImmunoResearch, West Grove, Pennsylvania USA), and Nissl staining with NeuroTrace® 435/355 Blue (Molecular Probes, Inc., Eugene, Oregon USA).

Following the initial analysis, additional DRG cryosections were evaluated from other experimental cohorts. Cohort B was composed of C57BL/6 mice that received AAV9-GFP (1.7×10^{11} vector genomes per injectate) by intrathecal delivery with mannitol pretreatment and with a 6-week endpoint (Schuster et al., 2014b). The vector was from the same vendor but an earlier supplier lot. Cohort C represented a subsequent experiment that utilized the same batch of AAV9-GFP as the initial cases but at a 1:50 dilution. In this study, ICR/CD-1 mice received AAV9-GFP, AAV9-human arginine

decarboxylase (hADC)-GFP, or saline with no pretreatment (Peterson et al., 2014). Incidentally, the reporter gene in the AAV9-hADC-GFP construct failed to express. Finally, Cohort D was composed of banked DRG sections from C57BL/6 mice that received intrathecal AAV5-GFP with mannitol pretreatment (as in Vulchanova et al., 2010; Schuster et al., 2014a).

Histopathology. In Cohort A, slides of L4 dorsal root and trigeminal ganglia were selected from the remaining tissues to include 3 to 6 sections from each animal as equally spaced as possible within the available set to reduce unintentional bias. The minimum distance between ganglia sections was 42 μm. Limited sections of other tissues from each animal, including spinal cord, liver, skeletal muscle, ileum, and colon, were included for general screening. For all other cohorts, only DRG sections were evaluated. The glass slides were submitted to the University of Minnesota Comparative Pathology Shared Resource for routine hematoxylin and eosin staining. The tissue thickness precluded sharp focus and along with the gel coating caused variation in the staining quality.

The ganglia sections were scored by a trained, blinded investigator for the presence and severity of mononuclear infiltration and neuron loss based on the lesion parameters summarized in Table 2-3. The overall variance in lesion severity was evaluated to fit the range of observed lesions into a qualitative, ordinal scoring system (Gibson-Corley et al., 2013). An ordinal score of 1 indicated the presence of increased numbers of mononuclear cells with no clear organization and no evidence of neuronal loss. Sections with evidence of neuronal loss and replacement by compact, discrete nodules of mononuclear satellite cells (nodules of Nageotte) were assigned a score of 2 if solitary

and 3 if multiple. An ordinal score of 4 was reserved for sections with multifocal neuronal loss along with exuberant mononuclear infiltration, including within the subcapsular space. All stained sections were scored for each animal. Given the limited number and varying quality of fields available for review, the maximum score evident in any of the sections was assigned for the whole tissue of that animal.

2.3.3 RESULTS

Group designations for the sensory ganglia assessed in the initial investigation included naïve (n = 1), IV vector pretreated with saline (n = 4) or mannitol (n = 4), and IT vector pretreated with saline (n = 4) or mannitol (n = 2). This final group was reduced in size due to the loss of two animals prior to the 3-week endpoint; one animal was found deceased and a second was euthanized due to progressive seizure activity. Regrettably, issues from these two animals were not available for analysis.

Lesions in sensory ganglia ranged in severity and included infrequent, discrete nodules of residual satellite glial cells replacing solitary neurons (nodules of Nageotte) to more exuberant mononuclear infiltration with multifocal neuronal degradation and loss (Figure 2-11 A-C). In the L4 DRG, lesions were restricted to animals that received AAV9-GFP by intrathecal administration (Figure 2-11 D) and seemed to be more consistently severe in the mannitol pre-treatment group. However, this interpretation may be biased by the limited sample size. The trigeminal ganglia were less severely affected with neuronal loss evident in only one animal (Figure 2-11 E), although low-grade lesions were also observed in one subject with intravenous AAV9-GFP and mannitol. No lesions were evident on cursory examination of spinal cord, liver, skeletal muscle, or enteric tissues,

although the variation in staining quality and thickness of the tissue sections may have masked subtle abnormalities.

Histopathological examination of L4 DRG was expanded to include several other experimental cohorts for comparison (Figure 2-12). In Cohort B, all subjects (n = 4) received a similar IT dose of AAV9-GFP following mannitol pretreatment but from a different supplier lot. The animals were also maintained for 6 weeks post-injection instead of 3 weeks. Unlike the inciting experiment, no mortality was reported. Neuronal loss was still apparent but less extensive. In Cohort C, mice of a different strain were administered the same vector IT as in the initial experiment at a reduced dose and without mannitol pretreatment. Neuronal degradation and loss was evident in all animals that received the AAV9-GFP vector (n = 3). No lesions were observed in animals treated with IT AAV9-hADC-GFP (n = 3) or saline (n = 2). In Cohort D, all the mice were treated with a different serotype of reporter vector, AAV5-GFP, which was administered IT and with mannitol pretreatment. No lesions were observed (n = 5).

Ideally, the tissue scoring system should have been compared to a relevant parameter of disease severity, such as behavioral or electrophysiological output measures, in order to validate whether the scoring method was meaningful. However, no such pathobiology data was collected. Quantitative analysis for evaluation of cell loss was also beyond the scope of this study. Therefore, the distinction in the number of neurons affected in an individual section may be arbitrary. Reducing the scoring system to a binomial method, the data were summarized based on the presence or absence of distinct neuronal damage (an ordinal score of 2 or greater). The incidence of sensory neuronopathy within the various treatment paradigms is summarized in Table 2-4.

2.3.4 DISCUSSION

We provide evidence that intrathecal administration of AAV9-GFP in mice was associated with unexpected sensory neuron degeneration and loss of variable severity. Neuron damage was observed with the use of two different supplier lots of the same viral construct, several vector dosages, and two strains of mice. No lesions were observed in the sensory ganglia of mice that received a different AAV9 construct in which GFP failed to express, AAV5-GFP, or saline by the same delivery method. However, this retrospective assessment was limited to available tissues, and clear relationships between lesion severity and the vector source, vector dose, or mouse strains could not be inferred.

The diagnostic quality of the cryosections was hampered by the tissue thickness, which while appropriate for immunofluorescence, was approximately three times thicker than a standard histologic section. Another challenge to morphological interpretation was cell shrinkage and resulting anatomical distortion, which is a known drawback of the perfusion fixation method in rodents (Scouten, 2010). Despite the obscured cellular details, histological staining demonstrated the occurrence of residual nodules of Nageotte, compact areas of satellite cell proliferation that remain at sites of DRG neuron loss (Ellison et al., 2008). In other sections, more exuberant mononuclear cells were evident within the subcapsular space suggestive of inflammatory infiltrates. It is unclear whether these lesions result from separate pathological processes or represent different temporal stages of the same process.

Potential toxicities from viral vector administration may result from the delivery procedure, the viral vector, or the specific transgene (Pleticha et al., 2014a). In these mice, intrathecal delivery was performed by direct lumbar puncture, which unlike periganglionic injection, has not been associated with parenchymal injury to the DRG. Lesions were also absent in mice that had received other vectors or vehicle controls by the same injection method. Potential contamination of the viral vector due to a fault in the purification method could not be excluded, as both vector lots were acquired from the same vendor. However, no lesions were evident on cursory examination of systemic tissues in animals with IV administration of vector. Damage as a result of the viral vector itself also seems unlikely. Recombinant AAV vector genomes display inefficient integration into the host chromosome, persisting instead in episomal form (McCarty et al., 2004), so the risk of insertional mutagenesis that may compromise the viability of transduced cells is very low. Recombinant AAV vectors also do not contain viral genes, and have been noted for their inability to elicit cellular immune responses in rodents (Tenenbaum et al., 2003; Beutler, 2010). AAV vector capsids do not replicate after cellular transduction and are likely cleared from tissues relatively quickly.

The specific transgene involved in all instances of sensory neuronopathy was the reporter gene GFP, which is classically considered to be biologically inert (Marshall et al., 1995). However, neurotoxicity resulting from excessive transgene expression has been reported for fluorescent reporter proteins (Furuta et al., 2001; Goto et al., 2003; Klein et al., 2006; Comley et al., 2011) and other transgene products (Grimm et al., 2006; Ulusoy et al., 2009; Ehlert et al., 2010). Cell stress and subsequent death result from excessive consumption of important cellular resources and oversaturation of endogenous pathways. The high efficiency of the AAV9 vector combined with the strong

CB7 promoter may have caused overproduction of the fluorescent reporter protein within certain cells. This pathogenesis is consistent with the observation of chromatolytic neurons with abundant cytoplasmic GFP, and may explain the finding of isolated, tombstone-like nodules of Nageotte in the absence of inflammatory infiltrates.

Expression of foreign proteins may elicit a cellular immune response, particularly if the vector has tropism for antigen-presenting cells. Notably, recent reports caution the use of AAV vectors with broad tropism to mediate expression of a non-self protein in the brain, as off-target transduction of antigen-presenting glial cells resulted in a destructive neuroinflammatory response in rats and nonhuman primates (Hadaczek et al., 2009; Cielsielska et al., 2013; Samaranch et al., 2014). Sensory neurons, like neurons of the central nervous system, fail to express major histocompatibility complex (MHC) molecules (Turnley et al., 2002), and are therefore unlikely to be involved in immune surveillance. However, satellite glial cells in the sensory ganglia, which tightly envelop the neuronal cell bodies, share some properties of antigen presenting cells (van Velzen et al., 2009). It seems possible that transduction of satellite glial cells by AAV9 encoding a foreign protein could elicit a cellular immune response. Indeed, careful scrutiny of the immunofluorescence micrographs from the inciting experiment revealed several instances of crescentic cells immediately adjacent to sensory neurons with GFP-positive cytoplasm, morphologically consistent with satellite glial cells (Figure 2-13). Similar cells were not apparent in immunofluorescence micrographs within areas of widespread neuronal loss, but it seems likely that such cells would have been destroyed. Further analysis is warranted to immunohistochemically confirm the identity of the putative satellite glial cells and determine the extent of AAV9-mediated transduction of this cell population.

No microscopic lesions were observed in mice that received a different AAV9 vector by the same route of administration, despite the vector encoding two non-syngeneic proteins. However, several uncertainties exist making a meaningful comparison between these vectors challenging. Each AAV9 vector was from a different vendor source. Data were not available on the tropism or expression levels of AAV9-hADC-GFP other than confirmation that the reporter gene product, encoded by the second gene after the promoter in the construct, was not detectable. The production of hADC may not have been so extensive as to cause cellular exhaustion. Similarly, the human and murine sequences of arginine decarboxylase may be sufficiently similar to not induce an immune response. Interestingly, the derivation product of hADC, agmatine, shows various neuroprotective effects (Hong et al., 2014), and while speculative, it seems possible that overexpression could potentially mitigate lesion formation. A more comprehensive investigation to clarify the relationships between vendors, tropism, dose, and immunogenicity of transgene products for this vector serotype may be warranted.

The pathobiological consequences of this unexpected sensory neuronopathy are unclear, as no behavioral outcome measures were available from the affected animals and the overall extent of neuron loss could not be quantified. The sudden mortality and progressive seizure activity of animals within the treatment group with the least impedance to vector biodistribution within the nervous system are certainly suspicious, and may suggest more extensive neuronal damage than in just the sensory ganglia. Random sensory neuronopathy may complicate data interpretation, particularly in studies investigating sensory neuron signaling. High efficiency GFP-encoding vectors

may also be inappropriate as transduction controls, especially if compared to viral-mediated expression of syngeneic proteins.

CONCLUSIONS

To test the hypothesis that VGF activity in sensory neurons modulates nociception and hypersensitivity in rodents, as measured by assays of pain-relevant behavior, we utilized viral-mediated gene transfer techniques to induce VGF overexpression in DRG sensory neurons. We provide evidence that intrasciatic administration of AAV5 yields predominately local transduction with inefficient and variable gene transfer to sensory and motor neurons. Intrathecal administration of AAV5-VGF by direct lumbar puncture resulted in successful transduction of the choroid plexus in the fourth ventricle. However, sensory neuron transduction by AAV5-VGF was not evident and the mechanisms precluding transgene expression in this cellular population are unclear. The potential for supraspinal structures to influence the behavior outcomes of spinal reflex-withdrawal assays may also warrant further consideration.

Any observed differences in mechanosensitivity thresholds between animals receiving the AAV5-VGF vector and those receiving saline were insufficiently robust to be statistically significant. However, this may be partly due to the limited group sizes available for final analyses, which were as low as three animals per group in some studies, and the imbalance between the numbers of treated and control animals. The data from these small, inconclusive trials can be used to estimate the needed sample sizes examining mechanosensitivity thresholds, benefiting future work. Sample sizes can be estimated using the difference in the means between groups (δ), the standard

deviation common to both treated and untreated groups (S), the desired significance level (α), and the power of the test (1-β). In the first rat experiment, the difference in the mean mechanosensitivity thresholds was most pronounced at 42 days post-injection (Figure 2-2 A). The sample size needed to demonstrate a significant difference between rats treated with intrasciatic AAV5-VGF or saline is 15 rats per group (α = 0.05, 1-β = 80%, δ = 0.215, S = 0.21). Applying the same approach to the mouse pilot study and using the day 42 data (Figure 2-8 A, C), the sample size needed to demonstrate a significant difference between mice treated with intrathecal AAV5-VGF or saline is 18 mice per group (α = 0.05, 1-β = 80%, δ = 2.05, S = 1.96). Viral-mediated gene transfer was not successful in all animals, so the group sizes would have to be adjusted accordingly to ensure sufficient samples. As the success rate of viral gene transfer in the rat experiments was approximately 50%, and the number of experimental and control animals should be matched, the estimated total number of rats needed to pursue the differences in mechanosensitivity thresholds between AAV5-VGF and saline treatments would be at least 45 (15 control + 15 successful AAV5-VGF + 15 unsuccessful AAV5-VGF). Another 30 rats would be needed if another vector treatment group (e.g. AAV5-GFP) was included for comparison.

Variability in the quality of AAV vectors between batches and vendors became increasingly evident throughout the course of this work. While we demonstrated repeated neurotoxicity associated with AAV9-mediated transduction of DRG sensory neurons and putative satellite glial cells, no sensory neuron damage was observed in later experimental work using the same serotype from the same vendor. The apparent biodistribution and intensity of GFP expression following intrathecal delivery of AAV5-GFP in mice also differed between the present experiments reported in section 2.2 and

in our previous work (Vulchanova et al., 2010), despite using the same vector source, vector dose, delivery method, and strain of mice. These findings raise some concerns regarding the use of AAV vectors in the DRG, and a more thorough assessment of quality control and method standardization is warranted.

FIGURES

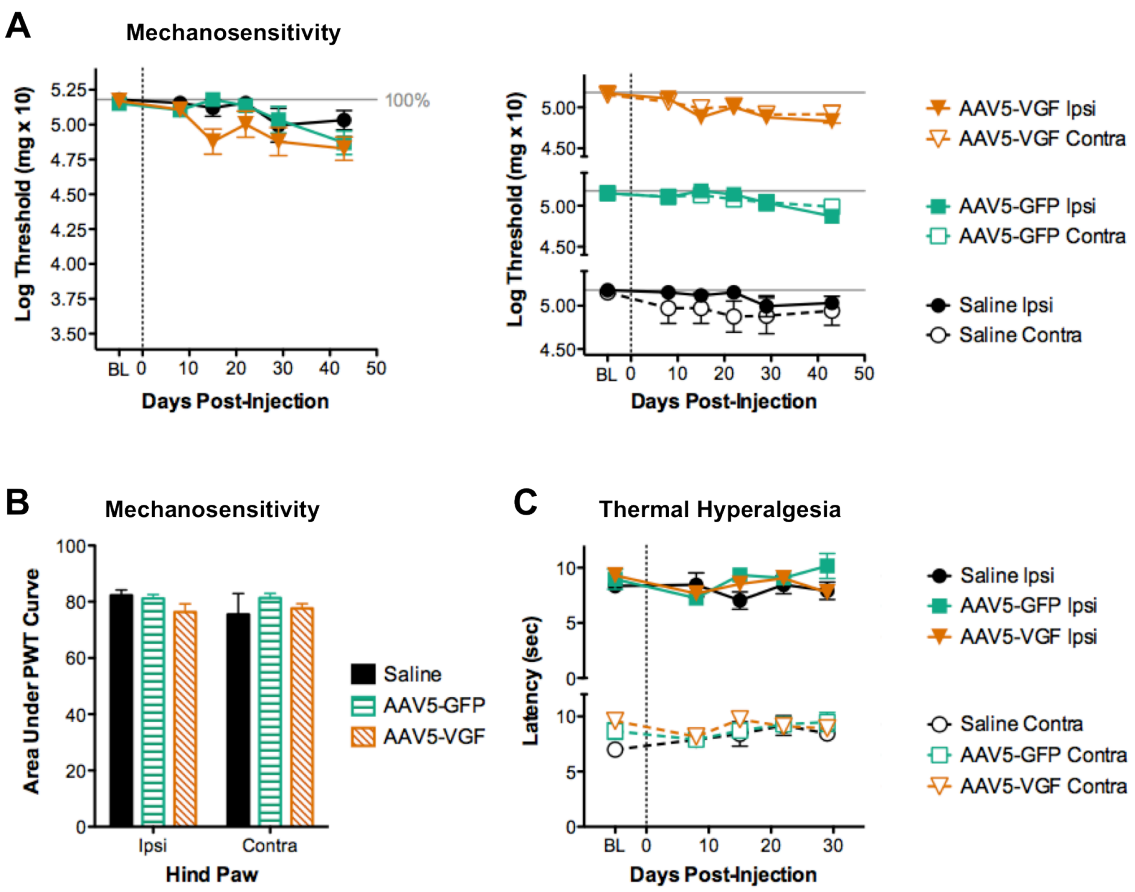

Figure 2-1, Behavior assay outcomes following intrasciatic administration of AAV5-VGF (n = 10), AAV5-GFP (n = 6), or saline (n = 4). **(A, left)** Mechanosensitivity thresholds determined by von Frey filament application were decreased for animals treated with AAV5-VGF as early as day 14 post-injection, but this trend was not statistically significant at any time point. A similar declining trend was observed for the AAV5-GFP treatment group at later time points. The grey solid line indicates the maximum possible value from the filament series. BL designates baseline measurements preceding intrasciatic injection. **(A, right)** Comparison of mechanosensitivity thresholds between the hind paws revealed striking similarities in responses despite the unilateral vector

administration. Closed symbols represent the left, affected hind paw (ipsilateral), and open symbols represent the right, naïve hind paw (contralateral). **(B)** The area under the paw withdrawal threshold curve was calculated for each subject to derive group averages. No significant differences were evident. **(C)** The latency to withdrawal of either hind paw from a radiant light heat source did not vary significantly over time.

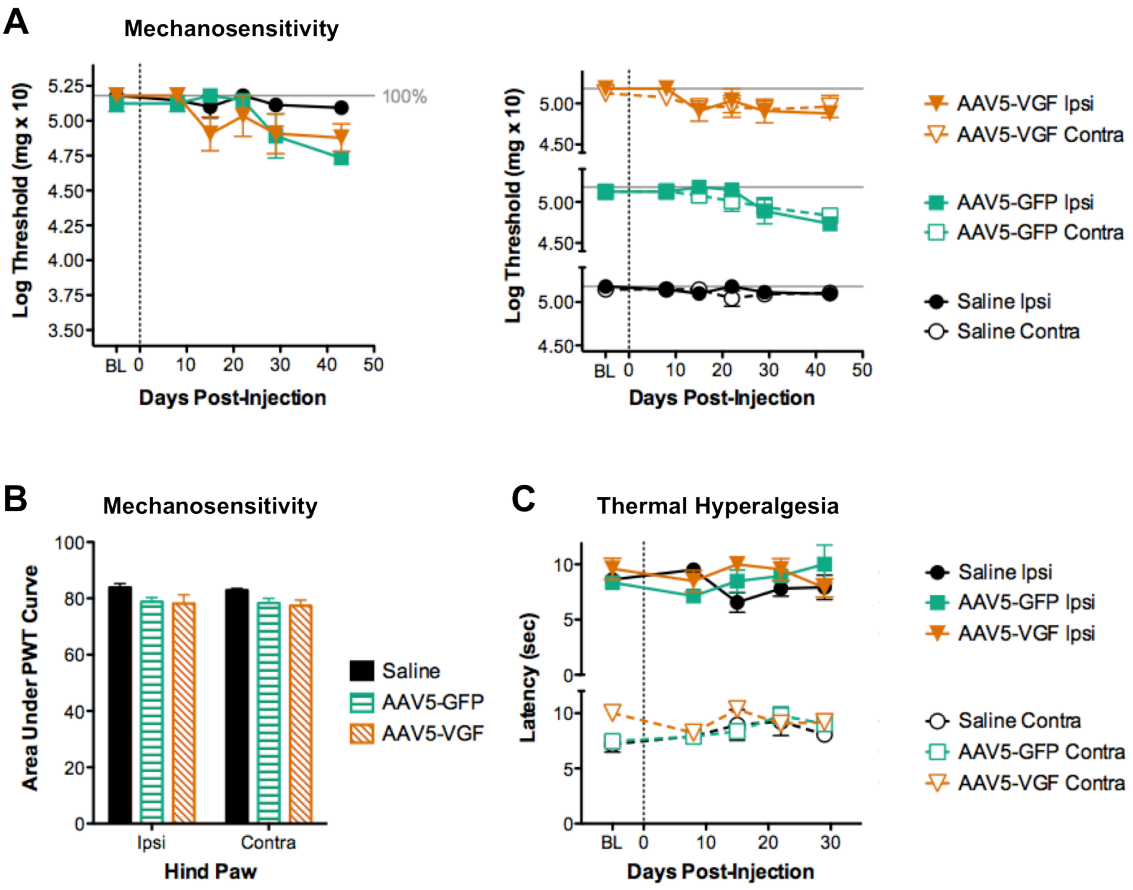

Figure 2-2, Behavior assay outcomes for animals with immunohistochemically confirmed vector transduction; AAV5-VGF (n = 5), AAV5-GFP (n = 3), and saline (n = 3). **(A, left)** Declining trends in mechanosensitivity thresholds were still evident in the vector-treated groups. The changes in tactile sensitivity were mirrored in the contralateral (right) hind paws, as seen in **(A, right)**. **(B)** Group means for the area under the paw withdrawal threshold curve were not significantly different. **(C)** Variations in the latency to paw withdrawal were more pronounced due to the reduced group sizes. There was no evidence of thermal hyperalgesia.

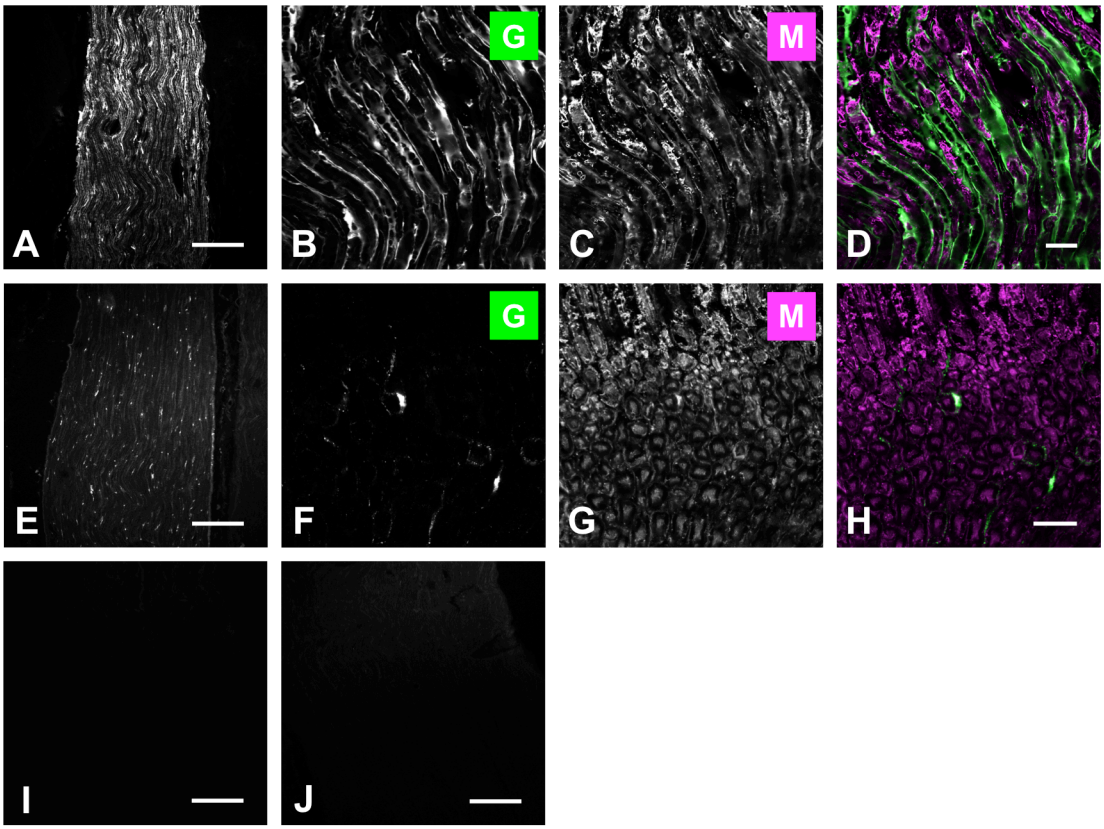

Figure 2-3, Representative immunofluorescence sections of rat sciatic nerves. **(A)** Widespread AAV5-mediated transfer of GFP within the sciatic nerve; scale bar = 250 μm. Higher magnification of tissue double-labeled with anti-GFP **(B)** and anti-MBP **(C)** suggests transduction of Schwann cells. Merged pseudocolored channels shown in **(D)**; scale bar = 25 μm. **(E)** Multifocal AAV5-mediated transfer of VGF in the sciatic nerve; scale bar = 250 μm. Double-labeling with anti-VGF **(F)** and anti-MBP **(G)** revealed limited colocalization in myelin sheaths. Merged pseudocolored channels shown in **(H)**; scale bar = 25 μm. Corresponding saline-injected controls for anti-GFP **(I)** and anti-VGF **(J)**; scale bar = 250 μm.

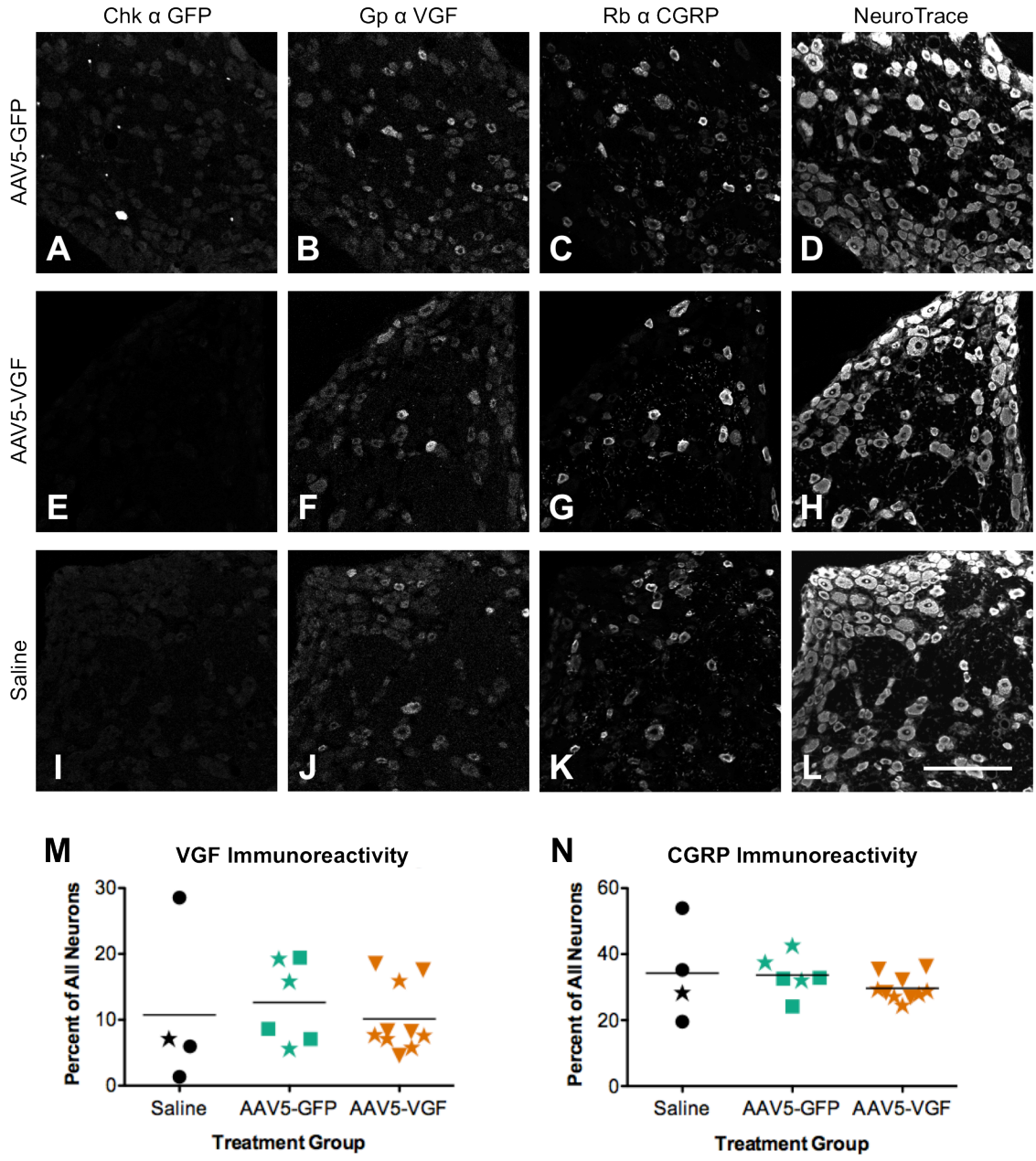

Figure 2-4. Representative images of the ipsilateral fifth lumbar (L5) DRG. **(A)** GFP-ir was observed in very low numbers of scattered sensory neurons in animals treated with AAV5-GFP. As expected, GFP-ir was absent in other treatment groups **(E, I)**. **(B, F, J)** Clear overexpression of VGF-ir was not evident between treatment groups. **(C, G, K)**

Expression levels of CGRP, a nociceptive signaling neuropeptide, were similar between treatment groups. **(D, H, L)** Corresponding images of NeuroTrace labeling; scale bar = 200 μm. **(M)** Semi-quantitative analysis of VGF-ir revealed similar levels of expression between treatment groups. Lines represent group means calculated from all individuals. Individual animals represented by star symbols (★) are those that were excluded in previous behavior analysis. Please refer to the text for exclusion criteria. **(N)** Semi-quantitative image analysis of CGRP-ir revealed no difference between treatment groups.

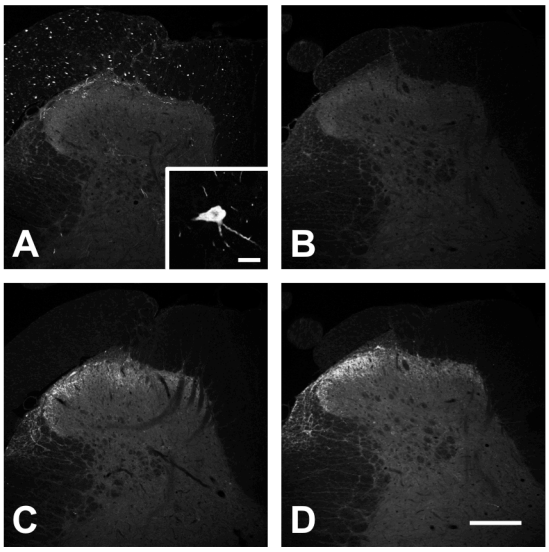

Figure 2-5, (A) Limited GFP-ir was evident in the dorsal root and superficial laminae of the ipsilateral dorsal horn. Ventral horn motor neurons were rarely transduced (inset, scale bar = 50 μm). **(B)** Corresponding saline-injected control. Transduced VGF **(C)** could not be discriminated from endogenous protein in saline controls **(D)**; scale bar = 250 μm.

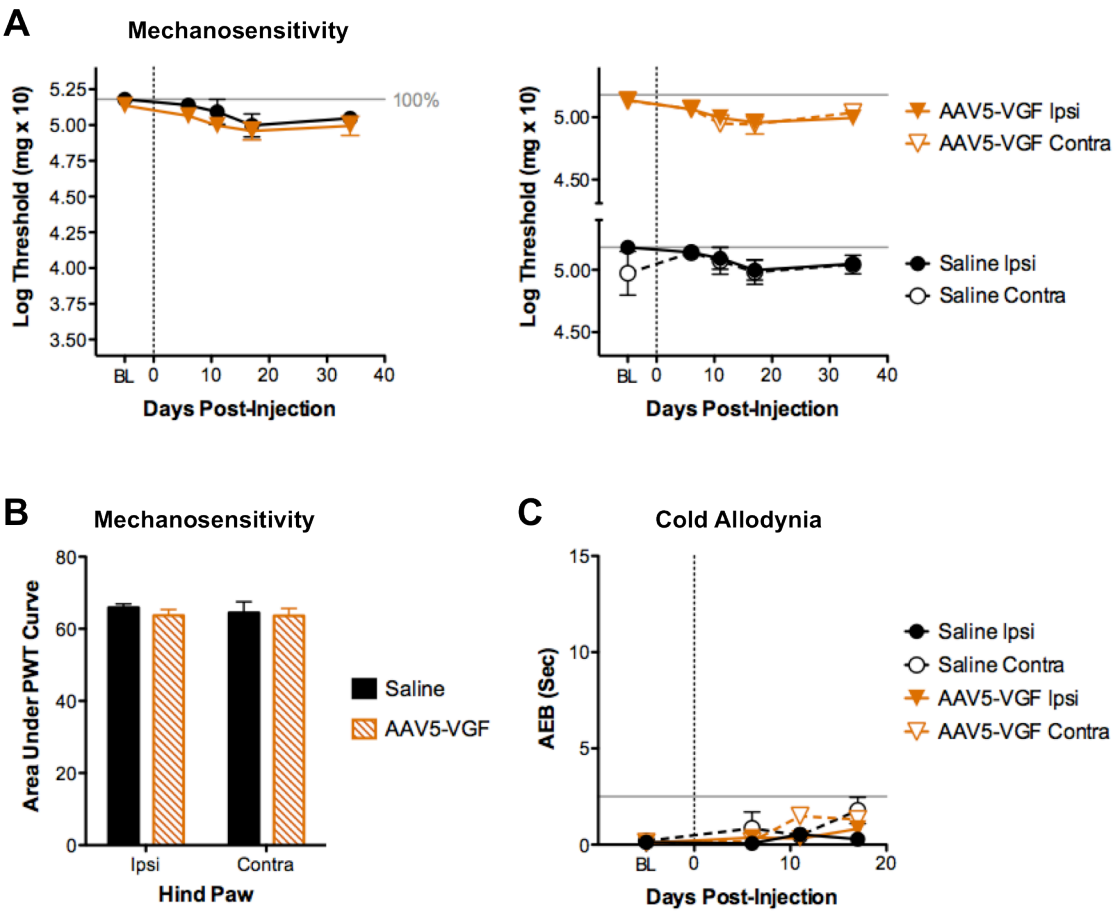

Figure 2-6, Behavior assay outcomes following intrasciatic administration of AAV5-VGF (n = 12) or saline (n = 4). **(A, left)** Mechanosensitivity thresholds were more stable over time in the second experimental cohort. **(A, right)** Paw withdrawal thresholds were very similar between the left hind paw (ipsilateral, closed symbols) and right hind paw (contralateral, open symbols). **(B)** As expected based on the appearance of the data, there were no significant differences in the area under the PWT curves. **(C)** All animals were monitored for 60 seconds for acetone-evoked behaviors (AEB), but responses were limited to rapid initial flinching and brief grooming of the paw. No group average

exceeded 2.5 seconds of total evoked behavior time (grey line). Prolonged evoked behaviors consistent with cold allodynia were not observed.

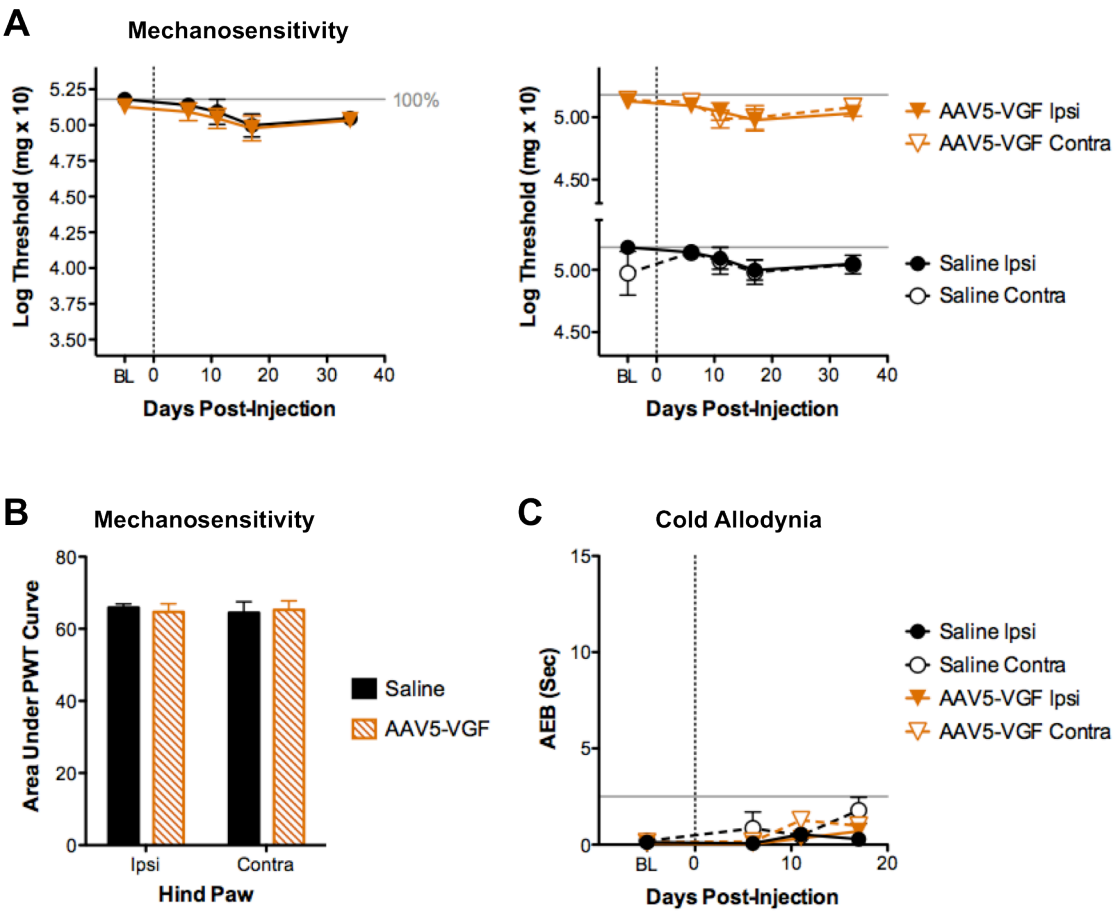

Figure 2-7, Behavior assay outcomes for animals with immunohistochemically confirmed vector transduction; AAV5-VGF (n = 8) and saline (n = 4). Limiting analysis to animals with evidence of VGF-ir in the sciatic nerve did not meaningfully alter the results of the mechanosensitivity assay **(A)**, comparison of the area under the PWT curves **(B)**, or assessment of acetone-evoked behaviors **(C)**. No significant differences were evident between treatment groups.

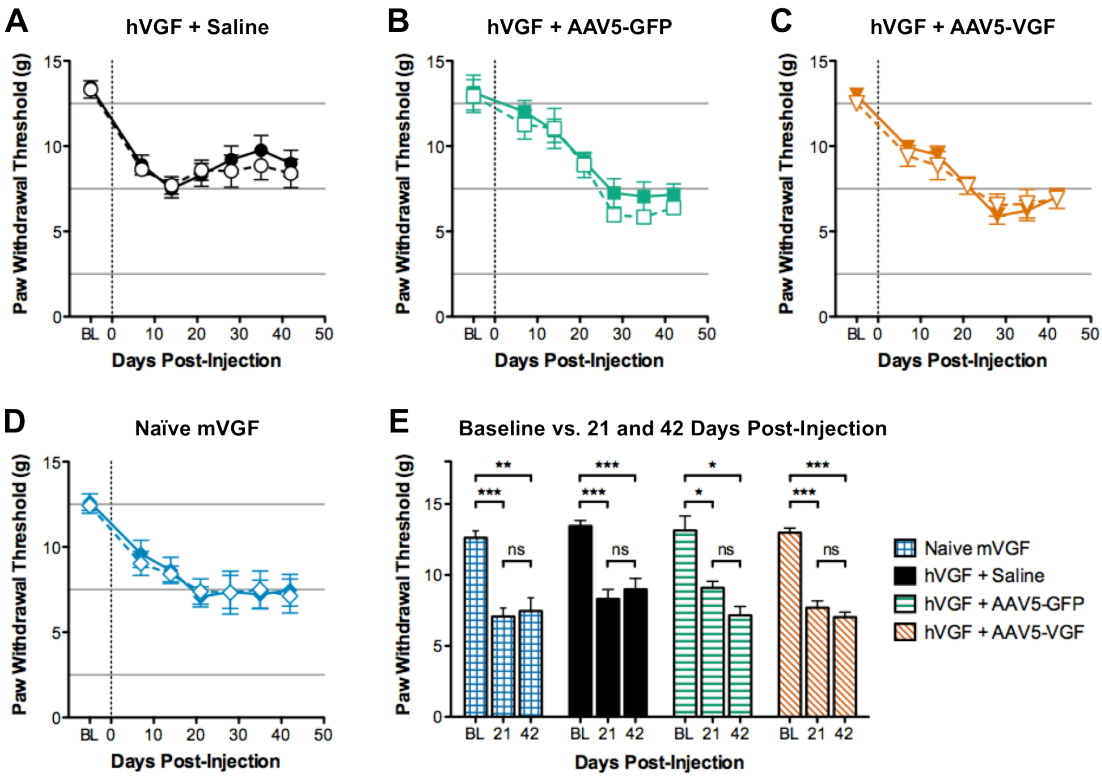

Figure 2-8, Mechanosensitivity thresholds determined by an electronic von Frey aesthesiometer. **(A-D)** In all treatment groups, paw withdrawal thresholds were consistent between the left hind paw (closed symbols) and right hind paw (open symbols). Thresholds unexpectedly declined sharply from baseline values over the first three weeks, then became relatively stable for the remainder of the experiment. **(E)** Within each group, mechanosensitivity thresholds were significantly lower than baseline at 3- and 6-weeks post-injection. There was no significant difference between 3- and 6-weeks post-injection (paired two-tailed t-test, * $p < 0.05$, ** $p < 0.01$, *** $p < 0.001$, ns = not significant).

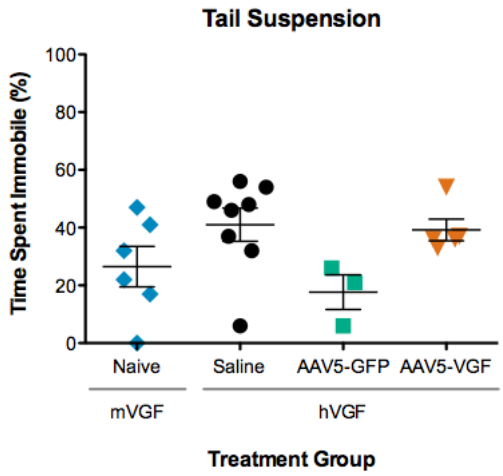

Figure 2-9, Immobility times during the tail suspension assay. Antidepressant-like behavioral effects were not evident in any treatment group.

Anatomic Area	AAV5-GFP	AAV5-VGF
Lumbar		
L4 DRG	3 / 6	–
Spinal cord	5 / 6	–
Supraspinal		
Choroid plexus	6 / 6	5 / 7
Brainstem	3 / 6	–
Cerebellum	1 / 6	–
Midbrain	–	–
Forebrain	–	–
Systemic		
Liver	–	–

Table 2-1, Immunohistochemical detection of viral-driven gene expression in vector-treated hVGF mice. The values indicate the total number of animals in which immunoreactivity was observed within the specified tissue out of the total number of animals in the group. The "–" symbol indicates no immunoreactivity was evident in the entire group.

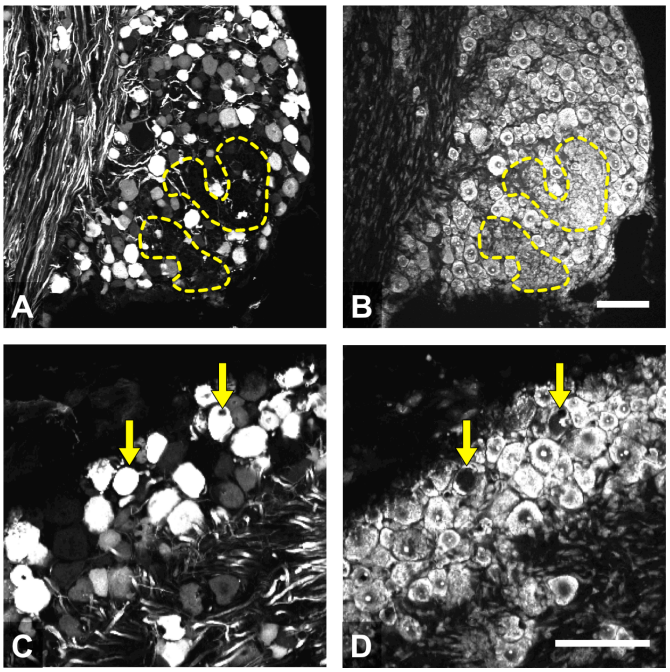

Figure 2-10, (A) AAV9-GFP mediated gene transfer to the mouse L4 DRG and **(B)** corresponding NeuroTrace labeling. Normal appearing transduced cells lie adjacent to mottled regions with indistinct cellular margins and uncharacteristic neuronal loss (dotted yellow outlines); scale bar = 100 μm. At higher magnification, labeling for GFP **(C)** and NeuroTrace **(D)** reveals GFP-positive neurons with absent or marginalized Nissl substance, suggestive of chromatolysis (yellow arrows); scale bar = 100 μm.

Cohort	Strain	Vector	Lot	Dose	Delivery
A	C57BL/6	AAV9-GFP	2	3.3×10^{11}	IV, IT, ± Mannitol
B	C57BL/6	AAV9-GFP	1	1.7×10^{11}	IT + Mannitol
C	ICR/CD-1	AAV9-GFP	2	6.6×10^{9}	IT
		AAV9-hADC-GFP	–	n/a	IT
D	C57BL/6	AAV5-GFP	–	$\sim 10^{11}$	IT + Mannitol

Table 2-2, Source of histopathology samples according to mouse strain, vector, and administration method.

Score	Lesion Rating	Description
0	None	No microscopic lesions
1	Minimal	Generally increased mononuclear cells without neuron replacement or loss
2	Mild	Distinct nodular aggregate of mononuclear cells replacing one neuron
3	Moderate	Discrete nodular aggregates of mononuclear cells replacing more than one neuron
4	Marked	Disseminated mononuclear infiltrates and nodular aggregates replacing at least three neurons

Table 2-3, Ordinal scores based on the distribution of lesions within sensory ganglia.

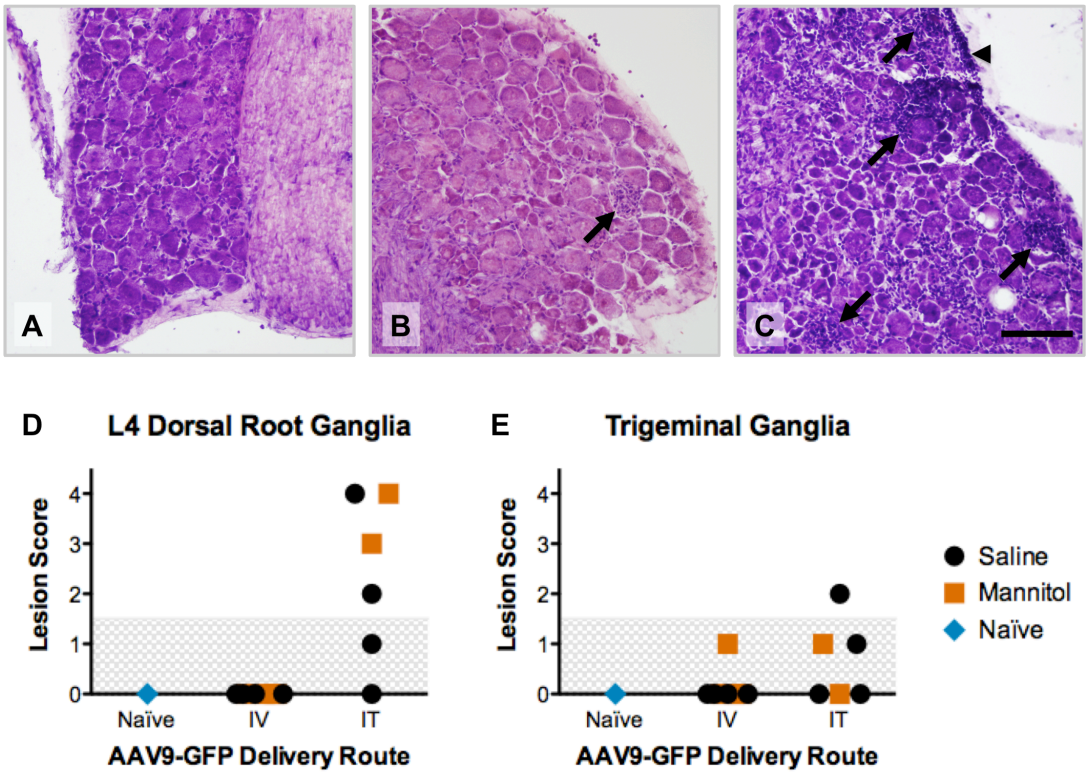

Figure 2-11, Hematoxylin and eosin scoring of mouse L4 DRG and trigeminal ganglia from Cohort A. **(A)** Naïve animal with no evidence of disease in the L4 DRG. **(B)** A single sensory neuron is replaced by a nodular aggregate of mononuclear cells (nodule of Nageotte, arrow). The DRG section represents a lesion score of 2. **(C)** Multiple neurons are replaced by dense aggregates of mononuclear cells (arrows), which also fill the subcapsular space (arrowhead). The DRG section represents a lesion score of 4. Some differences in appearance are due to variation in staining quality and cellular shrinkage artifacts. Thickness of sections (14 µm) precluded sharp focus. Scale bar = 100 µm. **(D)** Lesions in the L4 DRG were associated with intrathecal delivery of AAV9-GFP. **(E)** In the trigeminal ganglia, minimal to mild disease was evident in vector-treated

animals by either route of administration. An ordinal score of 2 or greater is indicative of neuronal loss.

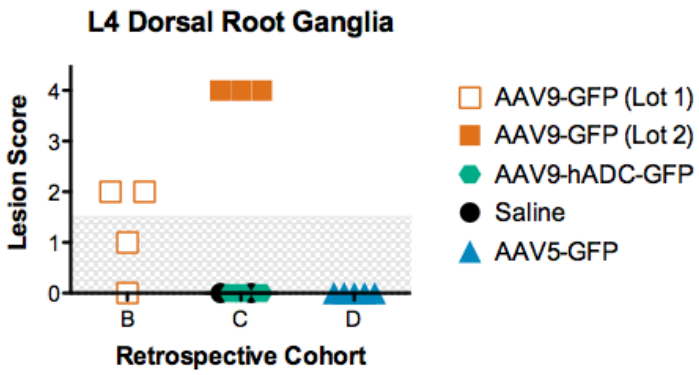

Figure 2-12, Hematoxylin and eosin scoring of mouse L4 DRG from retrospective Cohorts B, C, and D. Lesions were associated with IT administration of AAV9-GFP from either supplier lot. No lesions were observed following IT delivery of AAV9-hADC-GFP, saline, or AAV5-GFP.

Vector	Cohort	Route	Pretreatment	Neuronal Loss	%
AAV9-GFP (Lot 2)	A	IV	Saline	0 / 4	0
	A	IV	Mannitol	0 / 4	0
	A	IT	Saline	2 / 4	50
	A	IT	Mannitol	2 / 2	100
	C	IT	None	3 / 3	100
AAV9-GFP (Lot 1)	B	IT	Mannitol	2 / 4	50
AAV9-hADC-GFP	C	IT	None	0 / 3	0
AAV5-GFP	D	IT	Mannitol	0 / 5	0
Saline	C	IT	None	0 / 2	0
Naïve	A	–	–	0 / 1	0

Table 2-4, Scoring of L4 DRG for the presence or absence of neuronal loss.

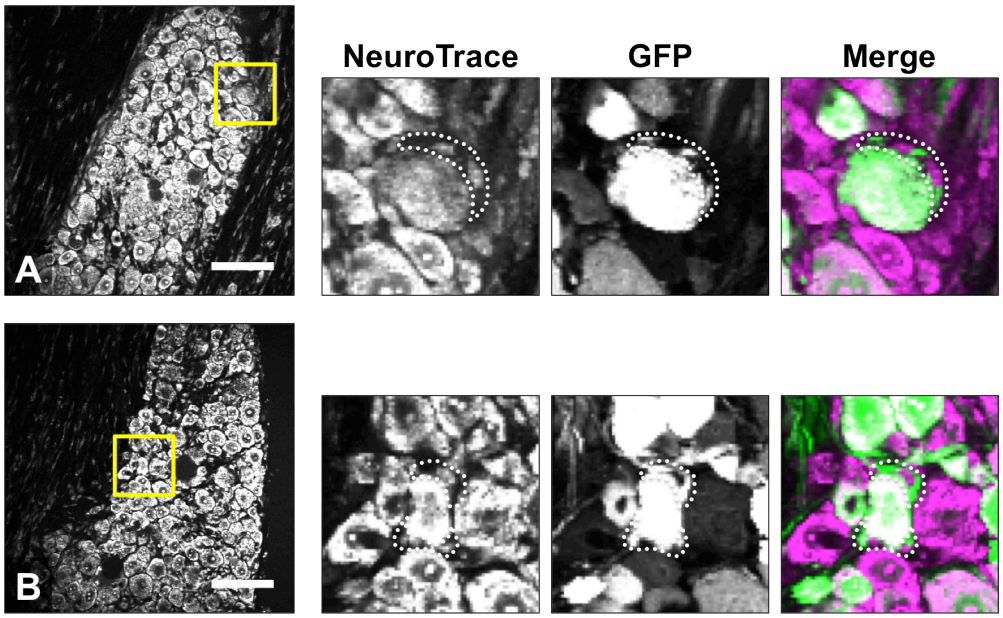

Figure 2-13, Putative AAV9-GFP mediated gene transfer to satellite glial cells in L4 DRG. Panels **(A)** and **(B)** show the original immunofluorescence micrograph with a yellow square indicating the location of the digitally enlarged images shown to the right. White dotted lines outline fusiform cells with Nissl-stained nuclei (magenta) that are closely associated with neuronal cell bodies, consistent morphologically with satellite glial cells. The cytoplasm of these cells is GFP-positive (green). Scale bars = 100 μm.

Chapter 3

Antibiotic-induced visceral hypersensitivity

3.1 Assessment of cutaneous referred allodynia in a murine model of antibiotic-induced visceral hypersensitivity

3.2 Novel utilization of a forelimb grip force assay to monitor antibiotic-induced visceral hypersensitivity in mice

3.3 Semi-quantitative image analysis of L6 dorsal root ganglion sensory neurons in a murine model of antibiotic-induced visceral hypersensitivity

SUMMARY

Deliberate antibiotic-induced perturbation of the gut microflora has been associated with the development of colonic hypersensitivity in murine models. We hypothesized that VGF plays a functional role in modulating nociception and hypersensitivity in viscero-specific sensory neurons. Antibiotic-induced dysbiosis in mice was not reliably associated with a behavioral phenotype of referred cutaneous allodynia of the abdomen or of axial stretching-induced discomfort. Other factors likely contributed to the lack of reliability of the dysbiotic model, including potential variability in the basal gut microflora. Thorough characterization of the microbial changes, including evaluation for pathogenic overgrowth, would complement and inform future work. Antibiotic treatment and presumed dysbiosis were associated with upregulation of CGRP, SP, and VGF in predominantly small-diameter sensory neurons of the sixth lumbar DRG. VGF expression was observed throughout the range of neuron sizes and colocalization with SP was limited, suggesting a role for VGF beyond peptidergic sensory neurons. Increased expression of nociceptive neuropeptides supports the potential utility of this experimental model for assessing visceral hypersensitivity, provided an appropriate behavioral assay is identified. As TRPV1 expression was unchanged following antibiotic treatment, the value in antemortem testing with capsaicin is unclear.

INTRODUCTION

Irritable bowel syndrome (IBS) is the most common functional gastrointestinal disorder, with key symptoms including abdominal pain or discomfort and altered lower bowel function (Sayuk and Gyawali, 2015). The prevalence is estimated to be 10-15% in Western countries, although as few as 25% of IBS sufferers actually seek professional care (Hungin et al., 2005). The multifactorial pathogenesis of IBS is incompletely understood, but involves psychosocial factors, altered signaling between the gut and brain, alterations in the normal composition of the gut commensal microbiota, and low-grade intestinal immune activation (Aguilera et al., 2015).

The neurobiological mechanisms of visceral pain differ from those involved in somatic pain, and the role of VGF-derived peptides in viscero-specific sensory neurons has not been investigated. As in our other work investigating the role of VGF in somatic sensory neurons (predominantly those of the sciatic nerve), we hypothesized that VGF plays a similar functional role in modulating nociception and hypersensitivity in viscero-specific sensory neurons. To explore this hypothesis, we utilized a mouse model originally developed to better understand the interplay between visceral hypersensitivity and altered intestinal microbiota in IBS.

3.1.1 ASSESSMENT OF CUTANEOUS REFERRED ALLODYNIA IN A MURINE MODEL OF ANTIBIOTIC-INDUCED VISCERAL HYPERSENSITIVITY

Deliberate antibiotic-induced perturbation of the gut microflora has been associated with the development of colonic hypersensitivity in murine models (Verdú et al., 2006;

Aguilera et al., 2015). In these reports, visceral sensitivity was assessed through responses to intraperitoneal acetic acid, intracolonic capsaicin, or colorectal distension via electromyography. However, these behavior assays may reflect a greater response of the somatic peritoneum than of the visceral organ of interest, or can be technically demanding, requiring intubation of the distal intestinal tract or surgery, respectively. Chemical stimulation assays are also typically performed once with short survival times after visceral stimulation due to ethical considerations, precluding their use in serial monitoring of progressive hypersensitivity development.

An alternative, simple, viscero-specific behavior assay proposed by Laird and colleagues (2001) is the examination of referred pain to the abdominal body wall using standardized von Frey filaments. Inspired by these findings, we questioned whether antibiotic-induced dysbiosis and subsequent visceral hypersensitivity could be monitored non-invasively through evaluation of referred cutaneous allodynia.

3.1.2 METHODS

Animals. The experimental procedures were reviewed and approved by the Institutional Animal Care and Use Committee of the University of Minnesota. Adult male C57BL/6 mice (20–25g; Harlan Labs, Madison, Wisconsin USA) were maintained in a conventional vivarium with a 12:12 light/dark cycle (lights on at 07:00 h) and ambient temperature of 21±2°C. The animals were socially housed in groups of 3–4 in transparent plastic cages with corncob bedding, compact cotton nesting material, and *ad libitum* access to water and standard rodent chow. The mice were allowed to habituate for at least 3 days under these conditions before the start of experimental manipulations.

Antibiotic administration. Mice received a combination of non-absorbable antibiotics by oral gavage once daily for ten days, in accordance with the method described by Verdú and colleagues (2006). Bacitracin and neomycin were diluted in sterile water (each to 4 mg/mL), with the addition of pimaricin (0.2 mg/mL) to prevent yeast overgrowth. For the final five days, the antibiotic concentrations were reduced to bacitracin 2 mg/mL, neomycin 2 mg/mL, and pimaricin 0.1 mg/mL. Control animals received sterile water (vehicle). The gavage volume was 100 µL per mouse. Alternatively, mice received the same combination of non-absorbable antibiotics in drinking water for seven days (Bercik et al., 2011). The concentrations throughout were bacitracin 5 mg/mL, neomycin 5 mg/mL, and pimaricin 0.1 mg/mL. The medicated water was changed daily. Control animals received non-medicated water.

To examine whether exposure to fecal pellets from mice without altered gut flora could protect against the antibiotic-induced changes in visceral sensitivity, select antibiotic-treated mice were cohoused with control mice. To replicate this exposure in select mice with medicated water, used bedding from cages with non-medicated water was transferred daily to cages with medicated water.

Mechanical stimulation of the abdomen. The frequency of withdrawal responses to the application of a von Frey filament to the abdomen was examined as a test of referred cutaneous allodynia (Laird et al., 2001). The filament was applied to the mid to lower abdomen for 1 to 2 seconds with a stimulus interval of at least 10 seconds. In most experiments, a von Frey filament with bending force of 0.16 g (filament number 3.22) was employed except in Cohorts 8 and 9, which used a 0.07 g (2.83) filament (Stoelting Co., Wood Dale, Illinois USA). The filament was applied 10 times, with care taken to not

stimulate the same point twice in succession. The behavior resulting from application of the filament was recorded by the experimenter blinded to the experimental condition.

Chemical stimulation of the colon. In certain experimental cohorts, spontaneous behaviors were evoked through the instillation of capsaicin (0.125% or 0.30% w/vol dissolved in 10% ethanol, 10% Tween 80, and 80% saline; Laird et al., 2001). Just prior to the intracolonic administration of capsaicin, petroleum jelly was applied in the perianal area to avoid accidental stimulation of somatic areas. A fine cannula with a rounded tip was gently introduced 4 cm into the colon via the anus, and the capsaicin solution was slowly injected. Spontaneous behavior was observed directly for 20 minutes by an experimenter blinded to the experimental condition. Postures quantified as capsaicin-induced pain-related behavior included licking of the abdomen, abdominal retractions, stretching of the abdomen, or squashing of the lower abdomen against the floor. Mice treated with capsaicin were sacrificed immediately following the behavior assessments.

Statistical analysis. Data were entered into a spreadsheet for analysis. Statistical tests were performed using GraphPad Prism (version 5.0d, GraphPad Software, San Diego, California USA, www.graphpad.com). Groups were compared by Student's t-test, one-way analysis of variance (ANOVA) with post-hoc Bonferroni's multiple comparison test, or two-way repeated measures ANOVA with post-hoc Bonferroni's multiple comparison test, where best applicable. Data are expressed and plotted as mean ± SEM. A p value of < 0.05 was considered significant.

3.1.3 RESULTS

Antibiotic administration. Naïve mice were randomly divided into up to four possible treatment groups: antibiotic treatment, antibiotic treatment with exposure to non-medicated animals or bedding, water treatment, or water treatment with exposure to medicated animals or bedding. Ten separate experiments with groups of 3–8 mice were performed. Antibiotics were administered by oral gavage in experimental cohorts 1–5 and 9–10, and through the drinking water in cohorts 6–8.

Referred cutaneous allodynia. The behavior experimenter described any reaction of the mouse to each filament application instead of directly interpreting whether the behavior of a mouse should be considered a positive withdrawal response. A total of sixteen possible behaviors were provided, ranging from no response to grooming to jumping. In order to quantify the positive response rate, the baseline data from all experimental cohorts were combined (n = 121 mice, 1210 filament tests) to determine behaviors that were common in naïve animals, as these responses were considered unlikely to represent pain-related behavior. The list was further refined by identifying those behaviors that were most compatible with the criteria suggested by Laird et al. (2001). The remaining behaviors were interpreted as positive withdrawal responses: (a) sharp retraction of the abdomen; (b) jumping; (c) immediate scratching of the filament application site; or (d) immediate flailing of one or both hind feet. The *post hoc* scoring metric was applied to the von Frey data from all experimental cohorts.

In Cohort 1, there was a significant but transient increase in the response rate to abdominal von Frey filament application in antibiotic-treated animals (Figure 3-1). This allodynia peaked five days after the cessation of antibiotic treatment (day 15), persisted at day 20, and was recovering at day 25. Multiple attempts were made to repeat this

finding in separate experimental cohorts with antibiotics administered through oral gavage (Figure 3-1) or drinking water (Figure 3-2). While the antibiotic-treated group occasionally trended toward a higher response rate than the control group, this difference was not statistically significant in any cohort. A reliable antibiotic-induced visceral hypersensitivity model could not be established.

In certain cohorts, antibiotic-treated mice were cohoused with control mice or provided with their soiled bedding. This was done to evaluate whether exposure to normal fecal microflora would rescue antibiotic-induced visceral hypersensitivity, as had been reported with probiotic therapy (Verdú et al., 2006). However, the inconsistency of behavior responses in antibiotic-treated animals precluded any meaningful interpretation on the impact of normal microflora exposure.

Behavior response to intracolonic capsaicin. In certain cohorts, visceral sensitivity was measured by quantifying the behavioral pain-related responses to the intracolonic instillation of capsaicin (Figure 3-3). In Cohort 4, there was a significant attenuation in capsaicin-induced behaviors in mice treated with antibiotics as compared to controls. This attenuation was not apparent in any of the following cohorts. The capsaicin dose was reduced in the later experiments in case differences between groups were being masked by a ceiling effect. However, no significant differences were observed.

The response rate to von Frey filament application to the abdomen was evaluated immediately before and following the intracolonic capsaicin test in two experimental cohorts (Figure 3-4 A). No significant differences were observed. The lack of demonstrable referred allodynia in any treatment group following intracolonic instillation

of capsaicin was concerning and prompted critique of the *post hoc* scoring metric used to define positive withdrawal responses. Behavior data from water-treated control animals before and after capsaicin administration were compiled for each cohort. Six behavior types were represented: arching the back, licking, recoiling from the filament, flailing one or both hind feet, jumping, or no observed response. Of these, recoiling, flailing, and jumping qualified as positive withdrawal responses in the scoring metric. In Cohort 5 (n = 3), only flailing of the hind feet was significantly increased from pre-capsaicin values, and in Cohort 6 (n = 6), no behavior significantly changed following capsaicin administration (Figure 3-4 B).

3.1.4 DISCUSSION

In this study, we questioned whether antibiotic-induced dysbiosis and subsequent visceral hypersensitivity could be monitored non-invasively through evaluation of referred cutaneous allodynia. Unfortunately, a reliable dysbiotic murine model of referred visceral pain could not be established.

The inconsistent behavior responses observed between experimental cohorts may be related to different states of dysbiosis despite using a similar antibiotic treatment. Specific microbial changes are likely influenced by many factors, including the strain of mouse, the source of the animals, the basal composition of the gut microbiota, the dose of antibiotics administered, and the environmental conditions (Aguilera et al., 2015). Treatment may also favor the expansion of antibiotic-resistant bacterial groups, which may or may not be pathogenic. In this study, all experiments utilized the same mouse strain from one commercial breeder and the antibiotic dose was kept consistent within

the delivery method. However, the mice were housed under conventional, non-sterile conditions, and although cleaned between uses, the behavior testing equipment was utilized for other rodent experiments. Characterization of the microbial changes within each cohort, including identification and quantification of the gut microbiota, went beyond the scope and expertise of this study. However, fecal pellets from mice at baseline and after ten days of antibiotic treatment were provided to collaborators. Their preliminary analysis revealed striking differences in the composition of the microflora after antibiotic treatment (T. Johnson, personal communication; data not shown). However, the basal composition of the microflora and the resulting changes induced by antibiotic therapy were not consistent between cohorts. Standardization of the basal microflora may be necessary to generate a predictable and reliable behavior model.

A disconcerting finding was the lack of referred allodynia following intracolonic instillation of capsaicin, particularly in control (water-treated) animals. The development of robust abdominal allodynia following the intracolonic administration of capsaicin (0.1% or 0.3%) in otherwise naïve animals has been repeatedly demonstrated in outbred Swiss mouse stocks, inbred mouse lines (including C57BL/6), and Sprague-Dawley rats (Laird et al., 2001; Galan et al., 2003; Kawao et al., 2004; Pitcher et al., 2007; Sanoja et al., 2010; González-Cano et al., 2013; Pitcher et al., 2013). Galan et al. (2003) also reported persistence of the referred allodynia, which was significant at all time points tested up to 24 hours post-instillation. Given a strong reaction to intracolonic capsaicin was evident in all treatment groups based on the number of pain-related behaviors observed over the 20 minute testing window, it seems likely that the capsaicin preparation was effective. This suggests the failure to detect the expected abdominal referred allodynia was more likely due to a fault in the detection method than to an absence of the secondary effect.

This not only is concerning for the tests involving capsaicin, but in all the preceding work solely evaluating dysbiosis-induced referred cutaneous allodynia. We considered several potential causes for the lack of success with the mechanical stimulation test.

Filament bending force. Laird et al. (2001) used von Frey filament application to the abdomen as a test of referred allodynia, and employed a series of five filaments with forces of 1, 4, 8, 16, and 32 mN (as in the Optihair$_2$-Set, Marstock Nervtest, Germany). They found the responses to mechanical stimulation of the abdomen following intracolonic instillation of capsaicin (0.1 or 0.3%) were significantly increased from baseline at all bending forces tested. Owing to differences in the sources of standardized sets of von Frey filaments, a filament with a bending force of 1 mN was not available. The 3.22 filament has a target bending force of 0.16 g or 1.6 mN, and the 2.83 filament has a target bending force of 0.07 g or 0.70 mN. These filaments each approximate the lower end of the reported testing series. Testing at a higher filament force could be considered.

Filament calibration. Von Frey filaments are subject to wear with repeated use. Given the number of required stimuli and the duration of the experiments, it is possible the filaments in use became uncalibrated over time, leading to spurious results. The bending force can be validated by advancing the filament carefully toward a sensitive balance, typically with the aid of a clamp or micromanipulator, and recording the output value. If there is a discrepancy in the exerted force and the filament target force, replacement of the filaments may be necessary.

Positive withdrawal responses. The determination of positive and negative responses to von Frey filament application was based on *post hoc* interpretation of observational behavior data. The behaviors were categorized as nocifensive or innocuous based on similarities to the criteria provided by Laird et al. (2001) and likelihood of occurrence at baseline. Only baseline data were included in the development of the scoring metric, since the experimenter performing the *post hoc* analysis was no longer blinded to the experimental manipulations. Also, the behavior descriptions may have been over simplified. For example, "licking" could refer to immediate attention to the filament application site, which would have been considered a positive response based on the published criteria, or to innocuous grooming behavior, which was common at baseline. Without the ability to distinguish these, "licking" was not considered a positive response. Ideally, baseline and experimental withdrawals should have been assessed directly at the time of testing.

The attenuation of capsaicin-induced pain-related behaviors in antibiotic-treated mice in one cohort is reminiscent of the recent findings of Aguilera et al. (2015), where following a 2-week treatment of bacitracin, neomycin, and amphotericin B, capsaicin-induced pain-related behaviors were unexpectedly reduced by 48% as compared to vehicle-treated control mice. This significant reduction was attributed to downregulation of certain cannabinoid and opioid receptors in the gut and the possible generation of an analgesic-like state. It is unclear whether this local neuro-immune response may also influence the likelihood of referred allodynia in this model.

3.2.1 NOVEL UTILIZATION OF A FORELIMB GRIP FORCE ASSAY TO MONITOR ANTIBIOTIC-INDUCED VISCERAL HYPERSENSITIVITY IN MICE

Given the limited success in using standardized von Frey filaments to assess referred cutaneous allodynia, other non-invasive methods of monitoring visceral hypersensitivity were considered. Stretch-induced discomfort, as measured by functional deficits in forelimb grip force, had been reported as a phenotype of deep tissue pain and chronic low back pain in mice (Kehl et al., 2000; Millecamps et al., 2011). Inspired by these findings, we conducted a pilot study to evaluate whether antibiotic-induced visceral hypersensitivity could be monitored non-invasively through movement-evoked axial stretching and functional deficits in forelimb grip strength.

3.2.2 METHODS

Animals. The experimental procedures were reviewed and approved by the Institutional Animal Care and Use Committee of the University of Minnesota. Adult male C57BL/6 mice (20–25g; Harlan Labs, Madison, Wisconsin USA) were maintained in a conventional vivarium with a 12:12 light/dark cycle (lights on at 07:00 h) and ambient temperature of 21±2°C. The animals were socially housed in groups of four in transparent plastic cages with corncob bedding, compact cotton nesting material, and *ad libitum* access to water and standard rodent chow. The mice were allowed to habituate for at least 3 days under these conditions before the start of experimental manipulations.

Antibiotic administration. Mice received a combination of non-absorbable antibiotics by oral gavage once daily for ten days, in accordance with the method described by Verdú and colleagues (2006). Bacitracin and neomycin were diluted in sterile water (each to 4 mg/mL), with the addition of pimaricin (0.2 mg/mL) to prevent yeast overgrowth. For the final five days, the antibiotic concentrations were reduced to

bacitracin 2 mg/mL, neomycin 2 mg/mL, and pimaricin 0.1 mg/mL. Control animals received sterile water (vehicle). The gavage volume was 100 µL per mouse. To examine whether exposure to fecal pellets from mice without altered gut flora could protect against the antibiotic-induced changes in visceral sensitivity, select antibiotic-treated mice in each cohort were cohoused with control mice.

Functional deficits in grip strength. Forelimb grip force was measured using a grip force analyzer (Bioseb, France). During testing, the mouse was held by its tail and carefully passed in a rostral-to-caudal direction over a wire mesh grid connected to a force transducer. The mouse was allowed to grip the grid using only the forepaws while steady horizontal pressure was applied via the tail to induce stretching. The peak force exerted by the forelimbs when pulling on the grid was recorded by the force transducer. Five grip force measurements were obtained and averaged for each animal with a minimum 5-minute interval between tests.

Statistical analysis. Data were entered into a spreadsheet for analysis. Statistical tests were performed using GraphPad Prism (version 5.0d, GraphPad Software, San Diego, California USA, www.graphpad.com). Groups were compared by one-way analysis of variance (ANOVA) with post-hoc Bonferroni's multiple comparison test. Data are expressed and plotted as mean ± SEM. A p value of < 0.05 was considered significant.

3.2.3 RESULTS

Forelimb grip force was evaluated as a possible measure of discomfort induced by axial stretching. In Cohort 9, the average forelimb grip force exerted by antibiotic-treated mice was significantly reduced compared to water-treated controls, but not significantly lower than the other groups. This attenuation of grip force was also not evident in antibiotic-treated mice cohoused with control mice. No differences were observed between treatment groups in Cohort 10.

3.2.4 DISCUSSION

A novel behavior assessment employed to quantify visceral pain was forelimb grip force, as a functional deficit in grip may indicate discomfort induced by axial stretching. Diminished average grip force was evident in one antibiotic-treatment group. However, a visceral pain phenotype was not confirmed in these mice by any other means. The reduced willingness or capability to maintain grip is nonspecific and could represent fatigue or malaise due to other physiological processes such as dehydration or systemic inflammation. This finding was also not repeated in the subsequent cohort, suggesting other confounding factors may be contributing to the reduced grip function.

3.3.1 SEMI-QUANTITATIVE IMAGE ANALYSIS OF L6 DORSAL ROOT GANGLION SENSORY NEURONS IN A MURINE MODEL OF ANTIBIOTIC-INDUCED VISCERAL HYPERSENSITIVITY

We hypothesized that VGF plays a functional role in modulating nociception and hypersensitivity in viscero-specific sensory neurons. To explore this hypothesis, we utilized a mouse model originally developed to better understand the interplay between

visceral hypersensitivity and altered intestinal microbiota in IBS. In the previous sections of this chapter, we questioned whether antibiotic-induced dysbiosis and subsequent visceral hypersensitivity could be monitored non-invasively. In addition, we expected this visceral hypersensitivity to be associated with DRG sensory neuron upregulation of nociceptive neuropeptides including VGF.

As a pilot study, tissues from the experimental cohort with a discriminatory behavioral phenotype, as revealed by the forelimb grip assay (Cohort 9), were selected for further evaluation. Semi-quantitative image analysis was performed to determine whether VGF upregulation was evident in viscero-specific sensory neurons. Previous work investigating the role of VGF-derived peptides focused solely on somatic sensory neurons (predominantly those of the sciatic nerve), and the neurobiological mechanisms of visceral pain differ from those involved in somatic pain.

3.3.2 METHODS

Tissue preparation. Animals were terminally anesthetized with isoflurane and sacrificed by transcardial perfusion with a pre-wash of calcium-free Tyrode's (in mM: 116 NaCl, 5.4 KCl, 1.6 $MgCl_2$•$6H_2O$, 0.4 $MgSO_4$•$7H_2O$, 1.4 NaH_2PO_4, 5.6 glucose, and 26 Na_2HCO_3), followed by modified Zamboni's fixative (4% paraformaldehyde and 0.2% picric acid in 0.1 M phosphate buffer, pH 6.9). Spinal cord, lumbar dorsal root ganglia (DRG), and descending colon were collected and incubated in 10% sucrose overnight at 4°C. Tissues were cryosectioned (14 µm) and thaw-mounted onto gelatin-coated slides.

Immunohistochemistry. Tissue sections of the L6 DRG were incubated in blocking buffer (PBS containing 0.3% Triton X-100, 1% bovine serum albumin, and 1% normal donkey serum) at room temperature for 30 min, then incubated overnight at 4°C in primary antisera prepared using blocking buffer as diluent. Primary antisera used were: guinea pig anti-transient receptor potential vanilloid 1 (TRPV1), 1:500 (ref. Guo et al., 1999), rabbit anti-calcitonin gene related peptide (CGRP), 1:1000 (24112; ImmunoStar, Hudson, Wisconsin USA), protein A-purified guinea pig anti-VGF, 1:1000 (ref. Riedl et al., 2009), and rabbit anti-substance P (SP), 1:1000 (Neuromics, Edina, Minnesota USA). After rinsing with PBS, sections were incubated with appropriate combinations of cyanine-dye conjugated secondary antisera (Jackson ImmunoResearch, West Grove, Pennsylvania USA) for one hour at room temperature. Sections were rinsed again in PBS, then incubated with NeuroTrace® 435/355 Blue (Molecular Probes, Inc., Eugene, Oregon USA) per manufacturer's instructions. The slides were coverslipped using glycerol and PBS containing 0.1% p-phenylenediamine (Sigma Chemical Co., St. Louis, Missouri USA). Images were collected using an Olympus FluoView1000 confocal imaging system, analyzed using ImageJ (National Institutes of Health), and processed for publication using Adobe Photoshop.

Cell counting. DRG were mounted and sectioned parallel to the nerve root axis. At least three equally spaced sections from each DRG separated by a minimum distance of 56 μm were selected for image collection. The region of interest for imaging was visualized on the NeuroTrace channel, and the entire neuron population was imaged as best possible with non-overlapping fields, resulting in an average of 5 images per animal. Neuron cell body size and intensity of fluorescence were analyzed in ImageJ,

using the Nissl-like NeuroTrace labeling to manually outline cell margins. Only cells with a visible nucleus were counted.

Image analysis. Semi-quantitative image analysis was conducted as described in detail in Chapter 4. Briefly, double-labeled fluorescent tissue sections were imaged to produce a separate 8-bit greyscale image for each color channel. The red (cyanine-3) and green (cyanine-2) channels were used for markers of experimental interest, while the blue channel was exclusively used for Nissl-like NeuroTrace labeling. All images from a specific antibody marker and within a particular color channel were compiled into a stack in ImageJ. The image stack was then binarized using the Auto Threshold ImageJ plugin (version 1.15, Landini G, fiji.sc/Auto_Threshold) using the stack histogram, which would include images from control and experimental animals. Splitting the stack back into individual images, each binarized version was saved with the original greyscale images.

For cell counting, images of the identical microscope field were compiled into stacks of seven images: greyscale blue, greyscale red, binarized red, greyscale green, and binarized green. Manual cell outlining was conducted in the blue (NeuroTrace) channel, and the mean grey value (MGV) and cross-sectional area were simultaneously measured for the outlined region of interest for all images in the stack. A cell was considered negative for a particular marker if the mean grey value of the binarized channel was 0 (all pixels black). To determine which cells had sufficient fluorescent intensity to be considered positive, the average greyscale MGV for the negative population of cells was calculated. The threshold to be considered positive was determined as 3 standard deviations above the average for the negative population.

Statistical analysis. Data were entered into a spreadsheet for analysis. Statistical tests were performed using GraphPad Prism (version 5.0d, GraphPad Software, San Diego, California USA, www.graphpad.com). Groups were compared by Student's t-test. Data are expressed and plotted as mean ± SEM. A p value of < 0.05 was considered significant.

3.3.3 RESULTS

Semi-quantitative image analysis was performed on labeled sections from the sixth lumbar (L6) DRG (Figure 3-6). All sections were derived from the same embedded tissue block. Cell counting was performed by a different investigator for each slide set in a blinded manner; all analysis was performed by one investigator. Two animals were ultimately excluded due to poor tissue section quality and/or insufficient (< 100) neurons available for analysis, one from the antibiotic-treatment group and one from the water-treatment group, reducing each group to three animals. The total number of neurons counted per animal was 611 ± 57. A cross-sectional area cutoff of 380 μm^2, which is equivalent to a calculated cell diameter of 22 μm, was selected as the cutoff for categorization of neurons by size based on the appearance of the neuron size histogram (Figure 3-7).

Antibiotic treatment was associated with increased sensory neuron immunoreactivity (-ir) to SP (22.4 ± 1.9% of all neurons vs. 9.4 ± 0.8%, $p < 0.01$) and VGF (18.4 ± 1.8% vs. 9.4 ± 2.7%, $p < 0.05$) as compared to water-treated controls (Figure 3-8 A). There was no significant difference between groups in CGRP-ir (25.3 ± 2.6% vs. 18.6 ± 1.4%) or TRPV1-ir (28.2 ± 1.3% vs. 26.5 ± 3.0%). Size distribution analysis revealed these

changes predominated in small (≤ 380 μm^2) sensory neurons (Figure 3-8 B-E). Interestingly, significant upregulation of CGRP was evident within small but not medium-to-large sensory neurons (Figure 3-8 B).

Colocalization analysis was performed within double-labeled slide sets. While there was no significant difference in the overall number of cells with immunoreactivity to CGRP and TRPV1, there was a small but significant increase in the percentage of TRPV1-ir cells also expressing CGRP in antibiotic-treated animals (Figure 3-9 A). The number of neurons immunoreactive to SP and VGF more than doubled in antibiotic-treated animals (5.0 ± 0.4% of all neurons vs. 2.1 ± 0.3%, $p < 0.01$). The proportion of SP-ir neurons also expressing VGF and vice versa did not change (Figure 3-9 B).

To further evaluate the neuron populations positive for SP and/or VGF, the image data from the two experimental groups were pooled and frequency histograms were generated (Figure 3-10). As expected, neurons with SP-ir were predominately within the peak of "small" neurons, with an average cross-sectional area of 258 ± 5.9 μm^2 in antibiotic-treated animals and 301 ± 10.1 μm^2 in water-treated controls. VGF-positive neurons were more broadly distributed, with an average cross-sectional area of 395 ± 11.6 μm^2 in antibiotic-treated animals and 435 ± 16.6 μm^2 in water-treated controls. As observed with the previous analysis, colocalization between the two markers was limited.

3.3.4 DISCUSSION

Sensory innervation from the descending colon follows two anatomic pathways, the lumbar splanchnic nerves and the paired pelvic nerves, which terminate in the thoracolumbar and lumbosacral spinal cord, respectively (Brierley et al., 2004). This is consistent with the bimodal distribution of labeled sensory neurons identified by retrograde labeling of the mouse descending colon, encompassing DRG levels T8-L1 and L6-S1 (Robinson et al., 2004). For this pilot study, we focused on the L6 DRG based on our previous work that identified an association between L6 sensory neuron transduction and anterograde labeling of fibers in the segment of descending colon just proximal to the pelvic inlet (Schuster et al., 2013). However, sensory neurons in the L6 DRG innervate several pelvic organs via the pelvic nerve, including the descending colon, urinary bladder, prostate, vagina, and cervix (Inskip et al., 2009; McCarthy CJ et al., 2015). Based on the experimental model, observed changes in the L6 sensory neurons are most likely attributable to disturbances in the colon; however, in future work the possibility of concomitant disease in other pelvic organs (e.g. urocystitis) should be excluded. Examination of the thoracolumbar DRG (T8-L1) may also be warranted, as sensory neurons of these DRG innervate the descending colon as well as the dermatomes of the ventral abdominal region tested for cutaneous referred allodynia (Patestas and Gartner, 2006).

Primary afferent neurons are divided into subclasses based on distinct morphological and molecular features. In general, the myelinated afferent fibers of medium-size type Aβ and large-size type Aα are responsible for innocuous tactile sensation and proprioception, while smaller myelinated Aδ and unmyelinated C-fibers carry thermal and nociceptive input (Lawson and Waddell, 1991; Patestas and Gartner, 2006). While there is some overlap in the size ranges, most small-diameter sensory neurons are

nociceptive. In this study, significant neuropeptide upregulation in antibiotic-treated animals as determined by immunohistochemistry was limited to small sensory neurons. While only non-specific behavior was observed with this cohort (discussed in 3.2.4), increased activity of nociceptive neurons suggests a pain-related phenotype may exist provided an appropriate detection method is utilized.

Small-diameter nociceptive sensory neurons can be divided into two major neurochemical subtypes that also differ anatomically in the region of termination in the dorsal horn of the spinal cord. Peptidergic neurons contain neuropeptides such as calcitonin-gene related peptide (CGRP) and substance P (SP), express the TrkA receptor, and project to lamina I and outer lamina II. Non-peptidergic neurons lack peptides but bind the plant lectin isolectin B_4 (IB_4), express the P2X3 receptor, and terminate predominantly in inner lamina II (Stucky and Lewin, 1999). Interestingly, TRPV1 receptors are restricted to peptidergic fibers in mice but not rats (Zwick et al., 2002).

Putative antibiotic-induced dysbiosis was associated with upregulation of CGRP, SP, and VGF in predominantly small-diameter sensory neurons. In neuropathic pain models and DRG neuron culture, VGF-derived peptides have been shown colocalized with SP, CGRP, TrkA, and P2X3 (Rizzi et al., 2008; Riedl et al., 2009). In this study, VGF expression was observed throughout the range of neuron sizes and colocalization with SP was limited (< 30%). This finding suggests the experimental condition is associated with upregulation of this VGF-derived peptide in nonpeptidergic C-fiber nociceptors and potentially in medium-sized Aδ or Aβ fibers as well, which are all associated with carrying afferent nociceptive information from the viscera (Patestas and Gartner, 2006).

The role of VGF in this context is unclear, and further investigation is warranted to better elucidate the involvement of VGF in visceral pain.

Increased protein expression levels of TRPV1 in sensory neurons have been reported for pathological pain conditions (Vilceanu et al., 2010), most notably in human biopsy specimens from patients with inflammatory bowel disease (Yiangou et al., 2001). In this study, sensory neuron expression levels of TRPV1 were not changed in antibiotic-treated animals. The TRPV1 channel is activated by capsaicin, heat, protons, and endovanilloids. The lack of TRPV1 upregulation in animals with putative antibiotic-induced dysbiosis may help explain the congruity in spontaneous, capsaicin-induced behaviors between antibiotic- and water-treated animals (discussed in 3.1.4).

CONCLUSIONS

Antibiotic-induced dysbiosis was not reliably associated with referred cutaneous allodynia of the abdomen in mice. However, the inconclusive results of the abdominal mechanical stimulation assay were complicated by the need to perform *post hoc* interpretation, and the method requires refinement. The only behavior assay with promising results was the functional deficit in forelimb grip force, which at best is nonspecific. Other factors likely contributed to the lack of reliable behavioral phenotype in the dysbiotic model, including variability in the basal gut microflora, potential for secondary infectious processes, and the lack of TRPV1 upregulation in viscero-specific sensory neurons, which likely influenced the results of capsaicin-induced behavior assays. Thorough characterization of the microbial changes, including evaluation for pathogenic overgrowth, would complement and inform future work.

Antibiotic treatment and presumed dysbiosis were associated with upregulation of CGRP, SP, and VGF in predominantly small-diameter sensory neurons of the sixth lumbar DRG. VGF expression was observed throughout the range of neuron sizes and colocalization with SP was limited, suggesting a role for VGF beyond peptidergic sensory neurons. Increased expression of nociceptive neuropeptides supports the potential utility of this experimental model for assessing visceral hypersensitivity, provided an appropriate behavioral assay is identified. As TRPV1 expression was unchanged following antibiotic treatment, the value in antemortem testing with capsaicin is unclear.

FIGURES

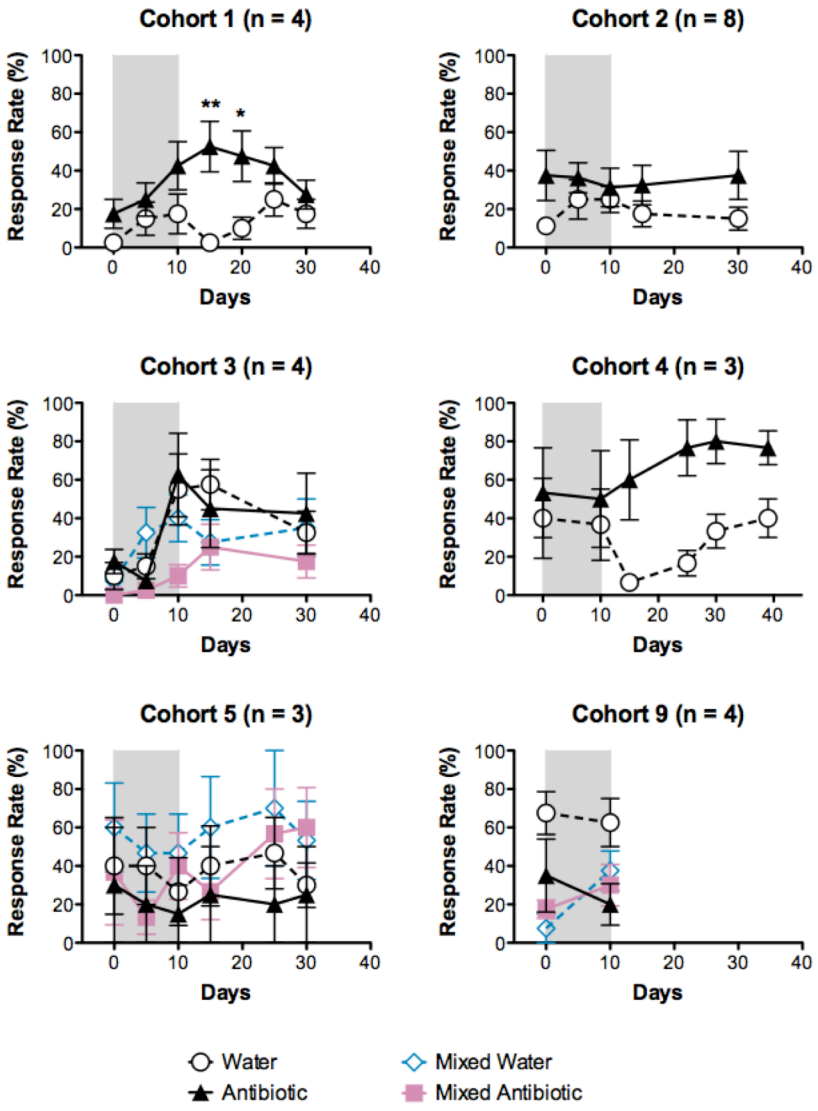

Figure 3-1, The frequency of positive withdrawal responses to von Frey filament application to the abdomen in mice treated by oral gavage. Group sizes in each cohort are specified. The grey shaded region indicates the 10 days of antibiotic treatment. In Cohort 1, the response rate of antibiotic-treated animals was significantly higher than water-treated controls on days 15 and 20 (two-way ANOVA with multiple comparisons, *

$p < 0.05$, ** $p < 0.01$). In Cohort 4, the response rate of antibiotic-treated animals trended higher but was not statistically significant at any time point.

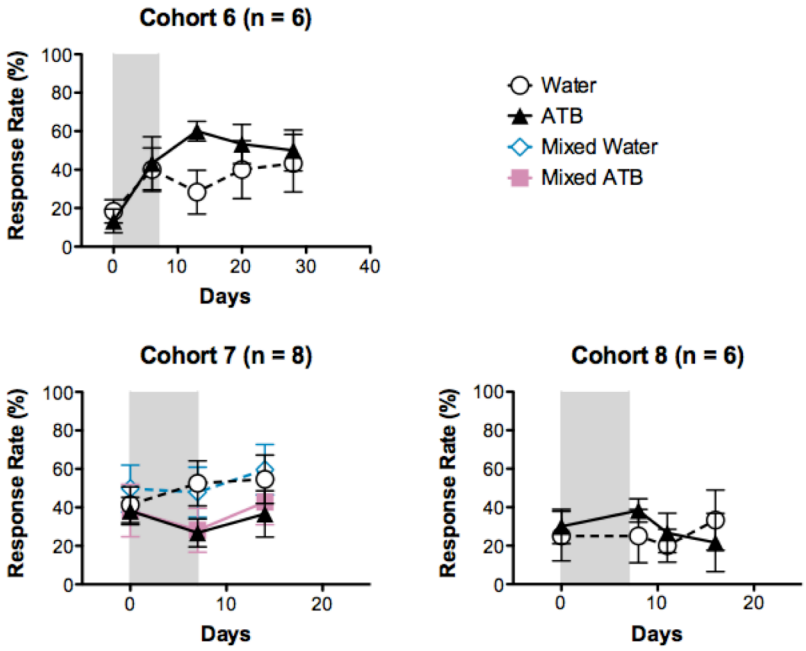

Figure 3-2, The frequency of positive withdrawal responses to von Frey filament application to the abdomen in mice treated via the drinking water. Group sizes in each cohort are specified. The grey shaded region indicates the 7 days of antibiotic treatment. The response rate between antibiotic-treated and water-treated animals was not statistically significant at any time point.

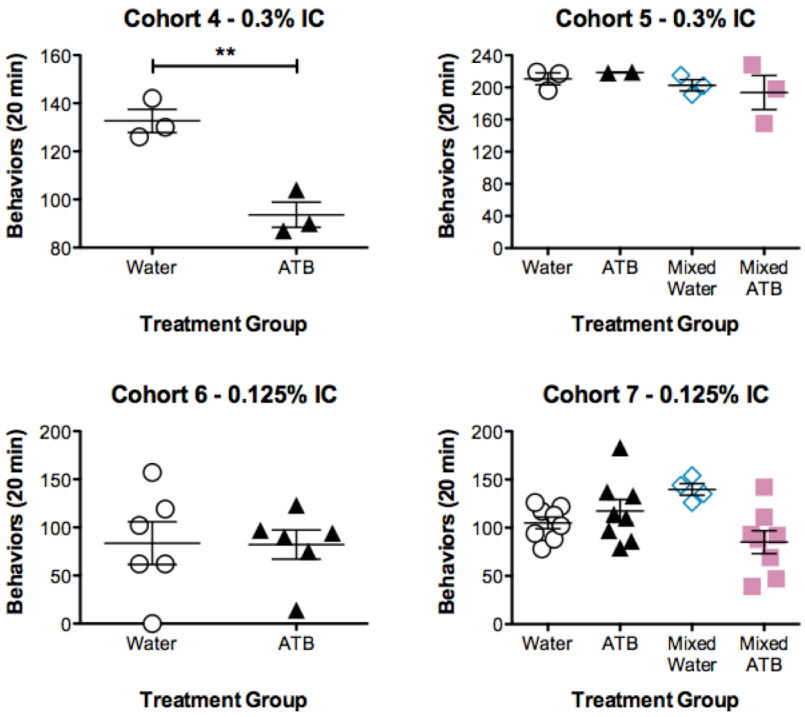

Figure 3-3, Spontaneous behaviors following intracolonic (IC) instillation of capsaicin in antibiotic-treated (ATB) and water-treated animals. Each symbol represents an individual animal. The timing of testing is as follows: Cohort 4 = day 46; Cohort 5 = day 30; Cohort 6 = day 28; and Cohort 7 = day 15. In Cohort 4, antibiotic treatment was associated with a significant attenuation in capsaicin-induced behaviors (unpaired two-tailed t-test, ** $p < 0.01$). This attenuation was not evident in any other cohort.

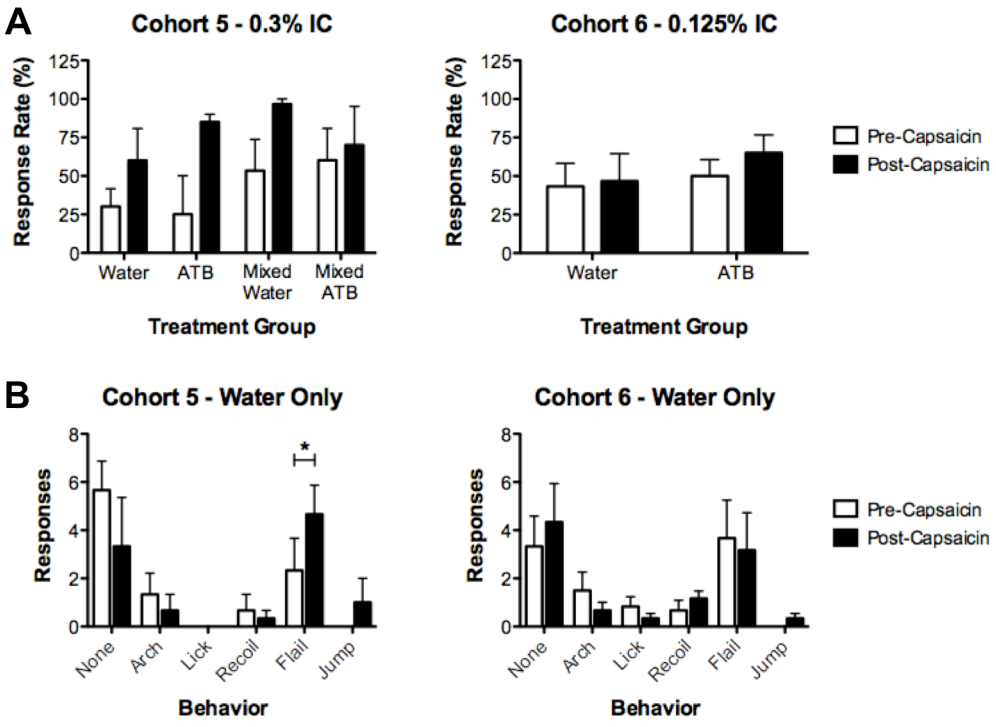

Figure 3-4, (A) Response rate to abdominal von Frey filament application before and 30 minutes after intracolonic (IC) instillation of capsaicin (white and shaded bars, respectively). Withdrawal responses were more frequent in animals following capsaicin administration in Cohort 5, but these trends were not significant in any treatment group. There were no significant differences in Cohort 6. **(B)** Response behaviors were re-evaluated in water-treated control animals from Cohort 5 (n = 3) and Cohort 6 (n = 6). Of the six possible responses recorded for animals before and after capsaicin treatment, a significant difference was only evident for one behavior type in Cohort 5 (paired two-tailed t-test, * $p < 0.05$). However, this difference was not observed in the subsequent cohort.

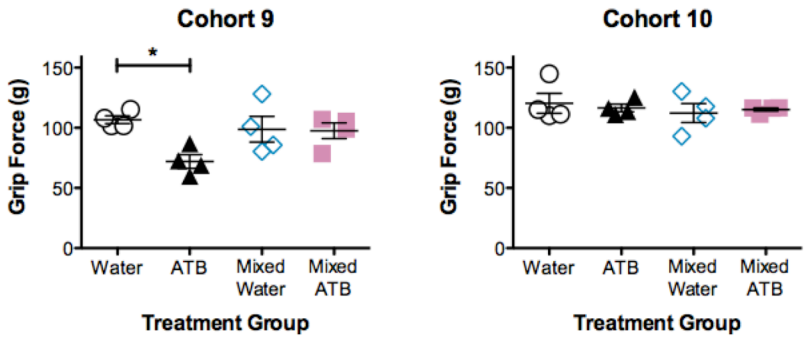

Figure 3-5, Forelimb grip force in animals treated by oral gavage. In both cohorts, testing occurred on day 11. Each symbol represents an individual animal. In Cohort 9, the average forelimb grip force was significantly reduced in antibiotic-treated mice as compared to water-treated controls (one-way ANOVA with multiple comparisons, * $p < 0.05$). This effect was not evident in the subsequent experimental cohort.

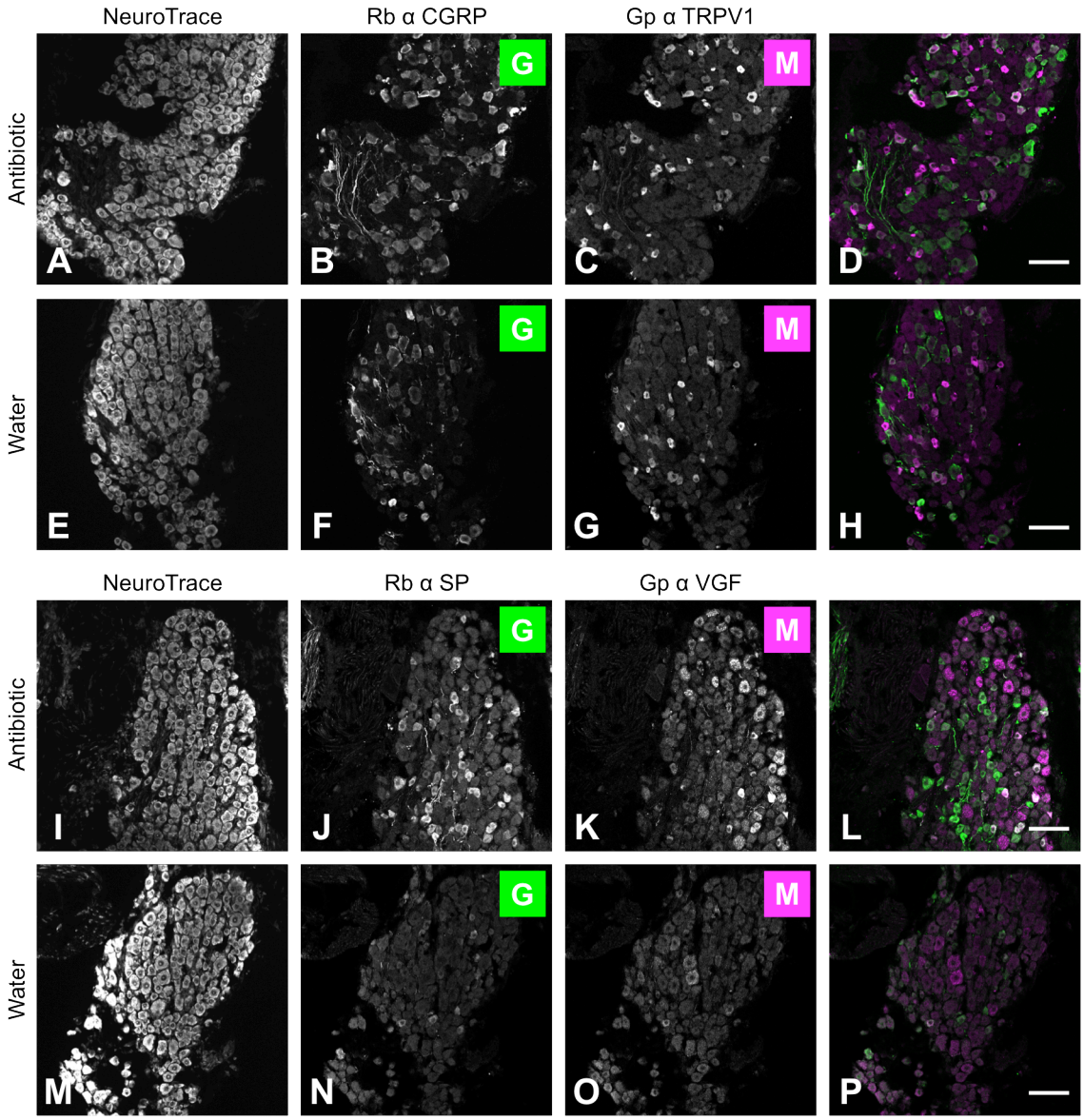

Figure 3-6, Representative pseudocolored immunofluorescence photomicrographs of mouse L6 DRG. **(A-H)** Double-immunofluorescence staining of sensory neurons expressing CGRP-ir (green) and TRPV1-ir (magenta). Occasional CGRP-positive cells also displayed positivity for TRPV1 (white in merge pictures, D and H). **(I-P)** Double-immunofluorescence staining of sensory neurons expressing SP-ir (green) and VGF-ir (magenta). Increased fluorescence intensity was apparent in antibiotic-treated animals.

Colocalization of SP and VGF was also increasingly evident (white in merge pictures, L and P). Scale bar = 100 μm.

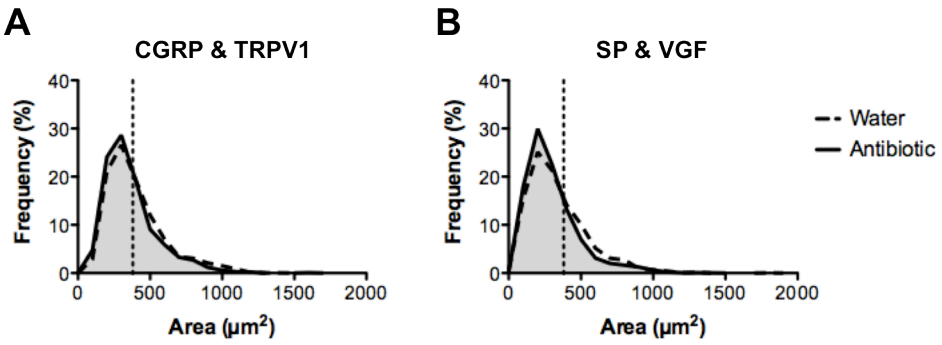

Figure 3-7, Frequency distributions of the cross-sectional area of quantified sensory neurons from L6 DRG sections. Double labeling was based on pairing primary antibodies raised in two different species, and equivalent slide sets were utilized. There were no significant differences in the cell size frequency distributions between the double-labeled slide sets (**A** and **B**) or between tissues from antibiotic-treated (solid line, grey shading) or control animals (dashed line) within slide sets. The vertical dotted line shows the cut-off used to categorize neurons as small (≤ 380 μm^2) or medium to large (>380 μm^2), and corresponds to a calculated cell diameter of 22 µm.

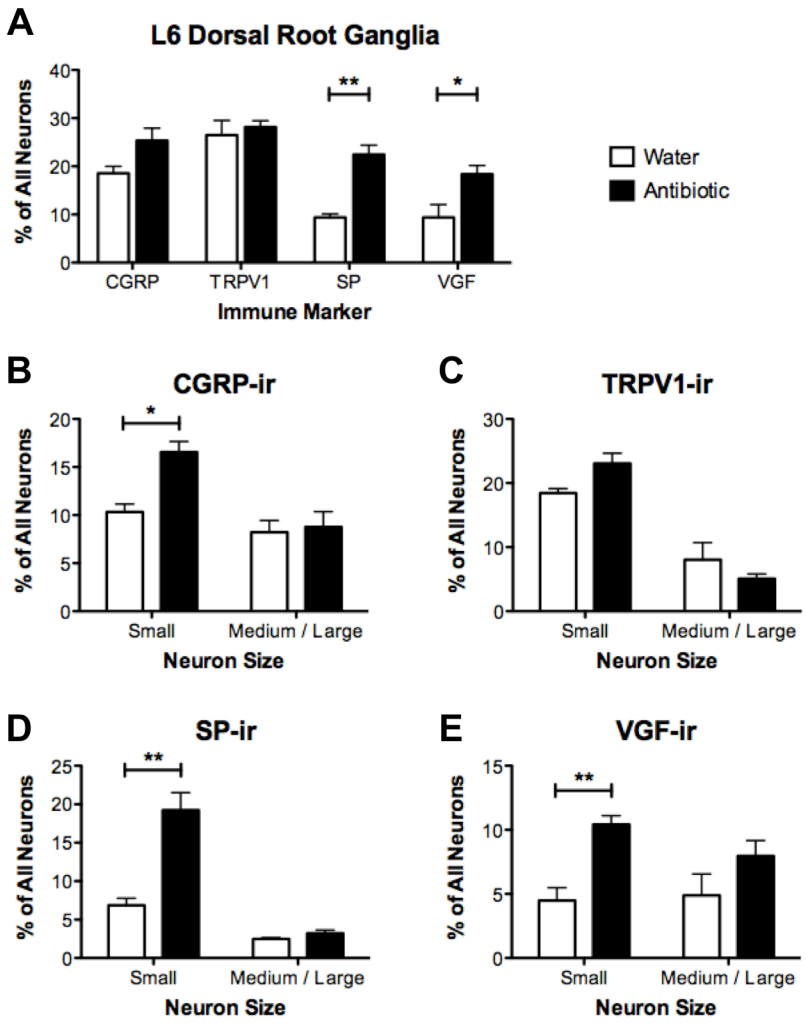

Figure 3-8, Quantification of double-immunofluorescence staining of L6 DRG sensory neurons expressing CGRP and TRPV1 or SP and VGF. **(A)** Antibiotic treatment was associated with significantly increased numbers of neurons immunoreactive to SP and VGF as compared to water-treated controls. **(B)** Size distribution analysis revealed a significant increase in CGRP-positive neurons in antibiotic-treated animals in small (<380 μm^2) neurons. **(C)** TRPV1 was not statistically changed in either neuron size category. **(D)** SP predominated in small sensory neurons and was significantly

increased following antibiotic treatment, while **(E)** VGF was evident in neurons of various size; (unpaired two-tailed t-test, * $p < 0.05$, ** $p < 0.01$).

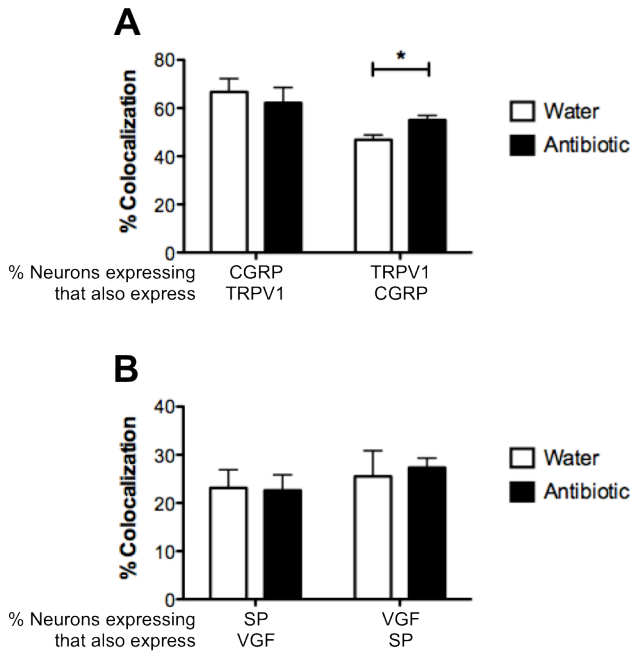

Figure 3-9, The percent colocalization between **(A)** CGRP and TRPV1 and **(B)** SP and VGF is shown for antibiotic- and water-treated mice. There was a significant increase in the percentage of TRPV1-ir neurons also expressing CGRP following antibiotic-treatment; (unpaired two-tailed t-test, * $p < 0.05$).

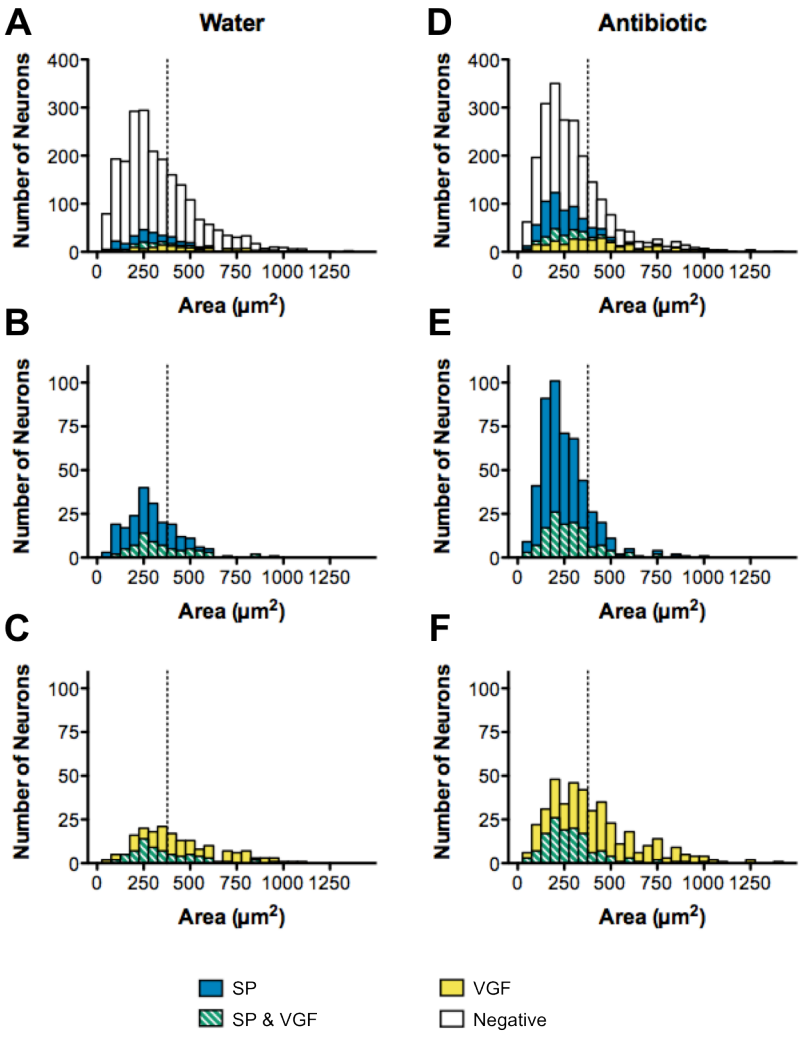

Figure 3-10, Stacked frequency distributions of the combined neuron counts of all animals within each group. The vertical dotted line approximately shows the cut-off used to categorize neurons as small or medium to large (380 μm^2). **(A-C)** In water-treated animals, low numbers of neurons were positive for SP (blue) or VGF (yellow). **(D-F)** In antibiotic-treated animals, the number of neurons positive for SP and/or VGF significantly increased. **(E)** SP immunoreactivity predominated in small sensory neurons, while **(F)** the VGF-derived peptide increased in small- to medium-sized

neurons. The proportion of sensory neurons with colocalization of SP and VGF (green) remained proportional.

Chapter 4

Refinement of methods

Use of binarization in semi-quantitative image analysis

to clarify immunofluorescence positive cutoff values

SUMMARY

A valuable tool in distinguishing sensory neuron subpopulations is the use of fluorescence microscopy. However, image analysis is needed to provide numerical data for statistically comparing fluorescence intensity. Distinguishing what shade of grey should be the cutoff between positive and negative is challenging and potentially subject to bias. To clarify immunofluorescence positive cutoff values for 8-bit images, we sought to develop an inexpensive, reliable, and adaptable method using only readily available software and techniques. Through the use of binarized images, the parameters of the negative cell population could be clearly defined and used to mathematically calculate an appropriate cutoff value. This approach takes advantage of automated processes in ImageJ and Microsoft Excel to expedite analysis, and can be applied to entire sets or to specific subsets of images. Currently, the main drawback of this method is the time investment necessary to create and apply the binarized images; however, it seems likely that this process could also be automated with appropriate macro coding.

INTRODUCTION

The neuron cell bodies in the DRG represent a heterogeneous population of neurons that convey sensory information from the periphery to the central nervous system. These primary afferent neurons are commonly classified by morphological and neurochemical signatures. A valuable tool in distinguishing sensory neuron subpopulations is the use of fluorescence microscopy, where fluorophore-labeled markers and stains are employed to locate interesting features. However, simply stating that the fluorescence appears brighter for a particular cell or treatment group is insufficient. Image analysis is needed to provide numerical data for statistically comparing fluorescence intensity.

The smallest units comprising a digital image are pixels. Each pixel in a fluorescence micrograph is a measurement of the light emitted by the sample from that point in space (Bankhead, 2014). In an 8-bit greyscale image, the intensity of each pixel is derived from a palette of 256 possible shades of grey, ranging from black to white. The pixel values are represented as integers, with values from 0 (black) to 255 (white). Ideally, a histogram of the grey values from a fluorescence image would reveal two distinct clusters: positive pixels from where the sample was emitting light (white) and negative pixels lacking fluorescence (black). In practice, this bimodal distribution is often merged, and distinguishing what shade of grey should be the cutoff between positive and negative is challenging and potentially subject to bias. While dedicated systems have been designed for image analysis in fluorescence immunohistochemistry, many require expensive software and hardware for image acquisition, analysis, and storage (Jensen, 2013).

Reviewing the scientific literature for inexpensive and reliable alternatives for image analysis became unrewarding, as most publications fail to disclose the exact image processing and analyses performed. One of the more commonly cited methods for sensory neuron image analysis was the approach of Fang and colleagues (2006), whereby the numeric intensity values for the sampled cell profiles were normalized to the brightest and dimmest intensity values in the same section or DRG. These relative immunointensity values were correlated to subjective scores to establish the cutoff between positive and negative, which in their case was 20% intensity. While the calculations required for this method are easily employed, application of this method was generally unsatisfying. Normalization of the data does nothing to affect the distribution of the intensity values other than change the units from an integer value to a percentage, and the cutoff value is still entirely subjective.

Semi-quantitative immunohistochemical analysis frequently takes advantage of ImageJ, a Java image processing and analysis program developed by Wayne Rasband and made available in the public domain through the National Institutes of Health (http://imagej.nih.gov/ij/docs/index.html). A multitude of free add-ons that extend the core functionality are also available from various sources. ImageJ can be readily employed to measure intensity values in manually-drawn regions of interest, as needed in analyzing the heterogeneous neuron populations in DRG. However, ImageJ can also be used for segmenting images into objects of interest – in this case, areas of fluorescence – from the background. In the resulting binary image, each pixel can only have one of two values, black or white. The binarized image is generated by identifying

pixels above or below a particular threshold value, which can be calculated from image histograms or manually applied.

As using ImageJ to define segmented regions is likely to be faster, more reproducible, and less biased, we developed a method utilizing binarized images to clarify immunofluorescence positive cutoff values in semi-quantitative image analysis of DRG sensory neurons.

IMAGE ANALYSIS WITH BINARIZATION

Image acquisition. Slide-mounted tissue sections of rat or mouse DRG were sequentially incubated with primary antisera, appropriate combinations of cyanine-dye conjugated secondary antisera, and NeuroTrace® 435/355 Blue Nissl stain (Molecular Probes, Inc., Eugene, Oregon USA), as discussed in detail in earlier chapters. The slides were coverslipped using glycerol and PBS containing 0.1% p-phenylenediamine (Sigma Chemical Co., St. Louis, Missouri USA).

Images were collected using an Olympus FluoView1000 confocal imaging system. Acquisition settings were determined for each color detection channel using the range finder look-up table, where blue pixels represent zero intensity and red pixels represent saturated intensity. The parameters were set so there was no oversaturation in areas of intense fluorescence and offset so the background intensity measured just above zero (Brown, 2007). The same image acquisition settings were maintained across the slide set and used for experimental and control tissues. The region of interest for imaging was visualized on the NeuroTrace channel, and the entire neuron population was

imaged as best possible with non-overlapping fields. Tissue sections were imaged to produce a separate 8-bit greyscale image for each color detection channel per field. In our hands, the red (cyanine-3, Cy3), green (cyanine-2, Cy2), and far-red (cyanine-5, Cy5) channels were used for markers of experimental interest, while the blue channel was used for Nissl-like NeuroTrace labeling. To allow the cell counting to be performed by a blinded investigator, each image set was numbered sequentially and a separate index was maintained to identify the animal number and group.

Image binarization. All greyscale images from a specific antibody label and within a particular color detection channel were compiled into a stack in ImageJ (National Institutes of Health). The image stack was then binarized (i.e. segmented into black and white) using the Auto Threshold ImageJ plugin (version 1.15, Landini G, fiji.sc/Auto_Threshold), which includes sixteen histogram-derived thresholding algorithm options. The threshold was computed based on the stack histogram, allowing data from both control and experimental animals to be considered concurrently, and was applied to all slices in the stack. Given that the stack histogram was typically comprised of a maximum peak near the right end of the histogram with a skew toward the left, the Triangle algorithm derived from the methods of Zack et al. (1977) often best segmented the data. Splitting the stack back into individual images, each binarized version was saved alongside the original greyscale images (Figure 4-1).

Cell counting. Images of the identical microscope field were compiled into stacks of three to seven images in ImageJ, depending on the number of detection channels utilized: greyscale blue (Nissl staining), greyscale red, and binarized red, with the addition of the greyscale and binarized versions of green and far-red as needed.

Manual cell outlining was conducted using the NeuroTrace image, and only cells with a visible nucleus were counted. The area and the mean grey value (MGV; the sum of the grey values of all the pixels in the selection divided by the number of pixels) were simultaneously measured for the outlined region of interest for all images in the stack (Figure 4-2 and Table 4-1).

Data analysis. The data values generated in ImageJ were exported to Microsoft Excel (Mac 2011 version 14.1.0, Microsoft Corporation) for analysis. A typical spreadsheet was composed of at least five columns: image number, cell area, and the MGV of the NeuroTrace, greyscale, and binarized slices. The data in each row represented an individual cell, and the data from all images within the same slide set were compiled. When blinding was no longer necessary, columns for the animal number and experimental groups were added, and the VLOOKUP function was utilized to efficiently translate the information from the image number index (entered into a separate worksheet).

For each experimental marker, a cell had two values: the MGV of the original fluorescence image and the MGV of the binarized image. Grey values of an 8-bit image range from 0 (black) to 255 (white). Ideally, the MGV of the fluorescence image would reveal two distinct neuron populations: positive cells with fluorescence (white) and negative cells lacking fluorescence (black). In practice, this bimodal distribution was often merged (Figure 4-3 A), and distinguishing the populations was challenging. What shade of grey was the appropriate cutoff between positive and negative? This problem was not directly resolved by the use of binarized images, as labels with patchy or granular immunoreactivity patterns still generated a mixture of black and white pixels.

The value in binarized images was not in revealing which cells were positive, but in clearly identifying which cells were negative. A cell was considered negative for a particular marker if the MGV of the binarized channel was 0 (all pixels black). The greyscale MGV of negative cells in the red (Cy3) and green (Cy2) channels typically followed a normal distribution (Figure 4-3 B). It was not uncommon for the negative distribution to be slightly skewed in the far-red (Cy5) channel, possibly due to higher background fluorescence with this detection modality.

By defining the parameters of the negative cell population, the criteria necessary for a cell to be considered positive could be established. Calculation of the mean and standard deviation of the greyscale MGV of the negative cells was expedited by the use of array formulas, which work with a series of data values. For example, consider a data table with values for 100 cells (rows 2 to 101), with the binarized MGV in column B and the greyscale MGV in column C. The mean greyscale MGV of the negative cells could be calculated by:

=AVERAGE(IF((B2:B101=0),C2:C101))

where values from column C (greyscale MGV) are averaged as long as the corresponding value in column B (binarized MGV) is equal to 0. It should be noted that array formulas are finished by holding the CTRL and SHIFT keys while pressing Enter; simply pressing Enter will yield spurious results.

The cutoff to consider a cell positive was defined as 3 standard deviations above the average greyscale MGV of the negative cells of the entire slide set for that particular immune marker and detection channel. This cutoff was universally applied to control and experimental animals alike.

Generating counts of the number of positive cells for a particular animal was facilitated by array formulas. Considering the previous hypothetical data set with binarized MGV data in column B, greyscale MGV data in column C, and the addition of animal identification numbers in column D, the count of positive cells for an individual could be calculated by:

=SUMPRODUCT((B2:B101>0)*(C2:C101>[cutoff])*(D2:D101="ID"))

which will return the number of neurons with a binarized MGV greater than 0 (non-negative), greyscale MGV greater than the calculated cutoff (positive), and with the specific animal identification. The total number of cells per animal can be determined through simpler means, such as the COUNTIF function.

DISCUSSION

This method of determining the positive cutoff value for 8-bit immunofluorescence images relies on histogram-derived algorithms and mathematical calculations using only readily available software. The approach can be applied to entire sets or to specific subsets of images. The binarized images are solely used to define the negative cell population; however, it may be possible to utilize the positive pixel data to establish other

cutoff parameters (e.g. determine whether a certain percentage of pixels being above threshold is informative). The method has been successfully utilized in discriminating populations of cells with various cytoplasmic markers, ranging from granular to patchy to diffuse. It is not known if it would work with purely membranous patterns (Cheuk and Chan, 2004), as the labeling of the periphery may not be sampled as cleanly with the manual cell outlining necessary in sensory neuron quantification.

The cutoff was set at 3 standard deviations above the mean of the negative population. A cutoff was still utilized as fluorescent signal noise could potentially "contaminate" a binarized cell, resulting in a non-zero MGV in a cell that would not otherwise be viewed as positive (as seen in the Cy3 channel of Neuron 3 in Figure 4-2). The choice in number of standard deviations was based on the conservative three-sigma rule-of-thumb, whereby data values falling more than 3 standard deviations from the mean of the negative population are likely outliers, in this case representing the other (positive) population (Nikulin, 2001).

Occasionally, when all images from a color detection channel were compiled, slide-to-slide variability in fluorescence intensity became evident. This variability precluded applying the same threshold to all images. However, this was easily remedied by considering each group of images from a particular slide separately. For this reason, it may be prudent to ensure control and experimental tissues are imaged from each slide.

The main drawback of this method is the time investment necessary to create the binarized images. When using more than one detection channel, the imaging system software creates a folder for each imaged field with separate images typically labeled as

"ImageNumber_C001" for the first channel, "ImageNumber_C002" for channel two, and so on. To create the image stack in ImageJ, copies of all images for a particular channel need to be sorted into a single folder (e.g. Folder C001). After the stack has been imported, thresholded, and split back into individual images, these images need to be saved and resorted back into their respective image number folders. Depending on the number of animals and species-related size differences in the DRG, complete imaging for a single DRG in a study may require at least 40 but often well over 100 images. Sorting of images back and forth is tedious and requires attentive naming conventions to ensure the original greyscale data is not lost. However, it seems likely that this process could be automated with appropriate macro coding.

While relying predominantly on mathematically-derived cutoffs to categorize cells as positive or negative, a subjective component could not be entirely eliminated. Segmenting the images into black and white was performed using an automated thresholding function, but the choice of algorithm and determination whether the threshold level was appropriate still relied on visual inspection.

CONCLUSIONS

The inclusion of binarized image values in semi-quantitative image analysis of DRG sensory neurons provides the necessary information to clearly define to parameters of the negative cell population and to objectively calculate the positive immunofluorescence cutoff value. The method utilizes only readily available software and is inexpensive, reliable, and adaptable. Currently, the main drawback of this method is the time

investment necessary to create and apply the binarized images; however, it seems likely that this process could also be automated to further expedite analysis.

FIGURES

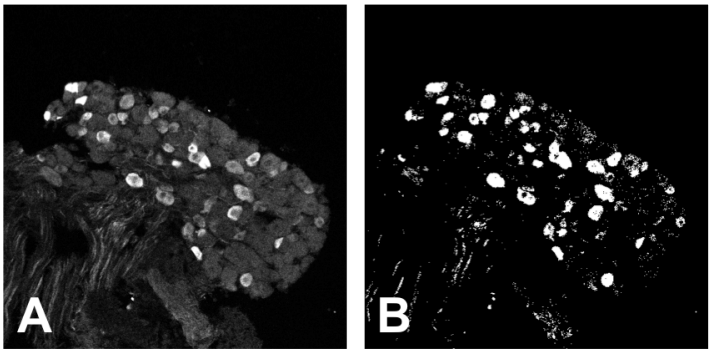

Figure 4-1, Representative immunofluorescence photomicrograph of a mouse DRG, showing **(A)** the original 8-bit greyscale image and **(B)** the resulting binarized black and white image.

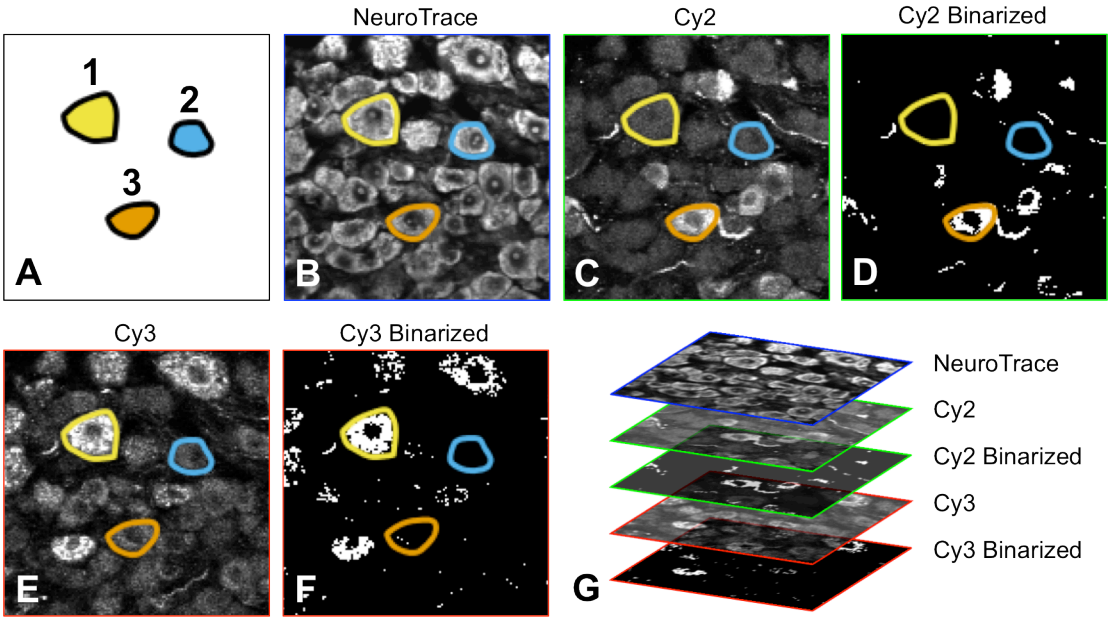

Figure 4-2, Counting of DRG sensory neurons**. (A)** Three cells were manually outlined and numbered for reference in Table 4-1, as shown in the layer mask. An ImageJ stack would be composed of the following slices: **(B)** NeuroTrace, **(C, E)** the original greyscale images of the other detection channels, and **(D, F)** the binarized images of the other detection images. Based on the binarized images, Neuron 1 is likely positive for Cy3 and negative for Cy2. Neuron 2 is negative in both channels. Neuron 3 is likely positive for Cy2 and negative for Cy3, although there are a few white pixels in the binarized cell. **(G)** An ImageJ stack is a set of related images or layers (slices) displayed in a single window. Only one slice is active at any one time. Manual cell outlining is performed on the top slice (NeuroTrace) to define a region of interest. By aligning the images in a stack, the MGV can be measured in the same region of interest in each slice simultaneously.

Neuron	Area (μm^2)	Mean Grey Value			
		Cy2	Cy2 Bin	Cy3	Cy3 Bin
1	809.8	71.52	0	162.85	145.71
2	461.2	63.98	0	58.70	0
3	543.0	152.84	123.15	69.59	2.17

Table 4-1, The area and mean grey values (MGV) for the three representative neurons shown in Figure 4-2. Neuron 1 (yellow) is likely positive on the Cy3 channel but negative for Cy2. Neuron 2 (blue) is negative for both markers, as evidenced by the completely black (0) binarized versions. Neuron 3 (orange) is likely positive for Cy2 and negative for Cy3. The non-zero value for the binarized Cy3 results from the few scattered positive pixels, which appear insufficient to otherwise consider the neuron positive. The MGV of the NeuroTrace channel is not informative and therefore not shown.

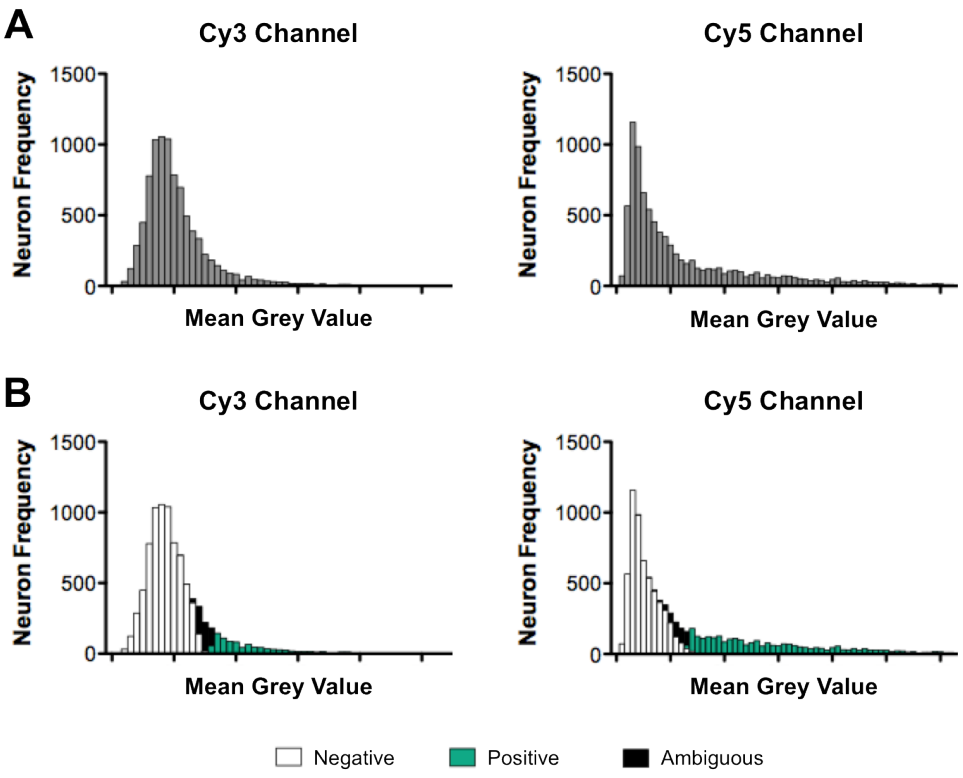

Figure 4-3, Representative frequency distributions of sensory neuron MGV from two detection channels. **(A)** The bimodal distribution of positive and negative neurons was often merged into a single skewed peak. **(B)** Stacked frequency distributions show the distribution of negative cells (white) typically followed a normal distribution for Cy3 (and Cy2, not shown) and often a slightly skewed distribution for Cy5. The cutoff to consider a cell positive (green) was defined as 3 standard deviations above the average greyscale MGV of the negative cells. Depending on the thresholding method and the amount of noise in the image, variable numbers of cells were considered ambiguous (black). These unknowns displayed positive pixels in the binarized image, but had an otherwise insufficiently high MGV to be considered positive.

Chapter 4

Refinement of methods

Critical examination of the simplified up-down (SUDO)

method of mechanical sensitivity assessment

SUMMARY

Mechanosensitivity is commonly assayed in animal models utilized in pain research. While frequently used to assess paw withdrawal thresholds, the classical up-down method of von Frey filament presentation is time-consuming and often inconsistent in the number of stimuli per animal. The simplified up-down (SUDO) method was recently reported as a reliable, efficient, user-friendly modification that provides greater standardization; however, the provided statistical justification was inadequate for comparing the two methods. We sought to validate the SUDO method for potential future use by investigating the agreement between the original and new methods and determining whether usable threshold estimates could be derived from retrospective data from mice and rats using the SUDO approach. The limits of agreement (-1.3 and 1.2 filament steps) did not preclude the SUDO method being used in place of the original method when assessing models of nerve injury-induced hypersensitivity, but may be too broad for other experimental applications. Further work is needed to ascertain whether the proposed standardization of the testing experience reduces intra-subject variability in threshold values.

INTRODUCTION

A commonly used assay for testing mechanical sensitivity involves the application of a von Frey fiber to a convenient body part, such as the hind paw, in an attempt to evoke a behavioral response. While various paradigms on the use of von Frey filaments have been described, the most widely applied in pain research is the up-down method of Dixon (Dixon, 1980) as applied to rodents by Chaplan and colleagues (1994). A recent literature survey found that in reports where von Frey filaments were used to assess mechanical sensitivity, over 60% used the up-down method or a modified up-down method to determine mechanical thresholds (Mills et al., 2012).

Testing is conducted with a conventional set of eight different von Frey filaments. These calibrated nylon monofilaments exert a reproducible vertical force level when pressed to the point of bending. The series of filaments used in the up-down method have logarithmically incremental stiffness, as indicated by the handle markings, with ranges of 0.41 – 15.14g in rats or 0.03 – 3.63g in mice (Table 4-2 and Figure 4-4). The maximum stimulus intensity is subject to physical limitations, as with increasing stiffness filaments are more likely to raise the entire limb of the animal rather than buckle.

For the up-down method, filaments are applied in sequential order starting at the middle of the series, with subsequent applications dependent on the prior response. If there is no response, the stimulus force is increased by one step in filament size. If a positive response (e.g. sharp withdrawal of the paw) is noted, the stimulus is decremented by one step. Stimuli are presented at intervals of 30 seconds or longer to allow resolution of any previous response. Testing is continued until six responses in the immediate

vicinity of the 50% withdrawal threshold are obtained or until the series is exhausted in either direction. The 50% paw withdrawal threshold (PWT) is determined as:

$$PWT = X_f + \kappa\delta$$

where X_f is the value of the final von Frey filament employed (in log units), κ is the tabular Dixon value for the positive/negative pattern, and δ is the mean difference (in log units) between stimuli (Mills et al., 2012). The threshold is converted from log units to gram units of force by:

$$50\%\ g\ threshold = (10^{(PWT)})/10{,}000$$

While a widely used method in pain research, the up-down method is not without faults. Depending on the particular pattern of positive and negative responses, the number of stimuli required for each animal will vary from four to nine per testing session, so all animals do not receive the same testing experience. Particularly with large cohorts of animals, resolving lengthy positive/negative response patterns is time-consuming. Attention must also be paid to accurately tracking and recording the response pattern throughout the trial, and then correctly tabulating the response pattern from the Dixon values.

To address these issues, Bonin and colleagues (2014) recently published a simplified up-down method (SUDO) for measuring mechanical sensitivity in rodents, which the authors posit is an efficient, user-friendly modification of the established up-down method. Key differences are that a fixed number of five stimuli are used per trial and the

PWT is estimated from the filament value and response to the fifth stimulus without the use of the Dixon look-up table. The authors allow that the proposed method lacks the precision in threshold calculation of the original up-down method, but suggest the simplified estimation should be sufficient.

To validate and inform its future use, we critically evaluated the mathematical basis of the novel SUDO method. Using archival mechanosensitivity measurements from mice and rats, we retrospectively compared the classical up-down method of Dixon/Chaplan to the SUDO method to determine whether the method produced usable PWT estimates.

METHODS

Retrospective von Frey data available for analysis included 512 measurements from rats (Sprague-Dawley, n = 36) and 1145 measurements from mice (C57BL/6 or congenic strains, n = 25; ICR, n = 49; mixed genetic background, n = 15). Testing was performed by the same experimenter following standard procedures: animals were allowed to acclimate to the testing room within their home cages for at least 40 minutes before being placed individually within the testing apparatus, where they were given at least 20 minutes to adjust to the testing environment. Efforts were taken to minimize auditory, visual, and olfactory disturbances in the testing room. The number of testing sessions per animal following baseline measurements ranged from 3 to 9 depending on the particular experimental design. Tests were performed on nonconsecutive days, typically spaced seven days apart. One response pattern was collected per animal at each testing session and was used to calculate the subject's PWT.

Data were entered into a spreadsheet for analysis. The PWT estimate was calculated from the response pattern using the methods described in Chaplan et al. or Bonin et al. Statistical tests performed included correlation, Bland-Altman method comparison, area under curve, one-way ANOVA with post-hoc Bonferroni's multiple comparison test, and two-way repeated measures ANOVA with post-hoc Bonferroni's multiple comparison test (GraphPad Prism version 5.0d, GraphPad Software, San Diego, California USA, www.graphpad.com). A p value of < 0.05 was considered significant.

RESULTS

Response patterns. The responses to sequential von Frey stimuli are recorded using the convention of X = withdrawal (positive) and O = no withdrawal (negative). The resulting pattern is compared against Dixon's lookup table of maximum likelihood estimates to determine the value of κ when calculating the PWT. The pattern cannot exceed the stimulus set in either direction and optimally contains six values in the vicinity of the threshold. If the initial response is positive (X), then this and the next five responses are considered the critical six values. If the initial response is negative (O), the threshold must be crossed (OX) and then the next four responses will complete the six critical values. Since the initial stimulus is in the middle of the series, the pattern length will vary from a minimum of four (XXXX, filaments 4-3-2-1) to a maximum of nine if the threshold is crossed at the seventh to the eighth filaments (such as in OOOOXOXOX, filaments 4-5-6-7-8-7-8-7-8).

There are a finite number of patterns possible within the boundaries of this testing paradigm. The lookup table in Chaplan et al. provides the tabular value for 250

positive/negative patterns. However, this list includes pattern options that exceed the upper or lower extreme of the stimulus series as well as truncated patterns that do not contain six critical values. For practical purposes, the up-down pattern list may be whittled down to 90 possible outcomes (Table 4-3).

Unlike the up-down method, the SUDO method maintains a fixed number of stimulus applications, so the pattern length has a maximum of five. Otherwise, testing progresses in a stepwise, sequential fashion according to the original method. Thus the SUDO pattern list consists of 31 possible outcomes (Table 4-4). Instead of using the tabular maximum likelihood estimate, an adjustment factor of ±0.5 is used, with the sign depending on the response to the fifth filament (positive for O and negative for X). To further simplify the calculations, the filaments are assigned whole number values instead of using the filament handle marking, with the corresponding average step size set at 1.

Correlation and agreement. Given that each assay yields a discrete set of values and the SUDO pattern can be derived from the longer up-down pattern, the tests can be compared over the whole range of possible values without the need for real-world rodent data. The PWT was calculated as shown above for the 90 up-down method patterns and the corresponding abridged SUDO patterns. To maintain the same units between methods, filaments were designated as the whole numbers 1 through 8 in ascending order of stiffness, which also kept the mean difference between stimuli at 1. The value of the adjustment factor κ was either the tabular Dixon value or ±0.5. In keeping with the findings of Bonin et al., the PWT estimates derived from the SUDO method correlate well with those from Dixon/Chaplan (Pearson $r = 0.942$, $p < 0.0001$; Figure 4-5 A).

However, while this finding of strong correlation shows that the two variables are linearly related, it does not demonstrate how well the results of the two methods agree.

Expanding on the findings of Bonin et al., we used the graphical method advocated by Bland and Altman (Bland and Altman, 1986) to plot the difference scores of the two measurements of PWT against the average of the two measurements in order to evaluate agreement (Figure 4-5 B). The average discrepancy or bias between the methods was -0.05 filament steps and the 95% limits of agreement were -1.3 to 1.2. Thus the SUDO method tends to give a slightly lower PWT estimate but may be 1.3 filament steps below or 1.2 filament steps above the PWT yielded by the Dixon/Chaplan method. By the Bland and Altman approach, the smaller the range between the two limits, the better the agreement.

The developers of the SUDO method advocated the constant adjustment factor of ±0.5 as it rendered the pattern lookup table unnecessary and simplified the calculations for the PWT estimate. The selection of the value 0.5 was based on the strength of correlation between the Dixon/Chaplan score and the resulting SUDO score. We questioned whether a different constant adjustment factor would improve the agreement between the methods. Using an iterative approach, the adjustment factor was varied in increments of 0.01 to determine the 95% limits of agreement. The narrowest range in the limits of agreement was obtained with a value of ±0.59, with a bias of -0.04 filament steps and 95% limits of agreement of -1.31 to 1.23 (Figure 4-6). However, the advantage of using this over of the conceptually simple value of 0.5 was negligible.

Given the lookup table in Chaplan et al. provides the tabular value for each of the positive/negative patterns in the SUDO outcome list, we next investigated whether using the corresponding maximum likelihood estimates instead of a constant adjustment factor would improve the agreement between the full pattern versus using a fixed number of stimuli. Calculations were performed as before using whole number designations for filaments (Figure 4-7). The PWT estimates derived from the modified SUDO method using the Dixon tabular values had slightly stronger correlation with the PWT estimates from Dixon/Chaplan (Pearson $r = 0.954$, $p < 0.0001$). The bias between the methods was further from zero (-0.14 filament steps), but the 95% limits of agreement were improved to -1.2 to 1.0. So even with using the tabular Dixon values, the five stimuli pattern promoted in the SUDO method tends to give a slightly lower PWT estimate and may be 1.2 filament steps below or 1.0 filament steps above the PWT yielded by the Dixon/Chaplan method.

Despite several mathematical approaches, limiting the response pattern to five stimuli results in limits of agreement with the complete pattern of around one full filament step. In assessing agreement between methods, the question of how close the measurements need to be is based on clinical context and is not determined statistically. If a difference of 1.0 to 1.3 filament steps in the estimated PWT does not meaningfully affect the interpretation of the results, then the SUDO method could be used as a replacement for the original method.

Retrospective data analysis. To frame the question within clinical context, we applied the SUDO method to mechanosensitivity measurements from rats and mice. The original measurements were conducted following the Dixon/Chaplan method and were

obtained by the same experimenter from animals at baseline or with varying degrees of experimental hypersensitivity. The resulting pooled data set was composed of 1657 positive/negative patterns from 125 individual rats and mice. All response patterns complied with the parameters of the Dixon/Chaplan method; accordingly, pattern length varied from four to nine. The average number of stimuli per trial was 6.3 with a standard deviation of 1.7. The total number of stimuli within the pattern set was 10,363. Filament presentations exceeding the advocated SUDO pattern length of five accounted for 21.3% of the total number of stimuli. If the SUDO method provides a reasonable estimate of the PWT, the reduction in the needed number of stimuli as compared to the original up-down method should result in more efficient use of experimenter time, particularly with large cohorts of animals.

The proponents of the SUDO method suggested that repeated testing could result in a change in responsiveness of the animal, and keeping the number of stimuli constant would help negate this potential confound. To ascertain whether following the up-down method could result in a change in responsiveness, from the retrospective data pool we identified a subset of control animals without experimental hypersensitivity that were tested at consistent intervals. The resulting subset was composed of 20 mice tested at baseline and then once weekly for three weeks (Figure 4-8). The average PWT decreased over time with increasing variability (baseline = 7.85 ± 0.09; day 21 = 7.43 ± 0.23; average ± SEM), although this trend was not statistically significant by one way ANOVA with post-hoc Bonferroni multiple comparison test ($p = 0.20$). The average change in PWT over three weeks was less than one filament step. From the limited data set, it was not clear if this threshold decay would progress with time, if the downward

drift in the control PWT would have significance in experimental context, or if animal responsiveness would be different if testing under the SUDO method.

In the complete pool of positive/negative patterns, the 90 possible patterns within the Dixon/Chaplan paradigm were not represented with equal frequency. Four patterns disproportionately accounted for 65.9% of the data set – XXXX, OOOOO, OOOOXOO, and OOOOXOXOX – and sixteen patterns were absent. Given the disparity in pattern occurrence, we questioned if this would influence subsequent assessments of correlation and agreement. The PWT estimates were calculated as above using whole number designations for the filaments and an adjustment factor of either the tabular Dixon value or ±0.5 (Figure 4-9). The strength of the correlation between the Dixon/Chaplan and SUDO scores was improved (Pearson $r = 0.980$, $p < 0.0001$), similar to the findings of Bonin et al. when the SUDO method was used to reanalyze existing measurements. The bias between the methods was further from zero (-0.19 filament steps), and the 95% limits of agreement were narrowed to -1.1 to 0.75. However, this still implies a potential difference in the estimated PWT of up to a full filament step.

To determine if the difference in the estimated PWT meaningfully affects the interpretation of the clinical results, we reanalyzed data within specific experiments. For each cohort, PWT estimates were calculated separately following the Dixon/Chaplan and SUDO methods. The final data were analyzed using two-way repeated measures ANOVA (time x treatment) with post-hoc Bonferroni multiple comparison test and by quantifying the area under the PWT curve (AUC) followed by one-way ANOVA. The three experiments selected for evaluation included animals with profound experimental hypersensitivity, no appreciable hypersensitivity, and moderate, variable hypersensitivity

as compared to non-allodynic controls. Two experiments utilized the murine spared nerve injury (SNI) model of peripheral neuropathic pain (Decosterd et al., 2000; Pertin et al., 2012), while the third experiment tested a potential hypersensitivity-inducing treatment in animals without nerve damage.

The first experiment evaluated four treatment groups with SNI against a control sham-operated group ($n = 4 – 6$). According to the original Dixon/Chaplan analysis, the mean PWT was significantly decreased in all groups with nerve injury as compared to the sham-operated control group at all time points evaluated following surgery ($p < 0.0001$; Figure 4-10 A). However, at no time post-operatively were the SNI groups statistically different from each other. Depending on the experimental context, a single measurement derived from the repeated measures may be considered more biologically meaningful. For hypersensitivity data, the most accessible is the AUC for each subject. Similar to the repeated measures analysis, the average AUC was significantly decreased in all SNI groups as compared to the sham-operated control ($p < 0.0001$), while there was no statistical difference between SNI groups (Figure 4-10 C).

We next performed all PWT calculations from the experimental data following the SUDO method to test whether levels of significance were changed. A slight upward shift was apparent in the PWT curves for all groups (Figure 4-10 B), which was also evident as increases in the calculated AUC means (Figure 4-10 C). However, the statistical relationships were consistent with the original analyses; reanalysis by the SUDO method did not cause statistical significance to be altered.

The second experiment evaluated two experimental treatments in animals without nerve injury compared to untreated controls (n = 7 – 8). Unlike the first experiment, no hypersensitivity was evident in either treatment group by either repeated-measures testing or by AUC analysis (Figure 4-11 A, C). Reanalysis by the SUDO method yielded observable variability in the PWT curves, but any differences between the groups remained non-statistically significant (Figure 4-11 B, C).

Given that the SUDO method resulted in no meaningful difference in interpretation at clinical extremes, we next questioned whether the same could be said for data in the middle of the PWT range. The third experiment evaluated two variations of the spared nerve injury surgery as compared to sham-operated controls in which recovery was expected in one of the injured groups (n = 6 – 9). The PWT of one surgical group was significantly decreased at all later time points, but only temporarily for the second surgical group (Figure 4-12 A). While perhaps less informative in this setting, the average AUC for both nerve-injured groups was also significantly decreased compared to sham-operated subjects (Figure 4-12 C). When reanalyzed by the SUDO method, statistical significance was not lost, but the strength of the evidence was diminished as indicated by larger p values (Figure 4-12 B, C).

DISCUSSION

We questioned the reliability of the recently proposed SUDO method for mechanosensitivity measurements in rodents. Our analysis generally supports the findings of Bonin and colleagues and expands upon the limitations of the testing method.

The only statistical comparison between the new and old techniques provided in the original report was the correlation coefficient. The use of the correlation coefficient for this type of comparison is misleading, as it measures the relationship between the values but not the agreement (Bland and Altman, 1986). For example, if the SUDO method always produced PWT estimates twice as big as the Dixon/Chaplan method, the PWT values would be highly correlated but would not agree. We wanted to know if the difference in the duplicate measurements was trivial, in which case the methods could be used interchangeably, or serious enough to preclude the meaningful interpretation of the results. Using Bland-Altman method comparison, we found the PWT estimate yielded by the SUDO method may be up to 1.3 filament steps above or below the Dixon/Chaplan PWT estimate. From clinical experience with neuropathic pain models, nerve injury typically produces tactile allodynia characterized by PWT estimates falling below the 50% point of the filament series, while the PWT estimates from non-injured controls stay within the stiffest three filaments of the series. In these cases, the disparity between hypersensitive and non-hypersensitive values should be sufficient to excuse the lack of precision from the SUDO method, which was evident from our retrospective data analysis. However, if more subtle variations in tactile sensitivity are being investigated, the potential difference of a full filament step in the final measurement may warrant following the Dixon/Chaplan method instead of the abridged method.

Another modification to streamline PWT estimate calculations was the use of a constant adjustment of ±0.5. While we explored other adjustment factors, including other constants between 0 and 1 as well as values from the Dixon look-up table, no substantial improvements in the final values were appreciated. The value of 0.5 is conceptually simple and facilitates easy mathematical derivations, particularly when

using whole number designations for the filaments and a filament step difference of 1.0. We elected to continue to use this adjustment factor in subsequent calculations due to the ease of use.

When examining archival von Frey measurements from rodents with varying levels of hypersensitivity, it was noted that response patterns did not occur with equal frequency. Patterns that did not occur within the data set tended to either represent the middle of the filament series (PWT estimates at filaments 3 – 5) or complete reversals in response, such as OOOOXXXXX. The patterns with the highest frequency were either near or at the maximum extreme of the series or the minimum extreme of the series. The most common cause of experimental hypersensitivity in the data set was standardized surgical nerve injury, which typically results in robust tactile allodynia. Given the inclusion of non-allodynic control animals, it is not surprising that measurements most often reflected either a high “normal” threshold or very low allodynic threshold, skirting the middle of the range. Other models of experimental hypersensitivity may better encompass the full range of possible PWT values. It seems likely that the experimental model may have more to do with pattern occurrence than the experience of the examiner, which contradicts the implication of Bonin et al. However, clarification of this issue would require further studies.

Another proposed advantage of the SUDO method is efficient use of experimenter time. Limiting the total number of stimuli recorded in the retrospective measurements to five would have resulted in 21.3% fewer filament presentations. If using a rough estimate of 30 seconds of experimenter time per filament presentation, generation of all the response patterns in the pooled retrospective data set required approximately 86 hours

of experimenter time, or an average of 3.12 minutes per pattern, which the SUDO method would have reduced to 68 hours or 2.46 average minutes per pattern. The standardized number of filament presentations would also influence the length of time animals spend within the testing apparatus, as removal of animals from their individual enclosures can be disruptive. All subjects remain on the testing apparatus until complete response patterns are obtained for the entire cohort. Using the same rough time estimate, twenty animals all representing the extremes of pattern length would take anywhere from 40 to 90 minutes to generate a complete response pattern for each subject. The SUDO method would limit this time to 50 minutes. Standardizing the time animals spent within the testing enclosures would eliminate a potential source of bias, particularly if animals within an experiment needed to be tested in batches due to space limitations in the testing area.

Prolonged testing sessions and variability in the number of stimuli have been identified as confounds that may result in a change in animal responsiveness over time (Chaplan et al., 1994). While unable to explore whether threshold decay is more or less evident in animals tested by the SUDO method, we attempted to determine whether changing thresholds were apparent in animals tested by the Dixon/Chaplan method. While limited by the number of animals that met the inclusion criteria, analysis did reveal a slight downward trend in the PWT that was not statistically significant. It would be interesting to determine if a constant number of filament presentations, fixed time in the testing apparatus, or both reduced intra-subject variability in PWT estimates over time.

An alternative method for measuring tactile sensitivity not addressed in the discussion of the SUDO method is to use an electronic von Frey apparatus instead of von Frey

filaments (Cunha et al., 2004; Martinov et al., 2013). An electronic anesthesiometer consists of a hand-held pressure meter fitted with a polypropylene tip of uniform diameter and suitable rigidity for the species being tested. The probe tip is applied with increasing force and measures the force when the paw is withdrawn. The experimental withdrawal threshold is typically calculated from the average of three such measurements. Advantages of electronic von Frey over classical filaments include not needing to switch between filament sizes during testing, fewer stimuli needed per trial, and availability of measurements outside the range physically allowed by filaments. In practice, electronic von Frey should provide the same improvements to stimuli presentation, time consumption, and mathematical complexity as the SUDO method without necessarily sacrificing precision in the threshold calculations.

However, electronic von Frey is not without disadvantages (as discussed in Chapter 2). The experimenter learning curve is steep and sufficient training is necessary to reach internal consistency in the application of probe force. The equipment must be appropriate for the species being tested and the electronic device requires prior calibration and consistent maintenance. The initial cost for the equipment is also considerably higher than for classical filaments: a recent price quote showed a 7-fold higher investment for an electronic von Frey anesthesiometer versus a standard 20-filament kit ($2,995.00 and $426.00, respectively; Stoelting Co., Wood Dale, Illinois USA, www.stoeltingco.com). To our knowledge, no studies are available investigating the agreement in rodent PWT estimates between electronic von Frey and either the Dixon/Chaplan up-down method or the SUDO method.

CONCLUSIONS

The SUDO method for mechanosensitivity testing using von Frey filaments provides a reasonable alternative to the Dixon/Chaplan up-down method, although some degree of precision is sacrificed for time efficiency and user-friendliness. The method appears best suited to experiments where robust hypersensitivity is expected and larger cohorts of animals require testing; the limits of agreement may be too broad for studies anticipating more subtle differences. Standard methods for electronic von Frey usage provide many of the same advantages, but the necessary equipment and expertise may not be as readily available. Further testing is required to determine whether the SUDO method reduces intra-subject variability and threshold decay over serial trials.

FIGURES

	Rats		Mice	
Filament	**Handle marking**	**Force (g)**	**Handle marking**	**Force (g)**
1	3.61	0.4	2.44	0.04
2	3.84	0.6	2.83	0.07
3	4.08	1.0	3.22	0.16
4	4.31	2.0	3.61	0.4
5	4.56	4.0	3.84	0.6
6	4.74	6.0	4.08	1.0
7	4.93	8.0	4.31	2.0
8	5.18	15.0	4.56	4.0

Table 4-2, Standard von Frey filament series for rats and mice. Traditionally, the handle marking is related to the bending force of the filament, calculated by Log_{10} of (10 x force in milligrams).

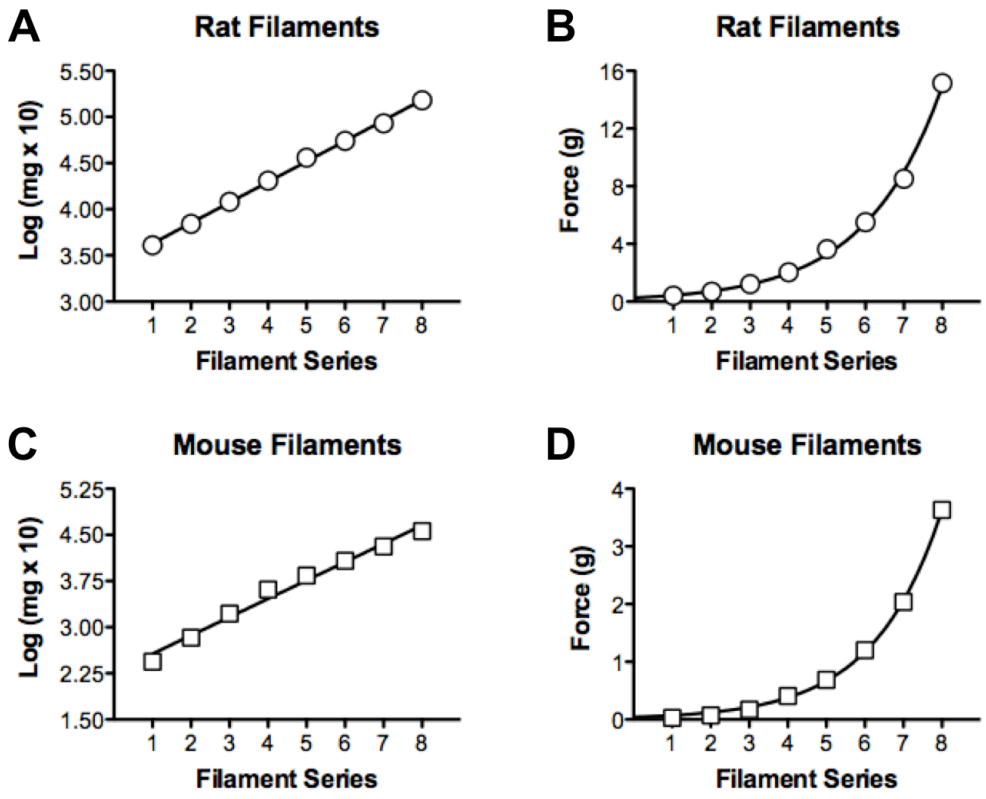

Figure 4-4, The series of filaments used in the up-down method have logarithmically incremental stiffness. The bending forces for the rat and mouse series are shown using a logarithmic scale **(A, C)** and a linear scale **(B, D)**.

Pattern	Value for κ	Pattern	Value for κ	Pattern	Value for κ
OOOOO	0.000	OOXOOOX	-1.247	OXXXXX	0.893
OOOOXOO	0.315	OOXOOXO	0.380	XOOOOO	-0.893
OOOOXOXOO	0.040	OOXOOXX	-0.144	XOOOOX	-1.603
OOOOXOXOX	-0.453	OOXOXOO	0.039	XOOOXO	0.043
OOOOXOXXO	1.248	OOXOXOX	-0.458	XOOOXX	-0.500
OOOOXOXXX	0.758	OOXOXXO	1.237	XOOXOO	-0.296
OOOOXXOOO	-0.263	OOXOXXX	0.732	XOOXOX	-0.831
OOOOXXOOX	-0.752	OOXXOOO	-0.266	XOOXXO	0.831
OOOOXXOXO	0.954	OOXXOOX	-0.763	XOOXXX	0.296
OOOOXXOXX	0.504	OOXXOXO	0.935	XOXOOO	-0.611
OOOOXXXOO	0.681	OOXXOXX	0.463	XOXOOX	-1.169
OOOOXXXOX	0.252	OOXXXOO	0.648	XOXOXO	0.500
OOOOXXXXO	2.014	OOXXXOX	0.187	XOXOXX	-0.022
OOOOXXXXX	1.496	OOXXXXO	1.917	XOXXOO	0.169
OOOXOOO	-0.154	OOXXXXX	1.329	XOXXOX	-0.372
OOOXOOXO	0.381	OXOOOO	-0.547	XOXXXO	1.250
OOOXOOXX	-0.142	OXOOOX	-1.250	XOXXXX	0.547
OOOXOXOO	0.040	OXOOXO	0.372	XXOOOO	-0.897
OOOXOXOX	-0.453	OXOOXX	-0.169	XXOOOX	-1.500
OOOXOXXO	1.247	OXOXOO	0.022	XXOOXO	0.169
OOOXOXXX	0.756	OXOXOX	-0.500	XXOOXX	-0.372
OOOXXOOO	-0.263	OXOXXO	1.169	XXOXOO	-0.169
OOOXXOOX	-0.753	OXOXXX	0.611	XXOXOX	-0.737
OOOXXOXO	0.952	OXXOOO	-0.296	XXOXXO	0.861
OOOXXOXX	0.500	OXXOOX	-0.831	XXOXXX	0.154
OOOXXXOO	0.678	OXXOXO	0.831	XXXOOO	-0.500
OOOXXXOX	0.244	OXXOXX	0.296	XXXOOX	-1.139
OOOXXXXO	2.000	OXXXOO	0.500	XXXOXO	0.432
OOOXXXXX	1.465	OXXXOX	-0.043	XXXOXX	-0.315
OOXOOOO	-0.547	OXXXXO	1.603	XXXX	-1.000

Table 4-3, The 90 relevant outcomes in Dixon's lookup table of maximum likelihood estimates.

Pattern	Value for κ	Pattern	Value for κ
OOOOO	0.5	XOOOO	0.5
OOOOX	-0.5	XOOOX	-0.5
OOOXO	0.5	XOOXO	0.5
OOOXX	-0.5	XOOXX	-0.5
OOXOO	0.5	XOXOO	0.5
OOXOX	-0.5	XOXOX	-0.5
OOXXO	0.5	XOXXO	0.5
OOXXX	-0.5	XOXXX	-0.5
OXOOO	0.5	XXOOO	0.5
OXOOX	-0.5	XXOOX	-0.5
OXOXO	0.5	XXOXO	0.5
OXOXX	-0.5	XXOXX	-0.5
OXXOO	0.5	XXXOO	0.5
OXXOX	-0.5	XXXOX	-0.5
OXXXO	0.5	XXXX	-0.5
OXXXX	-0.5		

Table 4-4, The 31 possible outcomes and adjustment factors in the SUDO method.

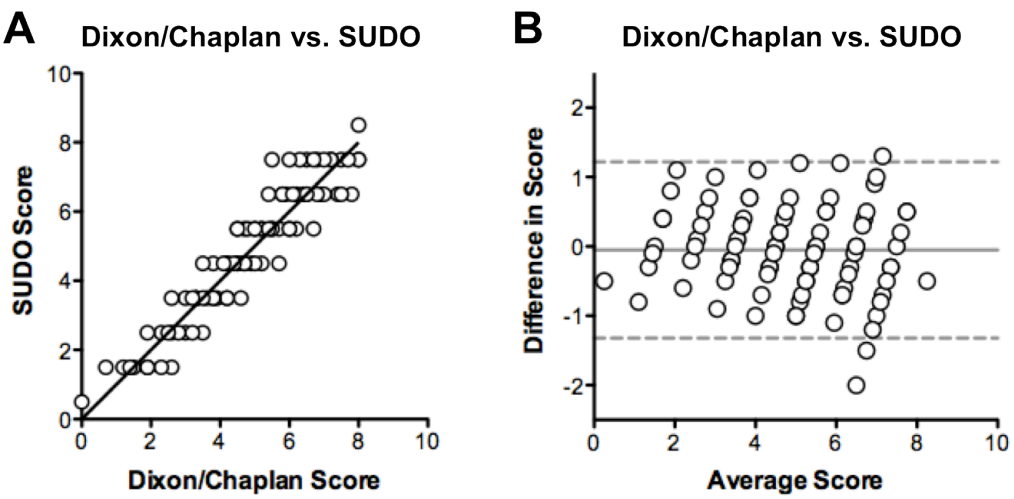

Figure 4-5, Analysis of the ninety potential outcome values of the Dixon/Chaplan up-down method and the corresponding SUDO value (using an adjustment factor of ±0.5)**.** **(A)** The outcome values of the Dixon/Chaplan up-down method and the corresponding calculated SUDO value, shown with a line of equality. The two methods demonstrate strong correlation (Pearson r = 0.942, $p < 0.0001$). **(B)** Bland-Altman plot of the same set of discrete values. The solid grey line represents the average discrepancy or bias (-0.05 filament steps) and the dashed grey greys represent the 95% limits of agreement (two standard deviations above or below the mean). The SUDO method tends to give a slightly lower PWT estimate but may be 1.3 filament steps below or 1.2 filament steps above the PWT yielded by the Dixon/Chaplan method.

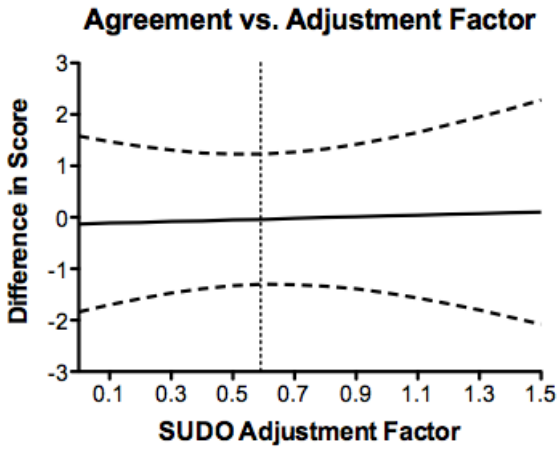

Figure 4-6, By the Bland and Altman approach, the smaller the range between the two limits (dashed lines), the better the agreement. Iteratively varying the SUDO adjustment factor in increments of 0.01 revealed the narrowest range in the limits of agreement between the Dixon/Chaplan and SUDO methods was obtained with a value of ±0.59. The advantage of this value over the conceptually simple value of 0.5 was negligible.

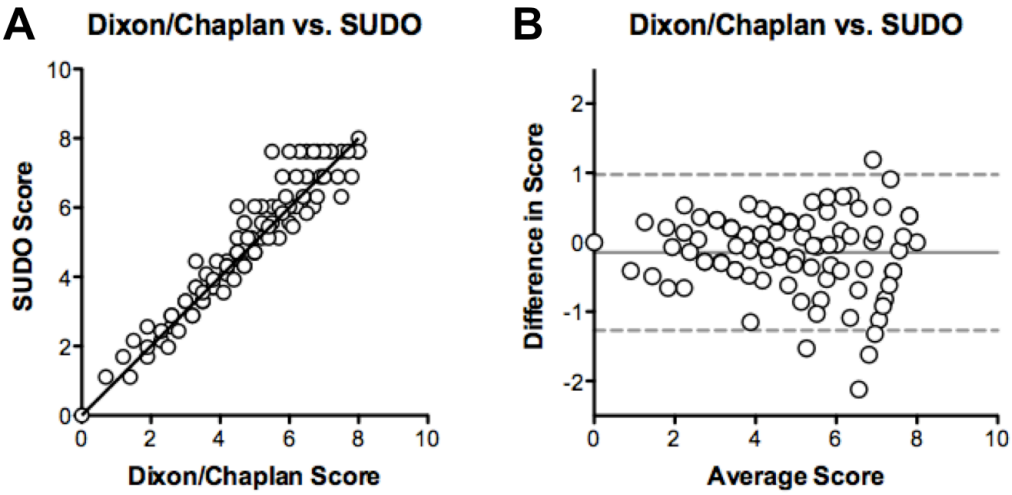

Figure 4-7, Analysis of the ninety potential outcome values of the Dixon/Chaplan up-down method and the corresponding SUDO value (using the tabular adjustment factor)**. (A)** Using the corresponding tabular Dixon maximum likelihood estimates rather than the constant SUDO adjustment factor improved the strength of correlation (Pearson r = 0.954, $p < 0.0001$); shown with line of equality. **(B)** Bland-Altman analysis revealed bias further from zero (-0.14 filament steps) and similar 95% limits of agreement (-1.2 to 1.0 filament steps) to use of the constant adjustment factor.

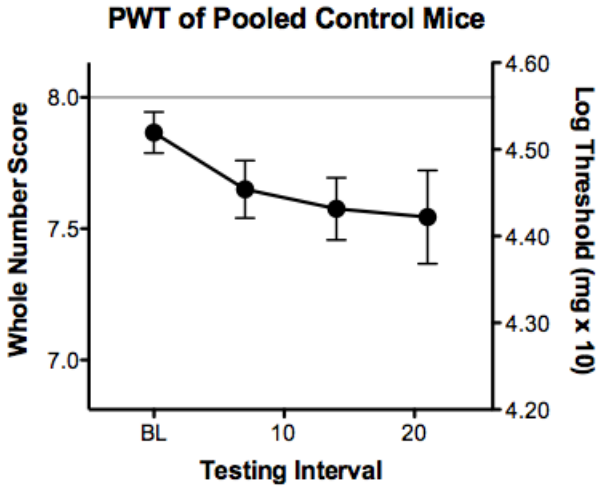

Figure 4-8, PWT values obtained by the Dixon/Chaplan method from 20 control mice pooled from several experiments. The average PWT decreased and became more variable over time, although this trend was not significant. The primary and secondary axes show the whole number score and equivalent filament force value.

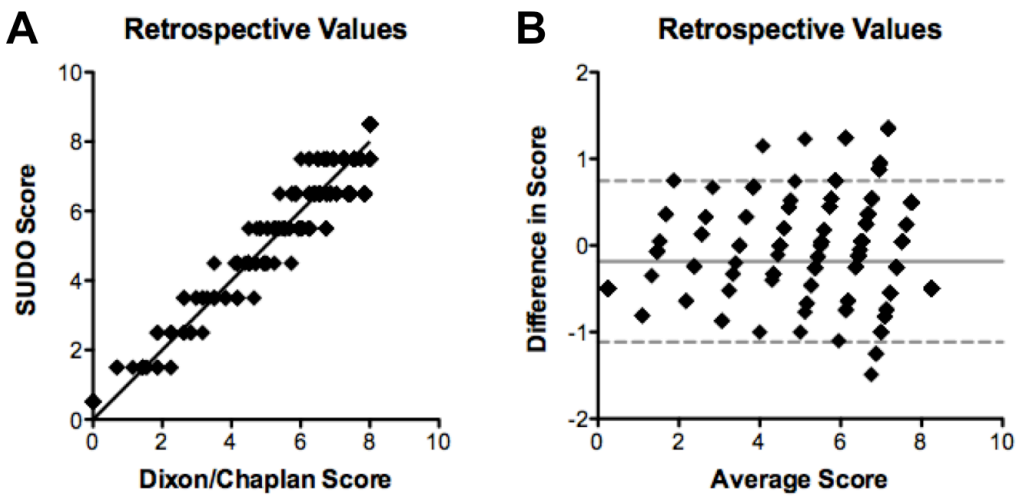

Figure 4-9, Correlation **(A)** and Bland-Altman analysis **(B)** of retrospective PWT data from rats and mice. The possible response patterns were not represented with equal frequency, resulting in stronger correlation (Pearson $r = 0.980$, $p < 0.0001$). The bias between the methods was further from zero (-0.19 filament steps), and the 95% limits of agreement were narrowed to -1.1 to 0.75. However, this still implies a potential difference in the estimated PWT of up to a full filament step.

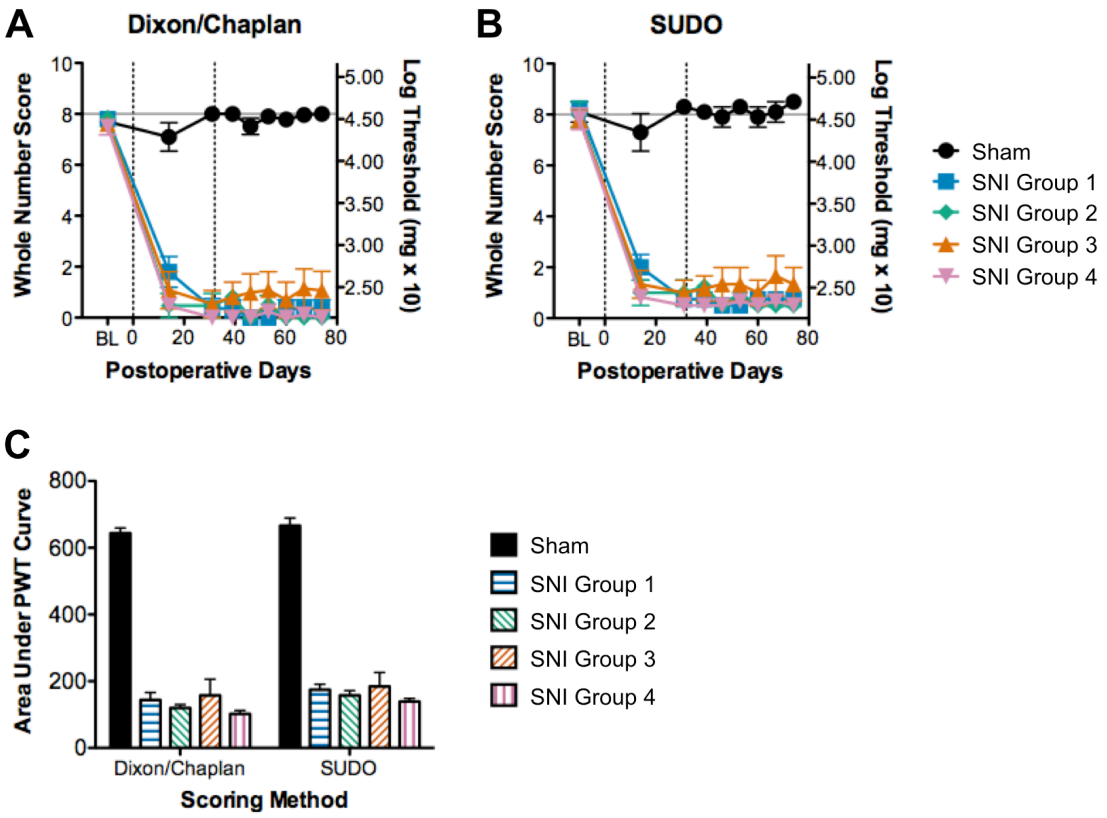

Figure 4-10, (A) By the original Dixon/Chaplan analysis, the mean PWT was significantly decreased in all SNI groups at all time points following surgery ($p < 0.0001$). The vertical dotted lines at day 0 and day 32 indicate the day of surgery and initiation of the experimental treatment, respectively. The primary and secondary axes show the whole number score and equivalent filament force value. **(B)** Converting the retrospective data to the SUDO method did not cause any statistical relationships to be altered. **(C)** The average area under the PWT curve was significantly decreased in all SNI groups as compared to the sham-operated control group ($p < 0.0001$). These relationships were changed following reanalysis by the SUDO method.

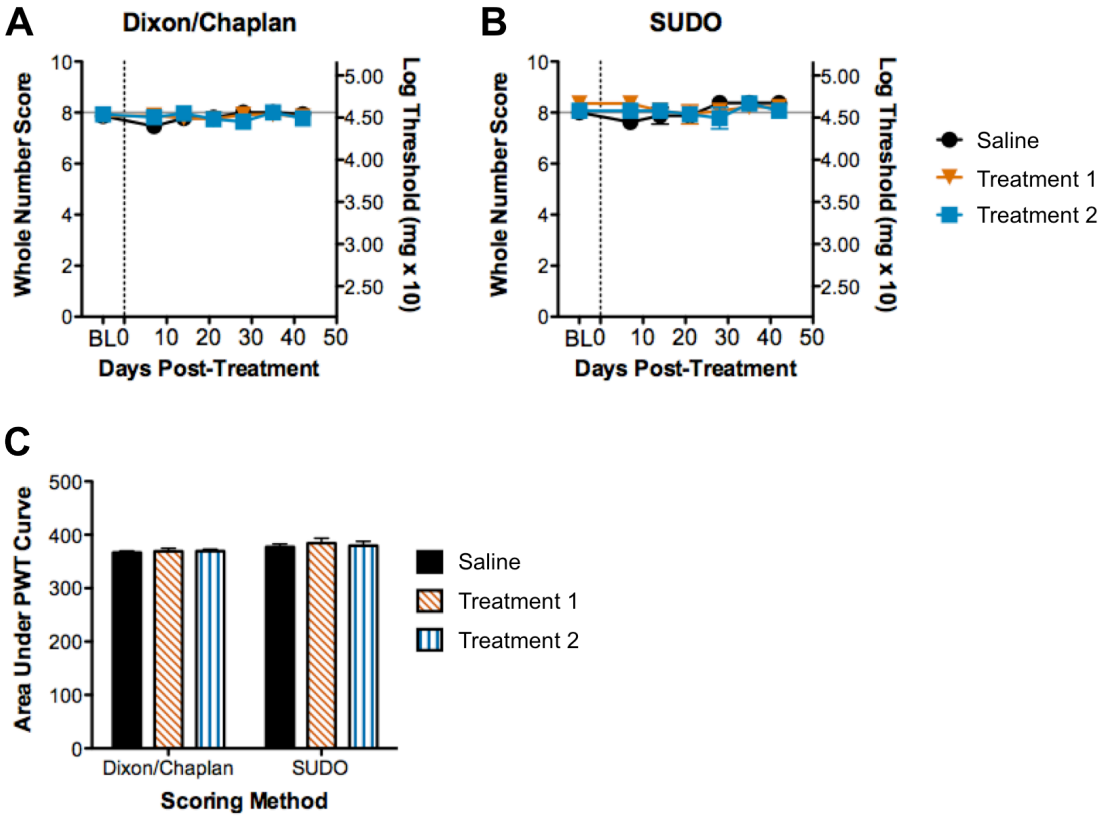

Figure 4-11, PWT values in mice without nerve injury evaluating two experimental treatments compared to saline-treated controls. No hypersensitivity was evident in **(A)** the original Dixon/Chaplan analysis, **(B)** the SUDO reanalysis, or in **(C)** the area under the PWT curves.

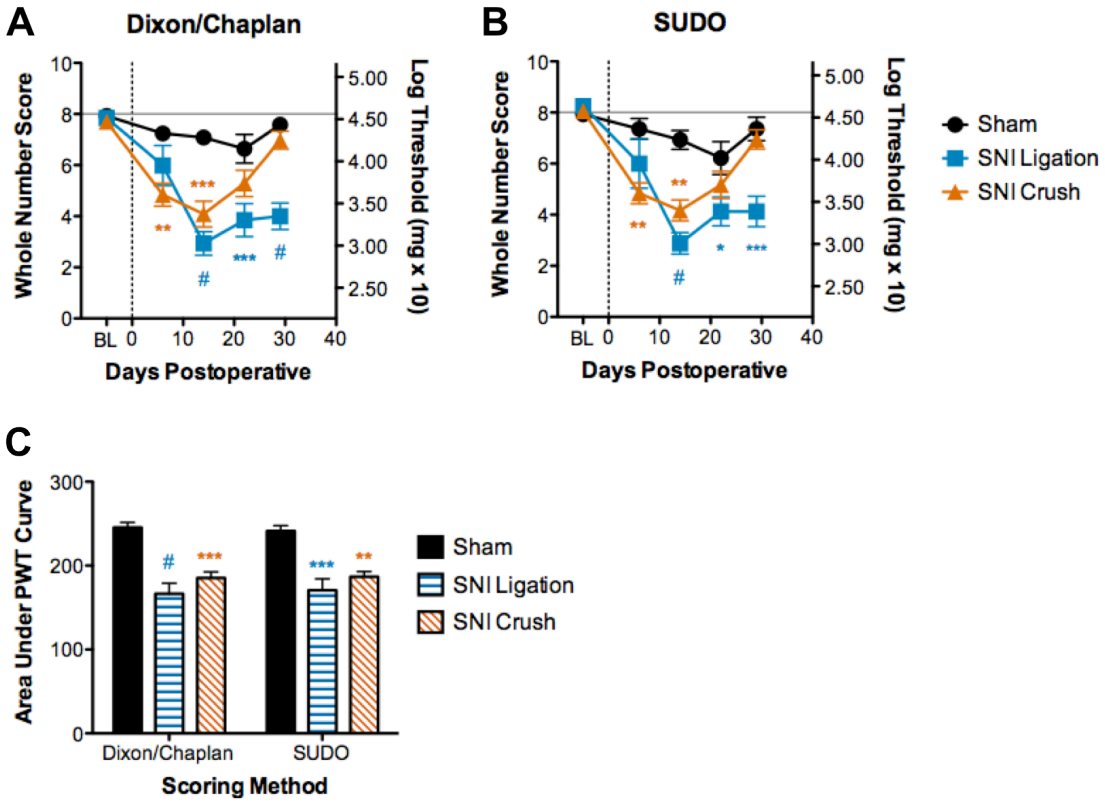

Figure 4-12, PWT values in mice with standard SNI (transection and ligation) and SNI in which the nerve was crushed and allowed to regenerate. **(A)** By the original Dixon/Chaplan analysis, the PWT was significantly decreased as composed to sham-operated controls at post-operative days 14, 21, and 28. In the nerve recovery group, the PWT was significantly decreased at post-operative days 7 and 14, but then returned to baseline. **(B)** With reanalysis of the converted SUDO values, statistical relationships were maintained, but the p values tended to be larger. **(C)** The area under PWT curve was significantly decreased compared to sham-operated controls in both SNI groups. Reanalysis with the SUDO method resulted in diminished p values (* $p < 0.05$, ** $p < 0.01$, *** $p < 0.001$, # $p < 0.0001$).

Chapter 5

Discussion

Theory is when you know everything but nothing works. Practice is when everything works but no one knows why. In our lab, theory and practice are combined: nothing works and no one knows why.

– Anonymous

The purpose of this research was to investigate the functional role of VGF-derived peptides in sensory neuron signaling and in the development of somatic and visceral pain-relevant behavior.

VGF was initially identified as a nerve growth factor-inducible transcript in PC12 cells by Levi and colleagues in 1985, with the accepted non-acronymic name deriving from culture plate V and nerve growth factor (Salton et al., 2000). Biological activities have since been described for a number of VGF-derived peptides. However, the challenge confronting investigators of VGF, as with other granins, is the paucity of information available on specific signaling pathways, cognate receptors, or cellular mechanisms of action (Bartolomucci et al., 2011). While daunting, these gaps in knowledge nonetheless provide opportunities for discovery, and there is increasing interest in the utility of granin-derived peptides in therapeutic intervention or as biomarkers of disease.

To further characterize the VGF signaling system in primary afferent neurons, we utilized animal models of viral-mediated gene transfer and antibiotic-induced visceral hypersensitivity. From this work, we learned intrasciatic administration of AAV5 (driving either GFP or VGF) yields predominately local transduction with inefficient and variable transduction of sensory and motor neurons, reminiscent of the AAV8 serotype and unlike AAV1, AAV2, and AAV6. Intrathecal administration of AAV5-VGF by direct lumbar puncture resulted in successful transduction of the choroid plexus in the fourth ventricle but poor expression in DRG sensory neurons. Antibiotic treatment and presumed dysbiosis were associated with up-regulation of VGF, as well as CGRP and SP, in small-diameter sensory neurons of the sixth lumbar DRG. Contrary to expectations, referred cutaneous allodynia associated with antibiotic-induced visceral hypersensitivity was not

readily detected using a non-invasive mechanical stimulation assay. Collectively, these findings encourage a re-evaluation of the tools employed to modulate VGF expression in primary afferent neurons *in vivo* while supporting the investigation of this novel signaling system beyond models of nerve injury.

Intrasciatic AAV5. We attempted to limit viral-mediated gene expression to primary sensory neurons by employing a specific route of administration. This method of transductional targeting was not successful, as we learned AAV5 demonstrates differential tropism following intraneural injection. It should be possible to restrict viral-mediated gene delivery to sensory neurons through intraneural delivery using a different AAV serotype that maintains neurotropism. However, a less-invasive administration method seems preferable, as iatrogenic neuron damage is an undesirable sequela of direct injection into peripheral nervous tissue.

An alternative approach would be to utilize transcriptional targeting to limit vector gene expression to specific cells. The promoter is the gene regulatory element that drives transcription and determines the strength and cell-type specificity of expression. For AAV vectors, the use of promoters that restrict gene expression to defined cellular subtypes is hampered by the small packaging capacity (up to 4.7 kb) and the typically large size of mammalian promoters (tens to hundreds of kilobases) (Dong et al., 1996; Betley and Sternson, 2011). Several compact, neuron-specific promoters have been developed and demonstrated to be AAV-compatible, including the neuron-specific enolase promoter (Peel et al., 1997) and human synapsin 1 gene promoter (Kügler et al., 2003). However, limiting vector-mediated gene expression to neurons would not resolve the issue of off-target transduction of neurons in the central nervous system.

A promising candidate for genetic manipulation of primary sensory neurons is the *Advillin* gene. *Advillin* encodes a protein in the actin binding family and is expressed almost exclusively in peripheral sensory neurons (Hasegawa et al., 2007). Using the upstream putative regulatory sequence of the gene, Zuborg and colleagues (2011) were able to develop a transgenic mouse line that expresses Cre-recombinase (Cre) exclusive to peripheral sensory neurons. To date, the particular sequence of the *Advillin* promoter has not been determined, and the large upstream promoter regulatory region used to generate the transgenic mouse line far exceeds the capacity of an AAV vector (168 kb). It is not currently possible to construct a sensory neuron-specific AAV vector.

To overcome these problems, a combined approach utilizing transgenic animals and AAV vectors may be warranted. Genetic modification of the mouse genome can take advantage of cell type-specific promoters that are too large to be accommodated by the AAV genome. Cre-dependent expression vectors utilize a strong, ubiquitous promoter but the activity is limited to cells selectively expressing Cre. Standard methods to generate the Cre-dependent vector construct include placing a stop cassette flanked by two loxP sites between the promoter and the transgene. Cre activates the transgene by excising the stop cassette. Unfortunately, stop cassettes occupy a substantial portion of the packaging capacity (1 to 2 kb), and "read-through" transcription is possible (Betley and Sternson, 2011). A strategy better adapted to AAV vectors is a flip-excision (FLEX) switch, which utilizes two pairs of heterotypic loxP sites and inversion of the transgene with respect to the promoter. In the presence of Cre, FLEX recombination changes the orientation of the coding sequence from anti-sense to sense. The FLEX switch is tightly regulated, highly efficient, and compact (0.30 kb) (Atasoy et al., 2008).

With respect to conditional VGF overexpression in sensory neurons, the adapted approach would require access to the *Advillin*-Cre driver mouse line and generation of a novel AAV vector construct. Back-of-the-envelope calculations suggest that there should be sufficient packaging capacity for a typical ubiquitous promoter sequence (~ 1000 bp, 22%), FLEX switch (~300 bp, 7%), and the VGF coding sequence (~1850 bp, 41%). The ideal serotype would demonstrate robust sensory neurotropism following intrathecal delivery, as has been described for AAV9 (Schuster et al., 2014b). Despite transport of the virus within the cerebrospinal fluid to distant, off-target sites, viral-mediated expression of the gene of interest would be selective to primary sensory neurons expressing Cre. However, the feasibility of this proposed approach is uncertain, as *Advillin*-Cre mice are not yet commercially available in the United States (The Jackson Laboratory, www.jax.org).

AAV9-induced sensory neuronopathy. While a useful tool, viral-mediated gene transfer to sensory neurons is not without risk. We provided evidence of unexpected and variable sensory neuron degeneration associated with robust sensory neurotropism and exuberant fluorescent reporter gene expression mediated by AAV9 vectors. Unfortunately, the pathobiological consequences of this unexpected sensory neuronopathy remain unclear, as no behavioral outcome measures were available from the affected animals and the overall extent of neuron loss could not be quantified.

A late revelation was the observation of GFP expression in putative satellite glial cells (SGCs). In the DRG, each sensory neuron soma is individually surrounded by a continuous envelope of multiple SGCs (Hanani, 2005). This complete ensheathment is

anatomically unique and not found in glial-neuron associations in the central nervous system. While long considered to merely give mechanical support, increasing evidence suggests that SGCs interact with neurons and have many essential functions, including controlling the extracellular microenvironment, receiving and transmitting chemical signals, and acting as the tissue-resident antigen presenting cells (Hanani, 2005; van Velzen et al., 2009).

SGCs may be distinguished from neurons immunohistochemically. The most useful marker is glutamine synthetase; glial fibrillary acidic protein is also expressed in activated cells, but may be negligible in resting SGCs. Specific staining for SGCs is not consistently described in reports evaluating AAV transduction of sensory ganglia. In the limited studies that include the satellite glia, no transduction of SGCs was evident with AAV6 (Towne et al., 2009; Yu et al., 2013). However, occasional expression of GFP was observed in SGCs transduced by AAV8 (Fischer et al., 2011). Transduction of glia-like cells in the DRG with crescentic morphology consistent with SGCs was reported in nonhuman primates treated with AAV7 and AAV9, but these cells were not characterized further (Samaranch et al., 2013).

The significance of unintentional SGC transduction may warrant further consideration. In this report, it seems likely that expression of a foreign protein in these antigen presenting cells elicited a destructive cellular immune response in certain animals. Additionally, the intricacies of the bidirectional communication between neuronal somata and SGCs are not well understood. With regards to viral-mediated expression of VGF, induced release of VGF-derived peptides by SGCs may not trigger the same signaling

pathways as endogenously produced VGF in sensory neurons, potentially leading to spurious, confusing results.

Pain-relevant behavior. Perplexity was already amply apparent with the mechanical stimulation assay used to non-invasively monitor putative antibiotic-induced visceral hypersensitivity. While some variability in response rates could be explained through differing states of dysbiosis, the absence of referred cutaneous allodynia following intracolonic instillation of capsaicin was particularly troubling. Meanwhile, the up-regulation of nociceptive neuropeptides in predominantly small-diameter primary afferent neurons in relevant DRG was consistent with increased pain signaling, despite the behavior assays only sporadically identifying a hypersensitive phenotype.

However, it could be argued that assays of mechanical allodynia and thermal sensitivity, as employed throughout these projects, are only measuring nociceptive reflexes and not what would be considered “pain” in the human experience. Spontaneous pain, arguably the most important human clinical symptom, cannot be objectively measured in rodents, and this has led to conflict in the field over the validity and translational value of rodent models (Mogil, 2009; Barrot, 2012). The challenge is that pain is a conscious, subjective, and emotional experience that is assessed by verbal expression, which is not possible in animal models. Additionally, rodents are prey species and are therefore motivated to not display disability to predators or conspecifics.

Recent work adapting tools developed in other fields of behavioral neuroscience has suggested that changes in emotional wellbeing can be objectively quantified in rodent pain. Decreased willingness to participate in spontaneous, rewarding behavior – such

as nest building, digging tasks like burrowing, or *ad libitum* consumption of sucrose solution – has been interpreted to represent an altered emotional state consistent with pain in several rodent models (Jirkof et al., 2010; Strekalova and Steinbusch, 2010; Yalcin et al., 2011; Andrews et al., 2012; Bura et al., 2013). However, incorporation of such assays must be planned judiciously. For, just as apparent negative changes in the global emotional state of the animal resulted in aberrantly decreased thresholds to mechanical stimuli (discussed in Chapter 2), the provision of enrichment materials has been shown to attenuate nerve-injury induced hypersensitivity to mechanical and thermal stimuli (Vachon et al., 2013).

Up-regulation of VGF after intestinal dysbiosis. Nociceptive sensory neurons are commonly classified by their neurochemical signatures. In the mouse, peptidergic nociceptors are demarcated from non-peptidergic by the expression of CGRP and/or SP, TRPV1, and the TrkA receptor, while non-peptidergic nociceptors bind IB_4 and express the P2X3 receptor (Price and Flores, 2007). In DRG culture and in models of neuropathic pain, up-regulated VGF in sensory neurons has been shown to co-localize with SP, CGRP, TrkA, and P2X3 (Rizzi et al., 2008; Riedl et al., 2009), suggesting that VGF induction is not restricted to a particular subset of sensory neurons.

As evidenced in our pilot work investigating a murine model of visceral hypersensitivity, up-regulation of VGF occurred in sensory neurons of varying size and neurochemistry, reminiscent of the previous findings in rats following nerve injury (Riedl et al., 2009). Only one time point was evaluated, with animal sacrifice and tissue collection occurring on the day after antibiotic treatment was completed. It is not clear whether this coincides with the peak of presumed visceral hypersensitivity, given the variability in behavioral

outcomes, for how long this increased expression would persist, or whether the up-regulation could be modulated by probiotic therapy. It should be noted, however, that further investigation of VGF expression in visceral pain would benefit from the use of a standardized model with a more robust, reliable behavioral phenotype.

Immunohistochemical analysis was pragmatically limited to the L6 DRG. However, as demonstrated by Robinson and colleagues (2004), the descending colon of the mouse receives sensory innervation from thoracolumbar DRG as well. Given the T8-L1 DRG also innervate the dermatomes of the ventral abdomen, involvement of nociceptive neurons from these segments may bear stronger correlation to the presence or absence of referred cutaneous allodynia. Provided an appropriate behavioral assay is identified to non-invasively monitor animals for referred hypersensitivity, investigation of DRG from this segment may be informative.

CONCLUSIONS

To further characterize the functional role of VGF-derived peptides in sensory neuron signaling and in the development of pain-relevant behavior, we utilized animal models, behavior analyses, and complementary morphologic and molecular techniques to pursue two approaches: using AAV vectors to modulate VGF expression in primary afferent neurons *in vivo*, and exploring whether VGF up-regulation is limited to somatic pain.

Unfortunately, we learned that AAV5-VGF, delivered intraneurally or intrathecally, was not a useful tool for investigating behavior outcomes of sensory neuron overexpression of VGF. We also witnessed sensory neuron degeneration and loss induced by AAV9,

raising some concerns regarding the use of this AAV serotype in DRG. Antibiotic-induced dysbiosis and presumed visceral hypersensitivity were associated with VGF up-regulation in DRG sensory neurons in a pattern similar to that seen in nerve injury, suggesting VGF also plays a functional role in visceral pain, but a reliable behavioral phenotype could not be established.

Collectively, these findings encourage a re-evaluation of the tools employed to modulate VGF expression in primary afferent neurons *in vivo*, support the investigation of this novel signaling system beyond models of nerve injury, and are presented such that they can be used as an aid in the design of future work.

Chapter 6

References

Abram SE, Yi J, Fuchs A, Hogan QH. 2006. Permeability of injured and intact peripheral nerves and dorsal root ganglia. *Anesthesiology* 105(1): 146-53.

Aguilera M, Cerdà-Cuállar M, Martínez V. 2015. Antibiotic-induced dysbiosis alters host-bacterial interactions and leads to colonic sensory and motor changes in mice. *Gut Microbes* 6(1): 10-23.

Andrews N, Legg E, Lisak D, Issop Y, Richardson D, Harper S, Pheby T, Huang W, Burgess G, Machin I, Rice ASC. 2012. Spontaneous burrowing behavior in the rat is reduced by peripheral nerve injury or inflammation associated pain. *Eur J Pain* 16: 485-495.

Aschauer DF, Kreuz S, Rumpel S. 2013. Analysis of transduction efficiency, tropism and axonal transport of AAV serotypes 1, 2, 5, 6, 8 and 9 in the mouse brain. *PLoS One* 8(9): e76310.

Atasoy D, Aponte Y, Hong Su H, Sternson SM. 2008. A FLEX switch targets Channelrhodopsin-2 to multiple cell types for imaging and long-range circuit mapping. *J Neurosci* 28(28): 7025-7030.

Bankhead P. 2014. *Analyzing fluorescence microscopy images with ImageJ.* Belfast, Northern Ireland: Queen's University Belfast. Retrieved from http://blogs.qub.ac.uk/ccbg/fluorescence-image-analysis-intro/

Barrot M. 2012. Tests and models of nociception and pain in rodents. *Neuroscience* 211: 39-50.

Bartolomucci A, Possenti R, Mahata S, Fischer-Colbrie R, Loh YP, Salton SR. 2011. The extended granin family: structure, function, and biomedical implications. *Endocr Rev* 32(6): 755-97.

Bercik P, Denou E, Collins J, Jackson W, Lu J, Jury J, Deng Y, Blennerhassett P, Macri J, McCoy KD, Verdu EF, Collins SM. 2011. The intestinal microbiota affect central levels of brain-derived neurotropic factor and behavior in mice. *Gastroenterology* 141(2): 599-609.

Bergner CL, Smolinsky AN, Hart PC, Dufour BD, Egan RJ, Laporte JL, Kalueff AV. 2010. Mouse models for studying depression-like states and antidepressant drugs. *Methods Mol Biol* 602: 267-82.

Betley JN, Sternson SM. 2011. Adeno-associated viral vectors for mapping, monitoring, and manipulating neural circuits. *Hum Gene Ther* 22(6): 669-77.

Beutler AS, Reinhardt M. 2009. AAV for pain: steps toward clinical translation. *Gene Ther* 16(4): 461-9.

Beutler AS. 2010. AAV provides an alternative for gene therapy of the peripheral nervous system. *Mol Ther* 18(4): 670-3.

Bland JM, Altman DG. 1986. Statistical methods for assessing agreement between two methods of clinical measurement. *Lancet* 1(8476): 307-10.

Bonin RP, Bories C, De Koninck Y. 2014. A simplified up-down method (SUDO) for measuring mechanical nociception in rodents using von Frey filaments. *Mol Pain* 10:26.

Boulis NM, Noordmans AJ, Song DK, Imperiale MJ, Rubin A, Leone P, During M, Feldman EL. 2003. Adeno-associated viral vector gene expression in the adult rat spinal cord following remote vector delivery. *Neurobiol Dis* 14(3): 535-41.

Brierley SM, Jones RC 3rd, Gebhart GF, Blackshaw LA. 2004. Splanchnic and pelvic mechanosensory afferents signal different qualities of colonic stimuli in mice. *Gastroenterology* 127(1): 166-78.

Brown CM. 2007. Fluorescence microscopy – avoiding the pitfalls. *J Cell Sci* 15(Pt 10): 1702-5.

Bura AS, Guegan T, Zamanillo D, Vela JM, Maldonado R. 2013. Operant self-administration of a sigma ligand improves nociceptive and emotional manifestations of neuropathic pain. *Eur J Pain* 17(6): 832-43.

Can A, Dao DT, Terrillion CE, Piantadosi SC, Bhat S, Gould TD. 2012. The tail suspension test. *J Vis Exp* 28(59): e3769.

Chaplan SR, Bach FW, Pogrel JW, Chung JM, Yaksh TL. 1994. Quantitative assessment of tactile allodynia in the rat paw. *J Neurosci Methods* 53(1): 55-63.

Cheuk W, Chan JK. 2004. Subcellular localization of immunohistochemical signals: knowledge of the ultrastructural or biologic features of the antigens helps predict the signal localization and proper interpretation of immunostains. *Int J Surg Pathol* 12(3): 185-206.

Ciesielska A, Hadaczek P, Mittermeyer G, Zhou S, Wright JF, Bankiewicz KS, Forsayeth J. 2013. Cerebral infusion of AAV9 vector-encoding non-self proteins can elicit cell-mediated immune responses. *Mol Ther* 21(1): 158-66.

Comley LH, Wishart TM, Baxter B, Murray LM, Nimmo A, Thomson D, Parson SH, Gillingwater TH. 2011. Induction of cell stress in neurons from transgenic mice expressing yellow fluorescent protein: implications for neurodegeneration research. *PLoS One* 6(3): e17639.

Cunha TM, Verri WA Jr, Vivancos GG, Moreira IF, Reis S, Parada CA, Cunha FQ, Ferreira SH. 2004. An electronic pressure-meter nociception paw test for mice. *Braz J Med Biol Res* 37(3): 401-7.

Daya S, Berns K. 2008. Gene therapy using adeno-associated virus vectors. *Clin Microbiol Rev* 21(4): 583-93.

Dayton RD, Wang DB, Klein RL. 2012. The advent of AAV9 expands applications for brain and spinal cord gene delivery. *Expert Opin Biol Ther* 12(6): 757-66.

Decosterd I, Woolf CJ. 2000. Spared nerve injury: an animal model of persistent peripheral neuropathic pain. *Pain* 87: 149-158.

Detloff MR, Clark LM, Hutchinson KJ, Kloos AD, Fisher LC, Basso DM. 2010. Validity of acute and chronic sensory testing after spinal cord injury in rats. *Exp Neurol* 225(2): 366-76.

Di Pasquale G, Davidson BL, Stein CS, Matins I, Scudeiro D, Monks A, Chiorini JA. 2003. Identification of PDGFR as a receptor for AAV-5 transduction. *Nat Med* 9(10): 1306-12.

Dixon WJ. 1980. Efficient analysis of experimental observations. *Annu Rev Pharmacol Toxicol* 20: 441-62.

Dong JY, Fan PD, Frizzell RA. 1996. Quantitative analysis of the packaging capacity of recombinant adeno-associated virus. *Hum Gene Ther* 7(17): 2101-12.

Eccleston PA, Funa K, Heldin CH. 1993. Expression of platelet-derived growth factor (PDGF) and PDGF alpha- and beta-receptors in the peripheral nervous system: an analysis of sciatic nerve and dorsal root ganglia. *Dev Biol* 155(2): 459-70.

Ellison DW, Perry A, Rosenblum M, Asa S, Reid R, Louis DN. 2008. Tumours: non-neuroepithelial tumours and secondary effects (paraneoplastic syndromes). In Love S, Louis D, Ellison DW (Eds.), *Greenfield's neuropathology,* 8th ed (pp. 2133-2139). Boca Raton, FL: CRC Press. Retrieved from http://books.google.com.

Ehlert EM, Eggers R, Niclou SP, Verhaagen J. 2010. Cellular toxicity following application of adeno-associated viral-vector-mediated RNA interference in the nervous system. *BMC Neurosci* 11:20.

Fairbanks CA, Peterson CD, Speltz RH, Riedl MS, Kitto KF, Dykstra JA, Braun PD, Sadahiro M, Salton SR, Vulchanova L. 2014. The VGF-derived peptide TLQP-21 contributes to inflammatory and nerve injury-induced hypersensitivity. *Pain* 155(7): 1229-37.

Fang X, Djouhri L, McMullan S, Berry C, Waxman SG, Okuse K, Lawson SN. 2006. Intense isolectin-B4 binding in rat dorsal root ganglion neurons distinguishes C- fiber nociceptors with broad action potentials and high Nav1.9 expression. *J Neurosci* 26(27): 7281-7292.

Fargali S, Garcia AL, Sadahiro M, Jiang C, Janssen WG, Lin WJ, Cogliani V, Elste A, Mortillo S, Cero C, Veitenheimer B, Graiani G, Pasinetti GM, Mahata SK, Osborn JW, Huntley JW, Phillips GR, Benson DL, Bartolomucci A, Salton SR. 2014. The granin VGF promotes genesis of secretory vesicles, and regulates circulating catecholamine levels and blood pressure. *FASEB J* 28(5): 2120-33.

Fischer G, Kostic S, Nakai H, Park F, Sapunar D, Yu H, Hogan Q. 2011. Direct injection into the dorsal root ganglion: technical, behavioral, and histological observations. *J Neurosci Methods* 199(1): 43-55.

Fu H, Muenzer J, Samulski RJ, Breese G, Sifford J, Zeng X, McCarty DM. 2003. Self-complementary adeno-associated virus serotype 2 vector: global distribution and broad dispersion of AAV-mediated transgene expression in mouse brain. *Mol Ther* 8(6): 911-7.

Furuta T, Tomioka R, Taki K, Nakamura K, Tamamaki N, Kaneko T. 2001. In vivo transduction of central neurons using recombinant Sindbis virus: Golgi-like labeling of dendrites and axons with membrane-targeted fluorescent proteins. *J Histochem Cytochem* 49(12): 1497-508.

Galan A, Cervero F, Laird JM. 2003. Extracellular signaling-regulated kinase-1 and -2 (ERK 1/2) mediate referred hyperalgesia in a murine model of visceral pain. *Brain Res Mol Brain Res* 116(1-2): 126-34.

Gibson-Corley KN, Olivier AK, Meyerholz DK. 2013. Principles for valid histopathologic scoring in research. *Vet Pathol* 50(6): 1007-15.

Gilron I, Watson CPN, Cahill CM, Moulin D. 2006. Neuropathic pain: a practical guide for the clinician. *CMAJ* 175(3): 265-75.

Glatzel M, Flechsig E, Navarro B, Klein MA, Paterna JC, Büeler H, Aguzzi A. 2000. Adenoviral and adeno-associated viral transfer of genes to the peripheral nervous system. *Proc Natl Acad Sci USA* 97(1): 442-7.

González-Cano, R, Merlos M, Baeyens JM, Cendán CM. 2013. σ1 receptors are involved in the visceral pain induced by intracolonic administration of capsaicin in mice. *Anesthesiology* 118(3): 691-700.

Goto H, Yang B, Petersen D, Pepper KA, Alfaro PA, Kohn DB, Reynolds CP. 2003. Transduction of green fluorescent protein increased oxidative stress and enhanced sensitivity to cytotoxic drugs in neuroblastoma cell lines. *Mol Cancer Ther* 2(9): 911-7.

Gray SJ, Foti SB, Schwartz JW, Bachaboina L, Taylor-Blake B, Coleman J, Ehlers MD, Zylka MJ, McCown TJ, Samulski RJ. 2011a. Optimizing promoters for recombinant adeno-associated virus-mediated gene expression in the peripheral and central nervous system using self-complementary vectors. *Hum Gene Ther* 22(9): 1143-53.

Gray SJ, Matagne V, Bachaboina L, Yadav S, Ojeda SR, Samulski RJ. 2011b. Preclinical differences of intravascular AAV9 delivery to neurons and glia: a comparative study of adult mice and nonhuman primates. *Mol Ther* 19(6): 1058-69.

Gray SJ, Kalburgi SN, McCown TJ, Samulski RJ. 2013. Global CNS gene delivery and evasion of anti-AAV-neutralizing antibodies by intrathecal AAV administration in non-human primates. *Gene Ther* 20(4): 250-9.

Grimm D, Streetz KL, Jopling CL, Storm TA, Pandey K, Davis CR, Marion P, Salazar F, Kay MA. 2006. Fatality in mice due to oversaturation of cellular microRNA/short hairpin RNA pathways. *Nature* 441(7092): 537-41.

Grubb T. 2010. Chronic neuropathic pain in veterinary patients. *Top Companion Anim Med* 25(1): 45-52.

Gu Y, Xu Y, Li GW, Huang LY. 2005. Remote nerve injection of mu opioid receptor adeno-associated viral vector increases antinociception of intrathecal morphine. *J Pain* 6(7): 447-54.

Haanpää M, Treede RD. 2010. Epidemiology and impact of neuropathic pain. *Pain: Clinical Updates* 18(7): 1-6.

Hadaczek P, Forsayeth J, Mirek H, Munson K, Bringas J, Pivirotto P, McBride JL, Davidson BL, Bankiewicz KS. 2009. Transduction of nonhuman primate brain with adeno-associated virus serotype 1: vector trafficking and immune response. *Hum Gene Ther* 20(3): 225-37.

Hahm S, Mizuno TM, Wu TJ, Wisor JP, Priest CA, Kozak CA, Boozer CN, Peng B, McEvoy RC, Good P, Kelley KA, Takahashi JS, Pintar JE, Roberts JL, Mobbs CV, Salton SR. 1999. Targeted deletion of the *Vgf* gene indicates that the encoded secretory peptide precursor plays a novel role in the regulation of energy balance. *Neuron* 23: 537-548.

Hanani M. 2005. Satellite glial cells in sensory ganglia: from form to function. *Brain Res Rev* 48(3): 457-76.

Hannedouche S, Beck V, Leighton-Davies J, Beibel M, Roma G, Oakeley EJ, Lannoy V, Bernard J, Hamon J, Barbieri S, Preuss I, Lasbennes MC, Sailer AW, Suply T, Seuwen K, Parker CN, Bassilana F. 2013. Identification of the C3a receptor (C3AR1) as the target of the VGF-derived peptide TLQP-21 in rodent cells. *J Biol Chem* 288(38): 27434-43.

Hansen J, Qing K, Kwon HJ, Mah C, Srivastava A. 2000. Impaired intracellular trafficking of adeno-associated virus type 2 vectors limits efficient transduction of murine fibroblasts. *J Virol* 74(2): 992-6.

Hasegawa H, Abbott S, Han BX, Qi Y, Wang F. 2007. Analyzing somatosensory axon projections with the sensory neuron-specific Advillin gene. *J Neurosci* 27(52): 14404-14.

Hayes C, Browne S, Lantry G, Burstal R. 2002. Neuropathic pain in the acute pain service: a prospective study. *Acute Pain* 4: 45-48.

Hirai T, Enomoto M, Machida A, Yamamoto M, Kuwahara H, Tajiri M, Hirai Y, Sotome S, Mizusawa H, Shinomiya K, Okawa A, Yokota T. 2012. Intrathecal shRNA-AAV9 inhibits target protein expression in the spinal cord and dorsal root ganglia of adult mice. *Hum Gene Ther Methods* 23(2): 119-27.

Hirai T, Enomoto M, Kaburagi H, Sotome S, Yoshida-Tanaka K, Ukegawa M, Kuwahara H, Yamamoto M, Tajiri M, Miyata H, Hirai Y, Tominaga M, Shinomiya K, Mizusawa H, Okawa A, Yokota T. 2014. Intrathecal AAV serotype 9-mediated delivery of shRNA against TRPV1 attenuates thermal hyperalgesia in a mouse model of peripheral nerve injury. *Mol Ther* 22(2): 409-19.

Hirakawa H, Okajima S, Nagaoka T, Kubo T, Takamatsu T, Oyamada M. 2004. Regional differences in blood-nerve barrier function and tight-junction protein expression within the rat dorsal root ganglion. *Neuroreport* 15(3): 405-8.

Hollis ER 2nd, Kadoya K, Hirsch M, Samulski RJ, Tuszynski MH. 2008. Efficient retrograde neuronal transduction utilizing self-complementary AAV1. *Mol Ther* 16(2): 296-301.

Homs J, Ariza L, Pagès G, Udina E, Navarro X, Chillón M, Bosch A. 2011. Schwann cell targeting via intrasciatic injection of AAV8 as gene therapy strategy for peripheral nerve regeneration. *Gene Ther* 18(6): 622-30.

Hong S, Son MR, Yun K, Lee WT, Park KA, Lee JE. 2014. Retroviral expression of human arginine decarboxylase reduces oxidative stress injury in mouse cortical astrocytes. *BMC Neurosci* 15:99.

Hungin AP, Chang L, Locke GR, Dennis EH, Barghout V. 2005. Irritable bowel syndrome in the United States: prevalence, symptom patterns, and impact. *Aliment Pharmacol Ther* 21(11): 1365-75.

Hunsberger JG, Newton SS, Bennett AH, Duman CH, Russell DS, Salton SR, Duman RS. 2007. Antidepressant actions of the exercise-regulated gene VGF. *Nat Med* 13(12): 1476-82.

Hylden JL, Wilcox GL. 1980. Intrathecal morphine in mice: a new technique. *Eur J Pharmacol* 67(2-3): 313-6.

Inskip JA, Ramer LM, Ramer MS, Krassioukov AV. 2009. Autonomic assessment of animals with spinal cord injury: tools, techniques and translation. *Spinal Cord* 47: 2-35.

Irving GA. 2005. Contemporary assessment and management of neuropathic pain. *Neurology* 64(Suppl 3): S21-S27.

Jensen EC. 2013. Quantitative analysis of histological staining and fluorescence using ImageJ. *Anat Rec (Hoboken)* 296(3): 378-81.

Jirkof P, Cesarovic N, Rettich A, Nicholls F, Seifert B, Arras M. 2010. Burrowing behavior as an indicator of post-laparotomy pain in mice. *Front Behav Neurosci* 4: 165.

Kawao N, Ikeda H, Kitano T, Kuroda R, Sekiguchi F, Kataoka K, Kamanaka Y, Kawabata A. 2004. Modulation of capsaicin-evoked visceral pain and referred hyperalgesia by protease-activated receptors 1 and 2. *J Pharmacol Sci* 94(3): 277-85.

Kehl LJ, Trempe TM, Hargreaves KM. 2000. A new animal model for assessing mechanisms and management of muscle hyperalgesia. *Pain* 85(3): 333-43.

Kehlet H, Jensen TS, Woolf CJ. 2006. Persistent postsurgical pain: risk factors and prevention. *Lancet* 367: 1618-25.

Klein RL, Dayton RD, Leidenheimer NJ, Jansen K, Golde TE, Zweig RM. 2006. Efficient neuronal gene transfer with AAV8 leads to neurotoxic levels of tau or green fluorescent proteins. *Mol Ther* 13(3): 517-27.

Kroll RA, Neuwelt EA. 1998. Outwitting the blood-brain barrier for therapeutic purposes: osmotic opening and other means. *Neurosurgery* 42(5): 1083-99; discussion 1099-100.

Kügler S, Kilic E, Bähr M. 2003. Human synapsin 1 gene promoter confers highly neuron-specific long-term transgene expression from an adenoviral vector in the adult rat brain depending on the transduced area. *Gene Ther* 10(4): 337-347.

Laird JMA, Martinez-Caro L, Garcia-Nicas E, Cervero F. 2001. A new model of visceral pain and referred hyperalgesia in the mouse. *Pain* 92(3): 335-42.

Lariviere WR, Chesler EJ, Mogil JS. 2001. Transgenic studies of pain and analgesia: mutation or background genotype? *J Pharmacol Exp Ther* 297(2): 467-73.

Lawson SN, Waddell PJ. 1991. Soma neurofilament immunoreactivity is related to cell size and fibre conduction velocity in rat primary sensory neurons. *J Physiol* 435: 41-63.

Le Bars D, Gozariu M, Cadden SW. 2001. Animal models of nociception. *Pharmacol Rev* 53(4): 597-652.

Levi A, Eldridge JD, Paterson BM. 1985. Molecular cloning of a gene sequence regulated by nerve growth factor. *Science* 229(4711): 393-5.

Lewis JE, Brameld JM, Jethwa PH. 2015. Neuroendocrine role for VGF. *Front Endocrinol (Lausanne)* 6: 3.

Loeser JD, Treede RD. 2008. The Kyoto protocol of IASP basic pain terminology. *Pain* 137: 473-477.

Marshall J, Molloy R, Moss GW, Howe JR, Hughes TE. 1995. The jellyfish green fluorescent protein: a new tool for studying ion channel expression and function. *Neuron* 14(2): 211-5.

Martinov T, Mack M, Sykes A, Chatterjea D. 2013. Measuring changes in tactile sensitivity in the hind paw of mice using an electronic von Frey apparatus. *J Vis Exp* 82: e51212.

Mason MR, Ehlert EM, Eggers R, Pool CW, Hermening S, Huseinovic A, Timmermans E, Blits B, Verhaagen J. 2010. Comparison of AAV serotypes for gene delivery to dorsal root ganglion neurons. *Mol Ther* 18(4): 715-24.

Mastakov MY, Baer K, Xu R, Fitzsimons H, During MJ. 2001. Combined injection of rAAV with mannitol enhances gene expression in the rat brain. *Mol Ther* 3(2): 225-32.

Mayorga AJ, Lucki I. 2001. Limitations on the use of the C57BL/6 mouse in the tail suspension test. *Psychopharmacology (Berl)* 155(1): 110-2.

McCarthy CJ, Tomasella E, Malet M, Seroogy KB, Hokfelt T, Villar MJ, Gebhart GF, Brumovsky PR. 2015. Axotomy of tributaries of the pelvic and pudendal nerves induces changes in the neurochemistry of mouse dorsal root ganglion neurons and the spinal cord. *Brain Struct Funct* (Epub ahead of print).

McCarty DM, Young DM Jr, Samulski RJ. 2004. Integration of adeno-associated virus (AAV) and recombinant AAV vectors. *Annu Rev Genet* 38: 819-45.

Millecamps M, Tajerian M, Sage EH, Stone LS. 2011. Behavioral signs of chronic back pain in the SPARC-null mouse. *Spine (Phila Pa 1976)* 36(2): 95-102.

Mills C, LeBlond D, Joshi S, Zhu C, Hsieh G, Jacobson P, Meyer M, Decker M. 2012. Estimating efficacy and drug ED_{50}'s using von Frey thresholds: impact of Weber's law and log transformation. *J Pain* 13(6): 519-23.

Mizisin AP, Weerasuriya A. 2011. Homeostatic regulation of the endoneurial microenvironment during development, aging and in response to trauma, disease and toxic insult. *Acta Neuropathol* 121(3): 291-312.

Mogil JS, Wilson SG, Bon K, Lee SE, Chung K, Raber P, Pieper JO, Hain HS, Belknap JK, Hubert L, Elmer GI, Chung JM, Devor M. 1999. Heritability of nociception I: responses of 11 inbred mouse strains on 12 measures of nociception. *Pain* 80(1-2): 67-82.

Mogil JS. 2009. Animal models of pain: progress and challenges. *Nat Rev Neurosci* 10(4): 283-94.

Moloney RD, O'Mahony SM, Dinan TG, Cryan JF. 2015. Stress-induced visceral pain: toward animal models of irritable-bowel syndrome and associated comorbidities. *Front Psychiatry* 6:15.

Moss A, Ingram R, Koch S, Theodorou A, Low L, Baccei M, Hathway GJ, Costigan M, Salton SR, Fitzgerald M. 2008. Origins, actions and dynamic expression patterns of the neuropeptide VGF in rat peripheral and central sensory neurones following peripheral nerve injury. *Mol Pain* 4:62.

Murlidharan G, Samulski RJ, Asokan A. 2014. Biology of adeno-associated viral vectors in the central nervous system. *Front Mol Neurosci* 7:76.

Nikulin MS. 2002. Three-sigma rule. In Hazewinkel M (Ed.), *Encyclopedia of Mathematics.* Dordrecht, the Netherlands: Kluwer Academic Publishers. Retrieved from http://www.encyclopediaofmath.org.

Patestas M, Gartner LP. 2006. Ascending sensory pathways. In *A Textbook of Neuroanatomy,* 1st ed (pp. 137-170). Malen, MA: Blackwell Science Ltd. Retrieved from http://www.blackwellpublishing.com/patestas/chapters/

Peel AL, Zolotukhin S, Schrimsher GW, Muzyczka N, Reier PJ. 1997. Efficient transduction of green fluorescent protein in spinal cord neurons using adeno-assoicated virus vectors containing cell type-specific promoters. *Gene Ther* 4(1): 16-24.

Pertin M, Gosselin R-D, Decosterd I. 2012. The spared nerve injury model of neuropathic pain. *Methods Mol Biol* 851: 205-12.

Peterson C, Braun P, Schuster D, Schnell S, Kitto K, Churchill C, Wilcox G, Vulchanova L, Fairbanks C. 2014. Expression of human arginine decarboxylase (hADC) in the spinal cord and dorsal root ganglia following intrathecal delivery of an AAV9-hADC vector reduces established chronic pain responses in rodents. Abstract presented at: 33rd Annual Scientific Meeting of the American Pain Society; Apr 30 – May 3; Tampa, Florida USA.

Pitcher MH, Price TJ, Entrena JM, Cervero F. 2007. Spinal NKCC1 blockade inhibits TRPV1-dependent referred allodynia. *Mol Pain* 3:17.

Pitcher MH, Nieto FR, Cervero F. 2013. Stimulation of cutaneous low threshold mechanoreceptors in mice after intracolonic capsaicin increases spinal c-Fos labeling in an NKCC1-dependent fashion. *J Pain* 14(1): 57-65.

Pleticha J, Heilmann LF, Evans CH, Asokan A, Samulski RJ, Beutler AS. 2014a. Preclinical toxicity evaluation of AAV for pain: evidence from human AAV studies and from the pharmacology of analgesic drugs. *Mol Pain* 10:54.

Pleticha J, Jeng-Singh C, Rezek R, Zailbak M, Beutler AS. 2014b. Intraneural convection enhanced delivery of AAVrh20 for targeting primary sensory neurons. *Mol Cell Neurosci* 60: 72-80.

Possenti R, Muccioli G, Petrocchi P, Cero C, Cabassi A, Vulchanova L, Riedl MS, Manieri M, Frontini A, Giordano A, Cinti S, Govoni P, Graiani G, Quanini F, Ghè C, Bresciani E, Bulgarelli I, Torsello A, Locatelli V, Sanghez V, Larsen BD, Petersen JS, Palanza P, Parmigiani S, Moles A, Levi A, Bartolomucci A. 2012. Characterization of a novel peripheral pro-lipolytic mechanism in mice: role of VGF-derived peptide TLQP-21. *Biochem J* 441(1): 511-22.

Price TJ, Flores CM. 2007. Critical evaluation of the colocalization between calcitonin gene-related peptide, substance P, transient receptor potential vanilloid subfamily

type 1 immunoreactivities, and isolectin B_4 binding in primary afferent neurons of the rat and mouse. *J Pain* 8(3): 263-72.

Riedl MS, Braun PD, Kitto KF, Roiko SA, Anderson LB, Honda CN, Fairbanks CA, Vulchanova L. 2009. Proteomic analysis uncovers novel actions of the neurosecretory protein VGF in nociceptive processing. *J Neurosci* 29(42): 13377-13388.

Rizzi R, Bartolomucci A, Moles A, D'Amato F, Sacerdote P, Levi A, La Corte G, Ciotti MT, Possenti R, Pavone F. 2008. The VGF-derived peptide TLQP-21: a new modulatory peptide for inflammatory pain. *Neurosci Lett* 441(1): 129-33.

Robinson DR, McNaughton PA, Evans ML, Hicks GA. 2004. Characterization of the primary spinal afferent innervation of the mouse colon using retrograde labeling. *Neurogastroenterol Motil* 16(1): 113-124.

Rothermel M, Brunert D, Zabawa C, Díaz-Quesada M, Wachowiak M. 2013. Transgene expression in target-defined neuron populations mediated by retrograde infection with adeno-associated viral vectors. *J Neurosci* 33(38): 15195-15206.

Ruben A. 2010. Surviving your stupid, stupid decision to go to grad school. New York, NY: Broadway Books.

Salton SR, Ferri GL, Hahm S, Snyder SE, Wilson AJ, Possenti R, Levi A. 2000. VGF: a novel role for this neuronal and neuroendocrine polypeptide in the regulation of energy balance. *Front Neuroendocrinol* 21(3): 199-219.

Samaranch L, Salegio EA, San Sebastian W, Kells AP, Bringas JR, Forsayeth J, Bankiewicz KS. 2013. Strong cortical and spinal cord transduction after AAV7 and AAV9 delivery into the cerebrospinal fluid of nonhuman primates. *Hum Gene Ther* 24(5): 526-32.

Samaranch L, San Sebastian W, Kells AP, Salegio EA, Heller G, Bringas JR, Pivirotto P, DeArmond S, Forsayeth J, Bankiewicz KS. 2014. AAV9-mediated expression of a non-self protein in nonhuman primate central nervous system triggers widespread neuroinflammation driven by antigen-presenting cell transduction. *Mol Ther* 22(2): 329-37.

Sanoja R, Tortorici V, Fernandez C, Price TJ, Cervero F. 2010. Role of RVM neurons in capsaicin-evoked visceral nociceptions and hyperalgesia. *Eur J Pain* 14(2): 120.e1-9.

Sayuk GS, Gyawali CP. 2015. Irritable bowel syndrome: modern concepts and management options. *Am J Med* Feb 27. Epub ahead of print.

Schultz BR, Chamberlain JS. 2008. Recombinant adeno-associated virus transduction and integration. *Mol Ther* 16(7): 1189-99.

Schuster DJ, Dykstra JA, Riedl MS, Kitto KF, Honda CN, McIvor RS, Fairbanks CA, Vulchanova L. 2013. Visualization of spinal afferent innervation in the mouse colon by AAV8-mediated GFP expression. *Neurogastroenterol Motil* 25(2): e89-100.

Schuster DJ, Belur LR, Riedl MS, Schnell SA, Podetz-Pedersen KM, Kitto KF, McIvor RS, Vulchanova L, Fairbanks CA. 2014a. Supraspinal gene transfer by intrathecal adeno-associated virus serotype 5. *Front Neuroanat* 8: 66.

Schuster DJ, Dykstra JA, Riedl MS, Kitto KF, Belur LR, McIvor RS, Elde RP, Fairbanks CA, Vulchanova L. 2014b. Biodistribution of adeno-associated virus serotype 9 (AAV9) vector after intrathecal and intravenous delivery in mouse. *Front Neuroanat* 8: 42.

Scouten CW. 2010. Frozen section technique in the animal research setting. In SR Peters (Ed.), *A practical guide to frozen section technique* (pp. 171-189). New York, NY: Springer.

Shevtsova Z, Malik JM, Michel U, Bähr M, Kügler S. 2005. Promoters and serotypes: targeting of adeno-associated virus vectors for gene transfer in the rat central nervous system *in vitro* and *in vivo.* *Exp Physiol* 90(1): 53.9.

Strekalova T, Steinbusch HW. 2010. Measuring behavior in mice with chronic stress depression paradigm. *Prog Neuropsychopharmacol Biol Psychiatry* 34(2): 348-61.

Stucky CL, Lewin GR. 1999. Isolection B_4-positive and –negative nociceptors are functionally distinct. *J Neurosci* 19(15): 6497-6505.

Tenenbaum L, Lehtonen E, Monahan PE. 2003. Evaluation of risks related to the use of adeno-associated virus-based vectors. *Curr Gene Ther* 3(6): 545-65.

Thakker-Varia S, Krol JJ, Nettleton J, Bilimoria PM, Bangasser DA, Shors TJ, Black IB, Alder J. 2007. The neuropeptide VGF produces antidepressant-like behavioral effects and enhances proliferation in the hippocampus. *J Neurosci* 27(45): 12156-67.

Towne C, Pertin M, Beggah AT, Aebischer P, Decosterd I. 2009. Recombinant adeno-associated virus serotype 6 (rAAV2/6)-mediated gene transfer to nociceptive neurons through different routes of delivery. *Mol Pain* 5: 52.

Turnley AM, Starr R, Bartlett PF. 2002. Failure of sensory neurons to express class I MHC is due to differential SOCS1 expression. *J Neuroimmunol* 123(1-2): 35-40.

Ulusoy A, Sahin G, Björklund T, Aebischer P, Kirik D. 2009. Dose optimization for long-term rAAV-mediated RNA interference in the nigrostriatal projection neurons. *Mol Ther* 17(9): 1574-84.

Vachon P, Millecamps M, Low L, Thompsosn SJ, Pailleux F, Beaudry F, Bushnell CM, Stone LS. 2013. Alleviation of chronic neuropathic pain by environmental

enrichment in mice well after the establishment of chronic pain. *Behav Brain Funct* 9: 22.

van Velzen M, Laman JD, Kleinjan A, Poot A, Osterhaus AD, Verjans GM. 2009. Neuron-interacting satellite glial cells in human trigeminal ganglia have an APC phenotype. *J Immunol* 183(4): 2456-61.

Verdú EF, Bercik P, Verma-Gandhu M, Huang XX, Blennerhassett P, Jackson W, Mao Y, Wang L, Rochat F, Collins SM. 2006. Specific probiotic therapy attenuates antibiotic induced visceral hypersensitivity in mice. *Gut* 55(2): 182-90.

Vilceanu D, Honore P, Hogan QH, Stucky CL. 2010. Spinal nerve ligation in mouse upregulates TRPV1 heat function in injured IB4-positive nociceptors. *J Pain* 11(6): 588-599.

Vulchanova L, Schuster DJ, Belur LR, Riedl MS, Podetz-Pedersen KM, Kitto KF, Wilcox GL, McIvor RS, Fairbanks CA. 2010. Differential adeno-assoicated virus mediated gene transfer to sensory neurons following intrathecal delivery by direct lumbar puncture. *Mol Pain* 6:31.

Wallace MS. 2005. Diagnosis and treatment of neuropathic pain. *Curr Opin Anaesthesiol* 18: 548-554.

Weerasuriya A, Mizisin AP. 2011. The blood-nerve barrier: structure and function. *Methods Mol Biol* 686: 149-173.

Wu Z, Asokan A, Samulski RJ. 2006. Adeno-associated virus serotypes: vector toolkit for human gene therapy. *Mol Ther* 14(3): 316-27.

Xu Q, Chou B, Fitzsimmons B, Miyanohara A, Shubayev V, Santucci C, Hefferan M, Marsala M, Hua XY. 2012. *In vivo* gene knockdown in rat dorsal root ganglia mediated by self-complementary adeno-associated virus serotype 5 following intrathecal delivery. *PLoS One* 7(3): e32581.

Xu Y, Gu Y, Wu P, Li GW, Huang LY. 2003. Efficiencies of transgene expression in nociceptive neurons through different routes of delivery of adeno-associated viral vectors. *Hum Gene Ther* 14(9): 897-906.

Yalcin I, Bohren Y, Waltisperger E, Sage-Ciocca D, Yin JC, Freund-Mercier MJ, Barrot M. 2011. A time-dependent history of mood disorders in a murine model of neuropathic pain. *Biol Psychiatry* 70: 946-953.

Yiangou Y, Facer P, Dyer NHC, Chan CLH, Knowles C, Williams NS, Anand P. 2001. Vanilloid receptor 1 immunoreactivity in inflamed human bowel. *Lancet* 357:1338-1339.

Yu H, Fischer G, Ferhatovic L, Fan F, Light AR, Weihrauch D, Sapunar D, Nakai H, Park F, Hogan QH. 2013. Intraganglionic AAV6 results in efficient and long-term gene transfer to peripheral sensory neurons. *PLoS One* 8(4): e61266.

Zack GW, Rogers WE, Latt SA. 1977. Automatic measurement of sister chromatid exchange frequency. *J Histochem Cytochem* 25(7): 741-53.

Zuborg S, Piszczek A, Martínez C, Hublitz P, Al Banchaabouchi M, Moreira P, Perlas E, Heppenstall PA. 2011. Generation and characterization of an Advillin-Cre driver mouse line. *Mol Pain* 7:66.

Zwick M, Davis BM, Woodbury CJ, Burkett JN, Koerber HR, Simpson JF, Albers KM. 2002. Glial cell line-derived neurotrophic factor is a survival factor for isolectin B4-positive, but not vanilloid receptor 1-positive, neurons in the mouse. *J Neurosci* 22(10): 4057-65.